NANYANG TECHNOLOGICAL UNIVERSITY

# DEVELOPMENT OF CALIBRATION CHAMBER FOR CONE PENETRATION TEST IN SAND

**ZHAO FENG**

**SCHOOL OF CIVIL AND ENVIRONMENTAL ENGINEERING**

**2008**

# Development of Calibration Chamber for Cone Penetration Test in Sand

**Zhao Feng**

School of Civil and Environmental Engineering

A thesis submitted to the Nanyang Technological University
in fulfilment of the requirement for the degree of
Master of Engineering

**2008**

# ACKNOWLEDGEMENTS

I would like to express my sincere gratitude to my supervisors, Professor Victor, Choa Choon Eng, and Associate Professor Chang Ming-Fang, for their enthusiasm, invaluable guidance, patience and constant encouragement. Their kindness and support during my study will be always in my mind.

I would also like to express my thanks to Dr. Cao Laifa for his warm-hearted guidance and help.

Thanks are given to Associate Professor Teh Cee Ing, the Chair of CEE, Associate Professor Leong Eng Choon, the Head of the Division of Infrastructure System & Maritime Studies, and other faculty members for their kind support and help.

Thanks also due to the staffs of Geotechnics Laboratory including Mr. Vincent Heng, Mr. Koh Sun Weng, Mr. Tan Hiap Guan and Mr. Tay Soon Leong for their assistance in the experimental setup and tests in the investigation.

The research scholarship offered by Nanyang Technological University is gratefully acknowledged.

Finally, my deep thanks to my parents and my wife, for their understanding, support and endless love in the period of my study.

# ABSTRACT

In-situ penetration test such as the cone penetration test (CPT) is increasingly being used in the characterization of sand fill that covers most recent reclaimed land space in Singapore. The usefulness of in-situ penetration test results for engineering applications relies heavily on the development of interpretation procedure in a calibration chamber (CC). A reliable and practical chamber for such purpose is yet to be developed. The chamber wall is the crucial element in the design of a calibration chamber due to the induced boundary effects.

The objective of this investigation is to explore an appropriate chamber wall design for a calibration chamber that can minimize the boundary effect for the calibration of cone penetration tests in sand. It is postulated that such a chamber would incorporate a suitable compressible layer inside the rigid wall.

In this study, a theoretical analysis based on cavity expansion theory has been developed to analyze the stress and displacement in the soil under the semi-infinite elastic half space and in a semi-confined cylindrical boundary. The analysis has subsequently been extended to arrive at a suitable criterion for the selection of the elastic stiffness and thickness of the compressible layer. Results of this analysis indicate that a close simulation of the field boundary condition as prevailed during cone penetration in a semi-infinite soil mass in a calibration chamber is possible if the induced radial stress can be stipulated at the soil-wall boundary. This can be accomplished by the incorporation of a compressible layer on the inner face of the rigid wall in a conventional chamber.

A series of CPT tests were carried out in the developed calibration chamber on Changi sand using a standard cone penetrometer. Results obtained from these calibration chamber tests were verified and interpreted to evaluate the performance of the developed calibration chamber with buffer wall that is capable of reducing and minimizing the boundary effect. The boundary effects of the calibration chamber with rigid wall for CPT tests are obvious and significant for medium dense and dense sand samples. For very loose sand, the boundary effects may be still existed but it is small enough and can be neglected. The CC tests results show that the boundary effects of the chamber can be reduced and minimized

by increasing the thickness of the buffer layer to a certain value for a selected material and the $q_c$ measured in chamber converges to value close to the in-situ $q_c$.

A comparison of the relationship of $q_c$ vs Dr of the sand between existing correlations proposed by other researchers and this research has also been made. The correlations proposed by Jamiolkowski et al. (1985) and Baldi et al. (1986) are applicable to Changi sand although some scatter exists.

# CONTENTS

# LIST OF TABLES

# LIST OF FIGURES

# LIST OF SYMBOLS

| | |
|---|---|
| $a$ | radius of cavity |
| $a_0$ | initial radius of cavity |
| $a_u$ | ultimate radius of cavity |
| $b$ | radius of elastic-plastic boundary |
| $C_0$ , $C_1$, $C_2$ | soil constants of Equation (2.6) |
| $C_g$ | intrinsic soil parameter |
| $C_U$ | coefficient of uniformities |
| $C_C$ | coefficient of curvature |
| $d_c$ | diameter of cone penetrometer |
| $D_c$ | diameter of chamber |
| $D_r$ | relative density |
| $e$ | void ratio |
| $e_g$ | intrinsic soil parameter |
| $e_{\min}$ | minimum void ratio |
| $e_{\max}$ | maximum void ratio |
| $E$ | Young's modulus |
| $E_{25}$ | secant Young's modulus at 25% of failure stress |

| | |
|---|---|
| $E_{50}$ | secant Young's modulus at 50% of failure stress |
| $E_c$ | Young's modulus of compressible layer |
| $E_w$ | Young's modulus of rigid wall |
| $F$ | function of soil parameters |
| $f_s$ | sleeve friction |
| $G$ | shear modulus |
| $G_o$ | initial small strain shear modulus |
| $G_b$ | secant shear modulus at the onset of yielding |
| $G_s$ | secant shear modulus |
| $G_S$ | specific gravity |
| $H_c$ | height of chamber |
| $I_D$ | density index |
| $K_o$ | coefficient of lateral stress |
| $K_{o(NC)}$ | coefficient of horizontal stress in normally consolidated soil |
| $K_{o(OC)}$ | coefficient of horizontal stress in over consolidated soil |
| $K_q$ | correction factor for chamber size effect |
| $M$ | constrained modulus |
| $M_o$ | initial tangent constrained modulus |
| $m_v$ | coefficient of volume change |

| | |
|---|---|
| $N_g$ | bearing capacity factor |
| $OCR$ | overconsolidation ratio |
| $p_a$ | atmospheric pressure |
| $p_c^{'}$ | consolidation pressure in triaxial test |
| $p_0$ | initial total mean stress |
| $p_l$ | limit cavity pressure in an unbounded medium |
| $p_{lc}$ | limit cavity pressure in a confined cylindrical medium |
| $q_c$ | cone tip resistance in an unbounded medium |
| $q_{cc}$ | cone tip resistance in a confined cylindrical medium |
| $q_{c,R}$ | cone tip resistance measured in rigid wall condition |
| $q_{c1}$ | Dimensionless normalized cone resistance $= \dfrac{(q_c / p_a)}{(s_v^{'} / p_a)^{0.5}}$ |
| $Q$ | Bolton's $Q$ parameter (Bolton 1986) |
| $Q_A$ | ageing factor of soil |
| $Q_c$ | compressibility factor $0.91 < Q_c < 1.09$ |
| $Q_{OCR}$ | overconsolidation factor |
| $r$ | radius |
| $r_{co}$ | initial outsider radius of compressible layer |
| $r_c$ | outsider radius of compressible wall |
| $r_{iw}$ | insider radius of rigid wall |

| | |
|---|---|
| $r_{ow}$ | outsider radius of rigid wall |
| $R_d$ | diameter ratio of chamber/cone |
| $u$ | displacement at radial direction |
| $u_c$ | displacement at $r_c$ |
| $V_s$ | shear wave velocity |
| $f$ | friction angle |
| $y$ | dilation angle |
| $a$ , $b$ | elastic parameters of sand |
| $a_M$ | factor in Equation (2.9) |
| $s_b$ | vertical pressure applied to piston at base of soil sample |
| $s_{mean}$ | mean total stress |
| $s'_{mean}, s'_m$ | mean effective stress |
| $s_h$ | horizontal soil pressure |
| $s_v$ | vertical soil pressure |
| $\Delta s_v$ | additional vertical soil pressure |
| $s_r$ | radial stress |
| $s_{rc}$ | radial stress at $r_c$ |
| $s_{rw}$ | radial stress at $r_{iw}$ |
| $s_q$ | circumferential stress |

| | |
|---|---|
| $s'_{vo}$ | initial effective overburden pressure |
| $s'_{ho}$ | initial horizontal effective stress, |
| $t$ | shear stress |
| $n$ | Poisson's ratio |
| $n_c$ | Poisson's ratio of compressible layer |
| $n_w$ | Poisson's ratio of rigid wall |
| $g$ | shear strain |
| $g_b$ | shear strain at elastic-plastic boundary |
| $e_r$ | radial strain |
| $e_q$ | circumferential strain |
| $e_v$ | volumetric strain |
| $r$ | dry density |
| $r_{max}$ | maximum dry density |
| $r_{min}$ | minimum dry density |
| $c$ | parameter of Equation (2.4) |

# CHAPTER 1 INTRODUCTION

## 1.1 Background

Additional land space formed by land reclamation is crucial to the economic development and survival of Singapore. Most of recently reclaimed land space is covered by thick sand fill. There is an increasing need for a reliable and rapid characterization of these sand fill.

The characterization of sand fill at reclaimed sites for the purpose of determining their engineering parameters such as strength and deformation properties is important for densification control and subsequent development of the reclaimed site. In-situ tests are often used because of difficulty of undisturbed sampling and the large sand mass involved in such a situation. Various in-situ tests are available, among which in-situ penetration tests, the cone penetration test (CPT), are by far the most popular.

Although methods are available for the interpretation of results from the CPT, they are site specific and highly empirical and may not be always applicable to sand at other project sites without some means of verification. Due to lack of the theoretical frameworks that simulate the CPT in sand, the usefulness of penetration test results for engineering application relies heavily on carefully controlled tests in calibration chambers (CC) conducted in laboratory. Unfortunately, results from conventional calibration chambers are strongly influenced by boundary effect due to limited chamber sizes that are practical (Parkin, 1988). Miniature penetrometers are sometimes used in attempt to overcome the boundary effects, but their use has not been very successful due to added scale effect. Methods for correction of effect of chamber sizes have been proposed (e.g. Jamiolkowski et al., 1985), but uncertainties exist.

Since its early development in the late 1960's, the calibration chamber has been an important research tool for establishing interpretation procedures for CPT in sand. A calibration chamber consists typically of flexible wall steel cylinder that holds the soil

and provides the necessary rigidity during chamber testing, and a set of top and base plates. The critical feature of a chamber lies mainly on the design of the chamber wall that controls the lateral boundaries. Calibration results obtained from various boundary conditions are generally not unique and usually required corrections and adjustments because of boundary effects from the limited size of the chamber that is practical. The ability of the chamber boundary to accommodate different lateral pressures induced by penetration in sand of different densities, elastic properties and shear characteristics will be a key consideration in the design of a new calibration chamber.

A field simulator that was recently developed by Hsu and Huang (1998) has shown very good results due to its highly sophisticated design and test procedure. There is however a need to develop a simpler calibration chamber of practical size that can be used more generally for the calibration of penetration tests involving normal size penetrometer in sand.

To minimize and overcome the boundary effects of conventional chamber, one potentially practical way is to design a new chamber with a double-wall system that incorporates an elastic compressible layer as a buffer between the sand mass and the rigid boundary. If the compressible material can be correctly chosen, it is possible that the radial stresses induced from the cone penetration would be able to produce strains that are comparable to those at the same radial location in a semi-infinite soil mass. The desirable elastic properties and the thickness of the compressible material are believed to vary primarily with the elastic properties and the shear characteristics of the sand to be calibrated, among other factors (Chang and Cao, 2001). A careful investigation of mechanism of deformation of sand when it is subject to penetration in a semi-confined space on basis of sound theoretical frameworks of cavity expansion theory and a suitable constitutive model such as that based on a power-law function constitutive model of sand will be of great importance in the development of such a calibration chamber.

## 1.2 Objectives

The objectives of this investigation are (1) to develop a theoretical framework for the analysis of the stress and deformation of sand around a penetrometer in a semi-confined space, (2) to determine on the basis of the theoretical framework, a suitable criterion for the selection of the stiffness and thickness of the compressible layer to be incorporated in a rigid-wall calibration chamber, and (3) to develop a calibration chamber that is capable of reducing and minimizing the boundary effects.

## 1.3 Scope of research

***Phase 1- Theoretical study***

A theoretical analysis of cavity expansion theory in sand that observes a suitable constitutive law in a semi-confined space has been formulated on the basis of relevant previous researches. The theoretical analysis enables the determination of changes in radial stress and displacement at various cylindrical boundaries at different distance away from the cavity wall as the cavity advances in a semi-infinite half space in the field and in a semi-confined space that prevailed in a conventional calibration chamber.

***Phase 2- chamber wall design***

A chamber wall aiming at reducing and minimizing the boundary effects has been designed and constructed and tested for the calibration of the cone penetration test in sand. The rigid-wall chamber incorporates an inner buffer layer consisting of elastic compressible material. A suitable criterion for the selection of the elastic properties and the thickness of the buffer has been drawn up on the basis of the theoretical framework developed in Phase 1.

***Phase 3- Fabrication of calibration chamber and cone penetration tests in chamber***

The main tasks in this phase included (a) characterization of Changi sand that tested in the chamber tests, (b) identification and characterization of suitable buffer material, (c) fabrication of a new calibration chamber using a selected steel tank available in the

university's Gotechnics Workshop, and (d) calibration chamber tests of a standard cone penetrometer available in the university's Geotechnics Laboratory.

***Phase 4- Verification and interpretation of calibration chamber test results***

A series of CPT tests were carried out in the developed calibration chamber on Changi sand using a standard cone penetrometer. Results obtained from these CC tests were verified and interpreted to evaluate the performance of the developed calibration chamber that is cable of reducing and minimizing the boundary effect.

## 1.4 Outline of the thesis

Chapter 2 presents a literature review of common in-situ penetration tests and their interpretation for the engineering parameters in sand fill. The development of different calibration chamber (CC) tests and interpretation methods for the cone penetration test (CPT) are included.

Chapter 3 describes the analysis of cavity expansion in semi-infinite sand mass. The distribution of stresses and associated strains around an expanding cavity in a semi-infinite half space has been investigated. Solutions for the stress, strain and displacement distribution of expansion of cylindrical cavities in sands are proposed.

Chapter 4 describes the analysis of cavity expansion in confined sand mass based on stress rotation analyses. If the limit cavity pressure in calibration chamber is equal to the limit cavity pressure in semi-infinite condition by choosing a suitable compressible buffer wall, the cone resistance measured in a calibration chamber will be the same as that measured in field. The selection criterion of the material of buffer wall is proposed.

Chapter 5 describes the laboratory tests to characterize the basic index properties and the stress-strain characteristics of the Changi sand tested in the calibration chamber.

Chapter 6 describes the laboratory compression test to characterize the stress-strain characteristics for determination of Young's modulus and Poisson's ratio of sponge rubber.

Chapter 7 presents the apparatus and setup for the new calibration chamber (CC) and the CPT tests in the chamber. The construction of calibration chamber was conducted in the Geotechnics Workshop of Nanyang Technological University (NTU) and it consists of a double-wall system, with a compressible layer attached to the inner face of the rigid wall. A series of cone penetration test (CPT) by using standard 36mm cone was carried in the new chamber on dry samples of Changi sand with different relative densities which were prepared by the sand pluviation method.

Chapter 8 presents the verification and interpretation of the results of calibration chamber tests to evaluate the performance of the new chamber wall design that is capable of reducing and minimizing the boundary effect in conventional calibration chamber.

Chapter 9 highlights the main conclusions of this study and some recommendations for future research of CPT tests in calibration chamber are proposed.

# CHAPTER 2 LITERATURE REVIEW

## 2.1 Introduction

In this chapter, common in-situ penetration tests and their interpretation for the engineering parameters in sand fill are briefly reviewed. The development of different calibration chamber (CC) tests and interpretation methods for the cone penetration test (CPT) are included.

## 2.2 In-situ penetration tests

### 2.2.1 General

The objective of any subsurface exploration in geotechnical engineering is to determine three main aspects: nature and sequence of the subsurface strata; groundwater conditions, and; in-situ physical and mechanical properties of the subsurface soils. There are many techniques available to meet the objectives of a site investigation and these include both investigation in the field and the laboratory. Laboratory investigation includes those that test elements of the ground, such as triaxial tests, and those that test prototype models, such as centrifuge tests. Field investigation includes drilling, sampling, in-situ testing and full scale testing. An ideal site investigation should combine the field and laboratory tests in a proper way.

In the in-situ test, the ground is tested in-place by instruments that are inserted in or penetrate the ground. In-situ tests are normally associated with tests for which a borehole is either unnecessary or is only an incidental part of the overall test procedure, required only to permit insertion of the testing tool or equipment. The role of the specialized in-situ testing for site characterization and the research and development of in-situ techniques have received important attention at least in the past 20 years. The use of specialized in-situ testing in geotechnical engineering practice became more and more popular all over the world and in Singapore. Improvements in apparatus, instrumentation, and technique of deployment, data acquisition and analysis procedure have been significant. The most common in-situ

tests used in geotechnical practice are the standard penetration test (SPT), the field vane test (FVT), the cone penetration test (CPT) and the piezocone penetration test (CPTU), the pressuremeter (PMT) and the dilatometer (DMT). Other common field tests include plate-bearing tests, pumping tests and other tests to determine hydraulic conductivity, and geophysical surveys.

Among the vast number of in-situ tests, the penetration tests such as the CPT and DMT, especially the CPT, are by far the most versatile tools available for the characterization of sand fill at reclaimed sites.

### 2.2.2 Cone penetration test (CPT) in site investigation

Cone penetration test (CPT) has played a significant role in evaluating the engineering characteristics of subsurface soils for decades. The result of CPT is often used in settlement analyses, allowable bearing pressure determinations, and density and friction angle estimations. Schmertmann (1978) and Robertson and Campanella (1983) performed detailed evaluations of the cone penetrometer that resulted in the early guidelines and recommendations for use of CPT in practice.

There are three main groups in existing CPT systems: (1) mechanical cone penetrometers; (2) electric cone penetrometers; and (3) piezocone penetrometers. A cone penetrometer with a 10 $cm^2$ base area cone with an apex angle of $60^{\circ}$ is the most common standard in geotechnical practice. The basic terminology of a cone penetrometer is described in Figure 2.1.

In the CPT test, a cone penetrometer is pushed into the ground at a constant rate (Standard rate of penetration = 20 mm/s) by a series of rods and nearly continuous or intermittent measurements are made of the resistance to penetration of the cone tip and the sleeve resistance. The cone tip resistance $q_c$ is defined as the value that the total force acting on the cone divided by the projected area of the cone. The sleeve friction $f_s$ is the ratio of the total force acting on the friction sleeve and the surface area of the friction sleeve. A standard electrical cone penetrometer uses separate load cells in two basic measurements of the tip and sleeve resistance. Additional sensors such as pore pressure transducers, inclinometers, and accelerometers have also been added to provide additional information in some cone penetrometers. The piezocone

penetrometer, for example, includes pore pressure transducers in addition to the two basic measurements.

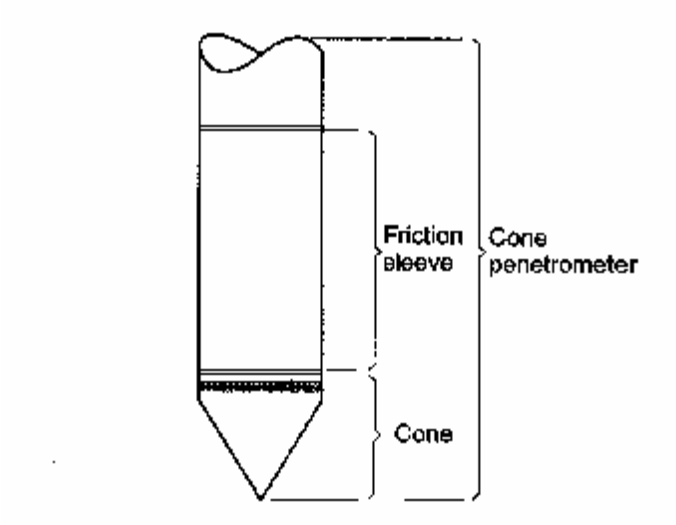


**Figure 2.1** Terminology for cone penetrometer

Three main applications of CPT results are:

(1) to determine subsurface stratigraphy and identify materials present,
(2) to estimate geotechnical parameters, and,
(3) to provide measurements for direct geotechnical design.

For the above applications the CPT tests may be supplemented by other tests, either in-situ or in the laboratory.

## 2.3 Interpretation of CPT tests in sandy soils

### 2.3.1 General

CPT has an important role in the exploration of cohesionless soils, because there is a lack of satisfactory alternative methods of investigation. CPT has been used very extensively as the key site investigation tool for the characterization of sand deposits for liquefaction potential study and for the characterization of sand fill and for fill densification control. Direct derivations from cone resistance of relative density, angle

of shearing resistance, and modulus values (either the constrained modulus or Young's modulus) depend on empirical correlations.

### 2.3.2 Relative density (density index)

For cohesionless soils, the relative density is often used as an intermediate soil parameter. Relative density $D_r$, is defined as:

$$D_r = \frac{e_{\max} - e}{e_{\max} - e_{\min}} \tag{2.1}$$

where $e$ is the in-situ void ratio, $e_{\max}$ and $e_{\min}$ respectively are the maximum and minimum void ratios that can be determined in the laboratory following appropriate procedures stipulated in relevant standards (e. g. ASTM 4253 and ASTM 4254).

Relative density has been used by engineers as a parameter to describe sand deposits and correlations have been developed relating $D_r$ to the angle of internal friction $f'$, liquefaction potential and so on. Former work in large calibration chamber (CC) has provided numerous correlations between cone penetration resistance and relative density for clean, predominantly silica sands.

The calibration chamber testing has shown that the cone resistance is controlled by sand density, in-situ vertical and horizontal effective stress and sand compressibility. Robertson and Campanella (1983) carried out a review of the available calibration chamber test results and showed that the correlations between cone resistance and effective stress at a given relative density were similar in shape but were strongly influenced by sand compressibility, as illustrated in Figure 2.2. Sands with a high compressibility would have a lower cone resistance than a sand at the same relative density with a lower compressibility.

The relationship between relative density and cone resistance of sand is greatly affected by its compressibility. At a given value of relative density and an effective overburden pressure, $s'_{vo}$, a sand of high compressibility has a lower $q_c$ than a sand of low compressibility.

Based on calibration chamber tests, Jamiolkowski et al. (1985) proposed a relationship between values of $D_r$ versus a function of $q_c$ and $s'_{vo}$ as illustrated in Figure 2.3.

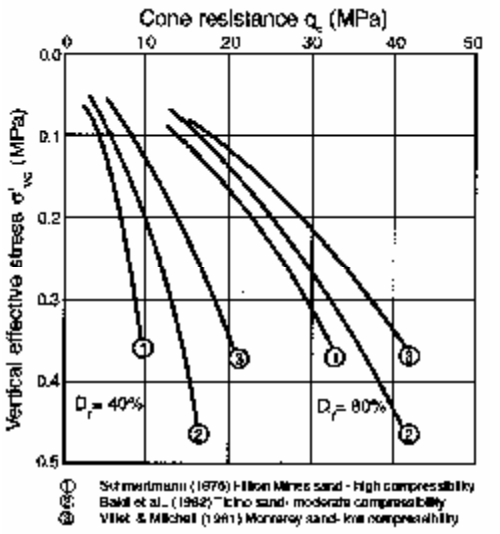


**Figure 2.2** Effect of sand compressibility on $q_c$, $s'_{vo}$, $D_r$ relationship (after Robertson and Campanella, 1983)

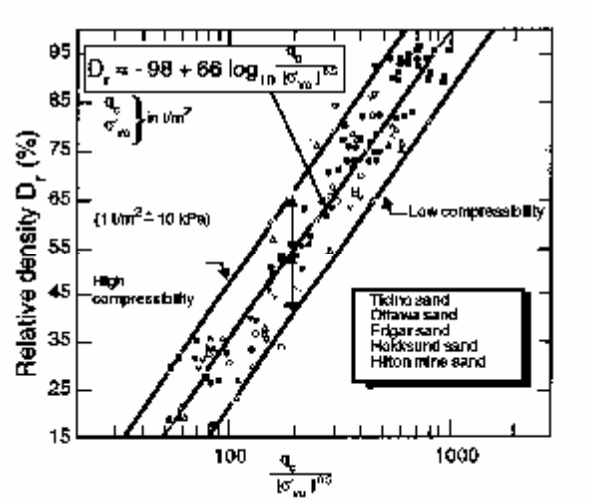


**Figure 2.3** Influence of compressibility on sands (after Jamiolkowski et al., 1985)

Figure 2.3 shows that, whereas sands of moderate compressibility (Ticino, Edgar, Hokksund) follow the regression line, the results for the highly compressible Hilton Mine sand tend towards the upper bound line, and those for the Ottawa 90 sand, of

low compressibility, tend towards the lower bound line. It is suggested, therefore, that these upper and lower bound lines can be taken to represent probable limit values of relative density for sands of very high compressibility and very low compressibility, respectively. Jamiolkowski et al. (1985) pointed out that a correction factor $K_q$ for accounting the chamber size effect is required. The proposed $K_q$ is given by:

$$K_q = 1 + \frac{0.2(D_r - 30)}{60} \tag{2.2}$$

The measured $q_c$ in the chamber needs be divided by $K_q$.

Chamber tests show that, for a given sand, $D_r$ is better correlated with initial horizontal effective stress, $s'_{ho}$, than with initial vertical effective stress, $s'_{vo}$. Figure 2.3 can therefore be used in OC sands by substitution of $s'_{ho}$ for $s'_{vo}$, if the in-situ effective horizontal stress is known or can be estimated. This should be regarded as only an approximation, with a possible error in $D_r$ of $\pm 20\%$. Values of in-situ horizontal stress can be estimated in the field using a self-boring pressuremeter. Failing this, and provided an estimation of the overconsolidation ratio (OCR) is available, values of $K_o$ (and hence of $s'_{ho}$) can be estimated using Schmertmann's (1975) proposed relationship:

$$K_{o(OC)} = (OCR)^{0.42} K_{o(NC)} \tag{2.3}$$

Schmertmann (1975) also suggested a relationship between $q_c$ for OC sand and $q_c$ for NC sand of the form:

$$q_{c(OC)} / q_{c(NC)} = 1 + c[(OCR)^b - 1] \tag{2.4}$$

where $c$ and $b$ have the values 0.75 and 0.42, respectively.

Baldi et al (1982) found that $b$ varies with relative density:

$$b \approx 0.275 + 0.26 D_r \tag{2.5}$$

and that $c$ varies decreasing with increasing $D_r$, approximately from 0.50 (OCR=2) to 0.25 (OCR=15).

Based on extensive calibration testing on Ticino sand, Baldi et al. (1986) recommended the following formula for estimating relative density:

$$D_r = \frac{1}{C_2} \cdot \ln\left( \frac{q_c}{C_o \left(s'\right)^{C_1}} \right) \tag{2.6}$$

where $C_o$, $C_1$ and $C_2$ are soil constants; $s'$ is effective stress in kPa, with $s'$ equal to either the mean effective stress $s'_m$ or the vertical effective stress $s'_{vo}$.

The correlations based on the above formula and soil constants are shown in Figure 2.4. To estimate the relative density of a given sand from the CPT, one requires an estimation of horizontal effective stress and the compressibility of the sand relative to those used in the calibration studies. Figure 2.4 (a) (using $s'_{vo}$) can be used to estimate $D_r$. For overconsolidated sands, one needs to use Figure 2.4 (b) and the effective mean stress $s'_m$.

The $D_r$ vs $q_c$ correlations above will lead to an overestimation of $D_r$ when applied to natural sand deposits. However, the same correlations will underestimate $D_r$ if applied to more crushable and compressible sands or sands containing more than 5% to 10% fines. Previous experience by former researchers has shown that an increase in grain size can increase cone resistance and an increase in coefficient of uniformity may decrease cone resistance at a given relative density. A visual classification of grain characteristics would improve the selection of appropriate $D_r$ correlation. The compressibility of sands tends to increase with increasing uniformity in grading, angularity of grains, mica or feldspar content, carbonate and fines content.

Kulhawy and Mayne (1990) proposed a simple formula for estimating relative density:

$$D_r^2 = \frac{q_{c1}}{305 Q_c \cdot Q_{OCR} \cdot Q_A} \tag{2.7}$$

where

$q_{c1}$ = Dimensionless normalized cone resistance $= \dfrac{(q_c / p_a)}{(s'_v / p_a)^{0.5}}$

$p_a$ = Atmospheric pressure in same units as $q_c$

$Q_c$ = Compressibility factor $0.91 < Q_c < 1.09$

$Q_{OCR}$ = Overconsolidation factor

$Q_A$ = Ageing factor

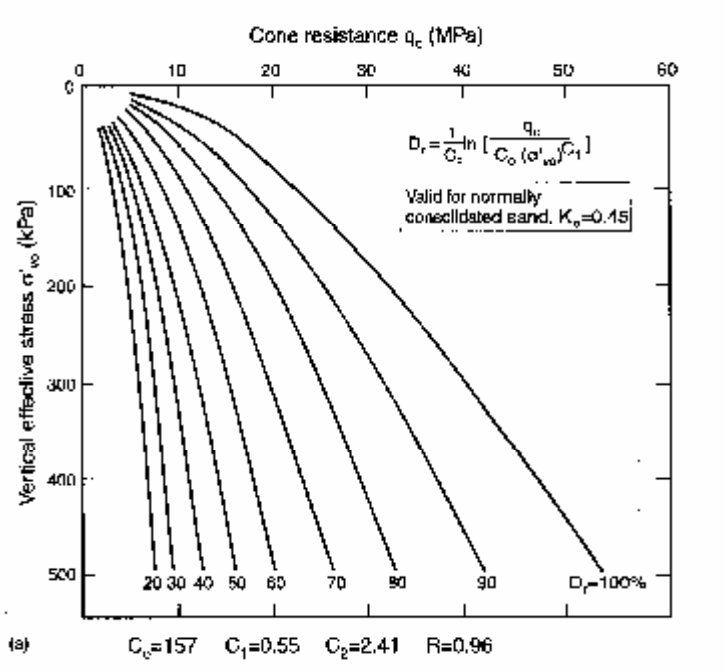


**Figure 2.4a** $q_c$, $s'_{vo}$, $D_r$ relationship for Ticino sand (NC) (after Baldi et al., 1986)

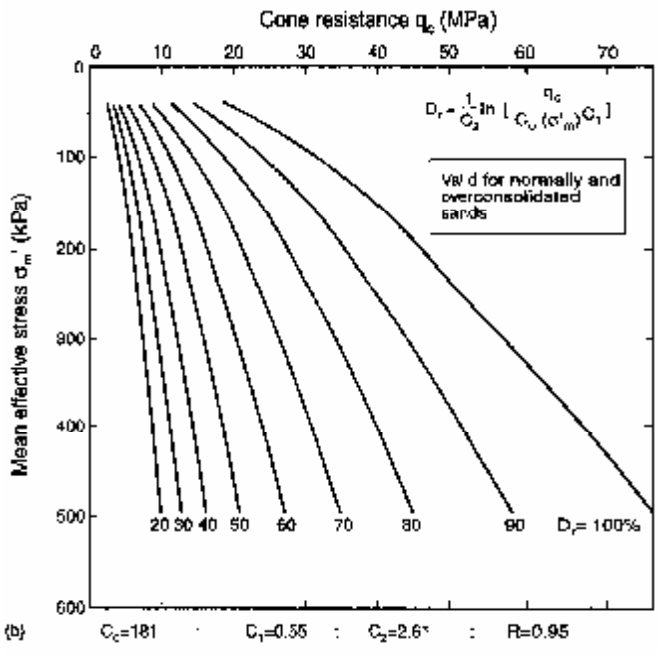


**Figure 2.4b** $q_c$, $s_m'$, $D_r$ relationship for Ticino sand (OC) (after Baldi et al., 1986)

### 2.3.3 Strength characteristics

It is possible to estimate the peak effective angle of shearing resistance, $f'$, of free-draining sands using relative density as an intermediate parameter. An existing relationship between relative $D_r$ and $f'$ is shown in Figure 2.5 (Schmertmann, 1978). Another approach is to use the Terzaghi bearing capacity factor for general shear, $N_g$ and $q_c$, as given by Muhs and Weiss (1971):

$$N_g = 12.5 q_c \qquad (2.8)$$

The correlation was derived from large-scale shallow footing tests on sand, and it takes no account of the overburden pressure. These procedures are less satisfactory than direct procedures for determination of $f'$, because of the uncertainty involved.

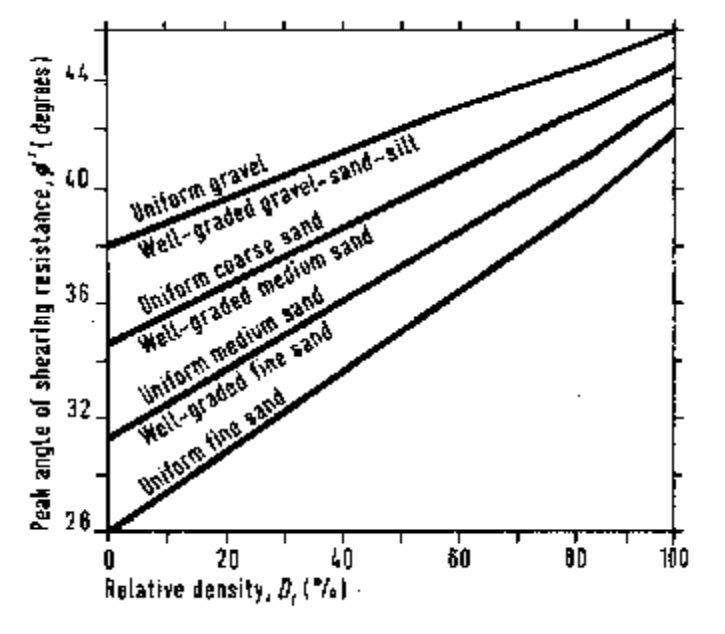


**Figure 2.5** Relationship between friction angle and relative density of sands (after Schmertmann, 1978)

A direct correlation between $q_c$ and $f'$ is shown in Figure 2.6. It is derived from a bearing capacity theory developed by Durgunoglu and Mitchell (1975), using a soil-to-cone interface friction angle of $0.5f'$ and a lateral earth pressure coefficient, $K_o = 1 - \sin f'$. The theory ignores the effects of soil compressibility.

A review by Robertson and Campanella (1983) of the results of chamber correlation tests by a number of researchers showed that the correlation provided by the Douglas and Mitchell's (1975) theory gives a reasonable lower bound of $f'$ for the type of sands tested. These were predominantly of quartz, with some of feldspar and in some cases a small amount of mica. Particle shapes ranged from round to sub-angular. The sands were in the medium and medium-to-coarse particle size range and fairly uniform in grading. In general, clean NC sands of this kind will have $f'$ ranging from the lower-bound values given in Figure 2.6 up to about $2°$ higher for the more compressible ones (angular grains, higher content of mica, more uniform). In highly compressibility sands (e.g. carbonate sands or glauconitic sands), $f'$ may be significantly higher than that would be derived from Figure 2.6.

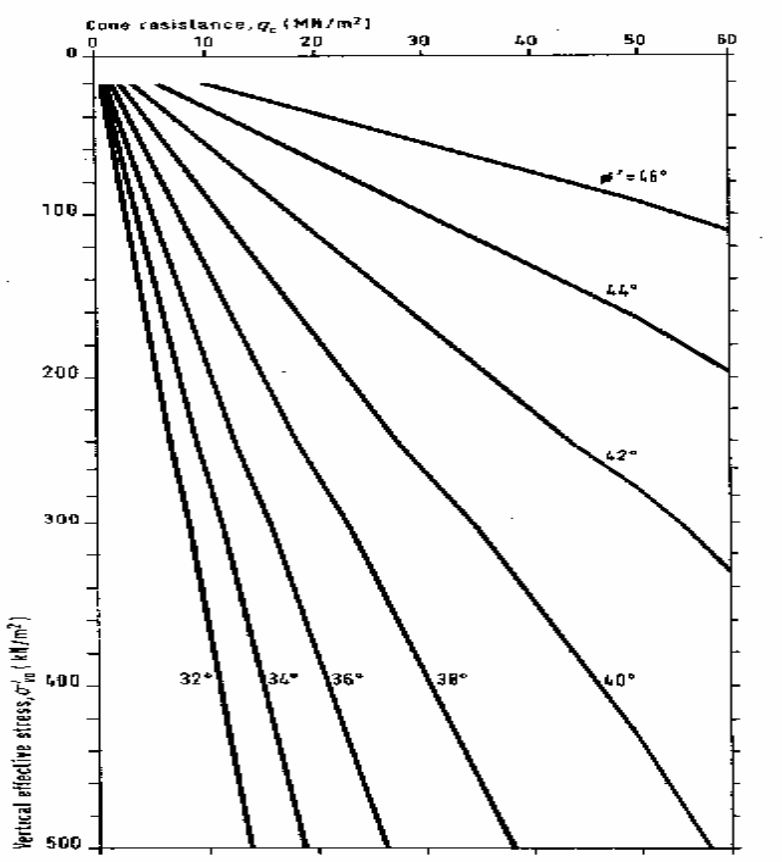


**Figure 2.6** Relationship friction angle and cone resistance of sand (after Dougls and Mitchell, 1975)

### 2.3.4 Deformability

A reliable determination of sand stiffness in-situ is of great practical interest to geotechnical engineer in view of the difficulties in obtaining representative deformation modulus from tests on laboratory specimens. This is mainly because of undisturbed sand samples are extremely difficult to obtain and often more or less impossible using conventional techniques, particularly because of the sensitivity of soil deformation to the fabric that is difficult to duplicate.

Depending on the problem under consideration, one will often need to evaluate one of three moduli: the constrained modulus $M$ (which is equal to the reciprocal of the oedometer vertical coefficient of volume change, $m_v$), the Young's modulus, $E$, or the shear modulus, $G$. The stress-strain curves for sands are normally nonlinear, it is necessary to know the stress range over which the deformation modulus is needed.

***Constrained modulus***

Correlations between constrained modulus, $M$ , and cone resistance, $q_c$ , are commonly expressed as

$$M = a_M \cdot q_c \tag{2.9}$$

and $a_M$ is often stated to be in the range 1.5 to 4.

Vesic (1970) suggested:

$$a_M = 2\left(1+\left(\frac{D_r}{100}\right)^2\right) \tag{2.10}$$

where the $a_M$ value is typically in the range 2.25 to 4. Lunne and Kleven (1981) summarized $a_M$ values from a number of chamber tests (Table 2.1). It can be seen that for NC sands, $a_M$ lies in the range of 3 to 11. The values are corresponding by higher values for OC sands. In general, $a_M$ decreases with increasing $q_c$, but for a given value of $q_c$, $a_M$ increases with increasing stress level.

**Table 2.1** Summary of calibration chamber results for constrained modular coefficient (after Lunne and Kleven, 1981)

| *Source* | *NC sand* | | *OC sand* | |
|---|---|---|---|---|
| | *No. of sands* | $\alpha_M$ | *No. of sands* | $\alpha_M$ |
| Veismanis (1974) | 3 | 3 to 11 | 3 | 5 to 30 |
| Parkin *et al.* (1980) | 1 | 3 to 11 | 1 | 5 to 30 |
| Chapman & Donald (1981) | 1 | 3 to 4<br>3 absolute lower limit | 1 | 6 to 15<br>(12 = average) |
| Baldi *et al.* (1982) | 1 | > 3 | 1 | 3 to 9 |

Lunne and Christoffersen (1983) made an extensive review of chamber test results. They proposed the following conservative values of the initial tangent constrained modulus, $M_o$, for NC sand:

$$M_o = 4q_c \quad \text{for} \quad q_c < 10\text{MN/m}^2 \tag{2.11}$$

$$M_o = 2q_c + 20 \quad \text{for} \quad 10\text{MN/m}^2 < q_c < 50\text{MN/m}^2 \tag{2.12}$$

and

$$M_o = 120\text{MN/m}^2 \quad \text{for} \quad q_c > 50\text{MN/m}^2 \tag{2.13}$$

For OC sand, with OCR>2, they propose

$$M_o = 5q_c \quad \text{for} \quad q_c < 50\text{MN/m}^2 \tag{2.14}$$

$$M_o = 250\text{MN/m}^2 \quad \text{for} \quad q_c > 50\text{MN/m}^2 \tag{2.15}$$

These recommendations are presented graphically in Figure 2.7.

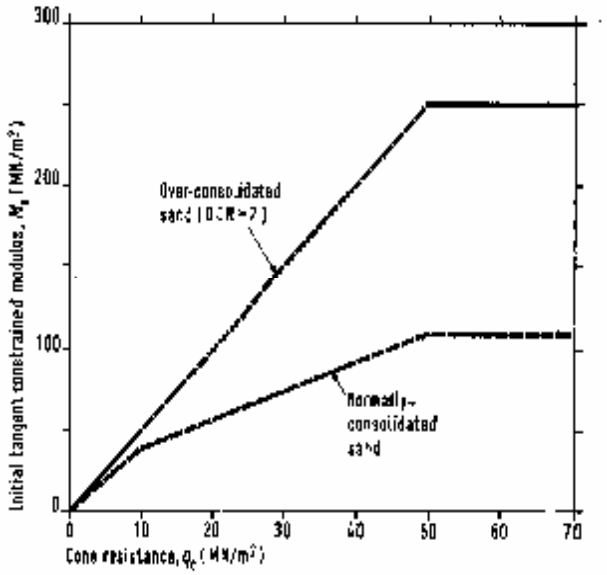


**Figure 2.7** Initial tangent constrained modulus for NC sand (after Lunne and Christoffersen, 1983)

For NC sands, the constrained modulus applicable for the stress range of $s'_{vo}$ to $s'_{vo} + \Delta s_v$ can be estimated as:

$$M = M_o \left( \frac{s'_{vo} + \Delta s_v / 2}{s'_{vo}} \right)^{0.5} \tag{2.16}$$

For overconsolidated sands, the exponent reduces with OCR, approaching zero for heavily overconsolidated sands.

***Young's modulus***

For other than one-dimensional cases, Young's modulus, $E$, is a more appropriate elastic modulus than the constrained modulus, $M$. Based on chamber test results, Robertson and Campanella (1983) proposed values of drained secant Young's modulus at 25% of failure stress ($E_{25}$) and at 50% of failure stress ($E_{50}$) for NC sands (Figure 2.8). Figure 2.8 shows that, expect at very low relative densities, $E_{25}$ varies between about $1.5q_c$ and just over $2q_c$, which is in reasonable agreement with the value of 2.0 recommended by Schmertmann (1970) for calculation of settlement of footings on sand.

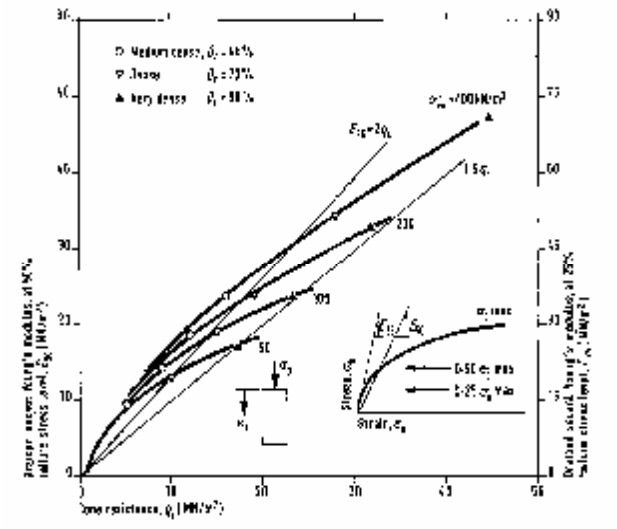

**Figure 2.8** Secant Young's modulus values for NC sands (after Robertson and Campanella,1983)

For OC sands, $E_{50}$ varies between $6q_c$ and $11q_c$ (Baldi et al., 1982). $E_{25}$ is some 50% higher for OCR up to about 3, but approximately equal to $E_{50}$ for OCR greater than 4 (ENEL et al., 1985). However, as a result of the limited data available, for OC sands, it is prudent to adopt $E$ values not more than twice those given in Figure 2.8 for NC sands.

***Small strain shear modulus***

The shear modulus is largest at very low strains and decreases with increasing shear strain. It has generally been found that the maximum shear modulus is constant for shear strains less than $10^{-3}\%$. This initial, small strain modulus often denoted $G_o$. Elastic theory relates the small strain shear modulus, $G_o$, to soil density, $r$, and shear wave velocity, $V_s$, as follows:

$$G_o = r V_s^2 \tag{2.17}$$

where $r =$ mass density of the soil.

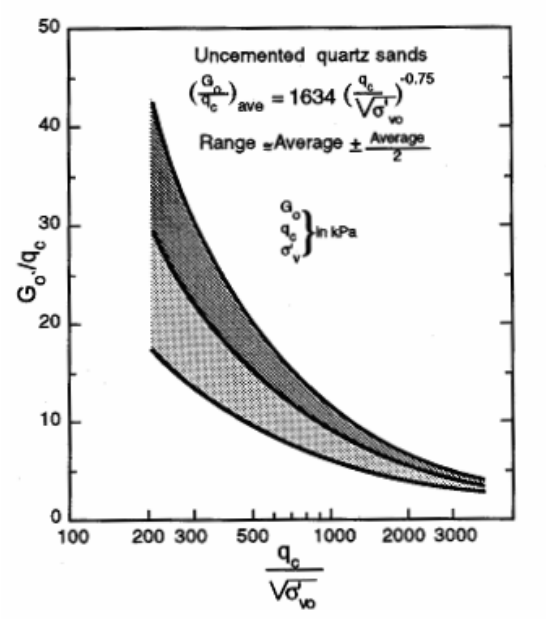


**Figure 2.9** $G_{max} / q_c$ (after Rix and Stokoe, 1992)

The value of $G_o$ can be found by measuring the shear wave velocity using the seismic CPT (Robertson et al., 1986). Alternatively, $G_o$ can be estimated using empirical correlations. Jamiolkowski et al. (1988) showed that the same variables of soil density and in-situ effective stresses controls both $q_c$ and $G_o$ can be found for uncemented and unaged cohesionless soils.

Based on calibration chamber results as well as field measurements, Rix and Stokoe (1992) suggested the correlation shown in Figure 2.9. The wide range of $G_o / q_c$ at low values of normalized cone resistance is most likely due to variations in soil compressibility. More compressible sands appear to produce lower values of normalized cone resistance and hence higher values of $G_o / q_c$.

## 2.4 Development of calibration chamber (CC) testing in sand

### 2.4.1 General

Theories or approaches for interpreting in-situ tests in terms of soil parameters need to be verified by experimental data. The interpretation methods are also often completely or partly based on correlations with experimental data. For cohesive material the basic soil characteristics (for instance, strength and deformation parameters) can be established from laboratory tests on undisturbed samples. For sandy soils, the problem of sample disturbance normally prevents this approach from being used. Calibration chamber (CC) testing has therefore been developed as the most efficient means of verifying interpretation theories and establishing engineering corrections for sands. Calibration chambers have been used for over thirty years to determine empirical correlations between test measurements and properties of the soil. Standard size or reduced size in-situ test apparatus (such as cone penetrometer and dilatometer) can be pushed into the sand in a large laboratory sample with a control density and subjected to a preselected applied stress. The corresponding responses can be monitored. Parallel standard size triaxial sand samples can be reconstituted to the same densities and consolidated to the same stresses as the CC sample for determining the basic stress deformation and strength parameters and providing the reference data for the development or verification of corrections.

Knowledge of the relationship between the cone penetration resistance $q_c$ and the relative density $D_r$ and the stress state is important for effective interpretation of cone penetrometer tests in sand. Calibration chambers may be used to study this relationship. In a calibration chamber test, a large cylindrical sand sample is deposited to the desired stress state. A cone penetration test (CPT) then may be performed along the axis of the sample. Every test provides one value of $q_c$ for the given values of $D_r$ and stress level. A large number of tests, covering the range of densities and stresses of interest, would provide the basis for regression analysis of the data and the empirical establishment of the relationship between $q_c$, $D_r$ and the stress state. Depending on the displacements and stresses at the sample boundaries, the boundary conditions imposed on the sand mass during penetration in a calibration chamber are usually one of the following four types. These are:

(1) BC1: constant lateral and vertical stresses,

(2) BC2: zero vertical displacement, and zero average lateral displacement,

(3) BC3: constant vertical stress and zero average lateral displacement, and

(4) BC4: zero vertical displacement and constant lateral stress

Four different boundary conditions of calibration chamber – BC1, BC2, BC3, or BC4 are illustrated in Figure 2.10. The boundary conditions for a soil mass, however, is believed to lie in between that under a constant lateral stress boundary (BC1 or BC4) and a zero lateral strain boundary (BC2 and BC3). It is now generally believed that test involving BC2 and BC4 boundary conditions should be discontinued as these boundary conditions are not compatible with those prevailed in the field. It has well known that the value of penetration resistance measured during the CC test is influenced by the conditions of boundary effects.

Most calibration chamber testing has been done using BC1. The difference between the four types of boundary conditions is in whether stress or displacement boundary conditions are imposed on the top, bottom, and circumferential surfaces of the sand sample. Circumferential boundary conditions are the most important. BC1 and BC4 (both corresponding to a constant lateral stress during cone penetration) generate approximately the same penetration resistance values, all other factors being equal.

Similarly, BC2 and BC3 generate comparable penetration resistance values under the same conditions. None of the four boundary conditions perfectly represents free-field conditions, so the measured $q_c$ in the calibration chamber generally is different from the measured $q_c$ in the field, all other parameters being the same. The difference between chamber and field $q_c$ values generally decreases as the ratio of chamber to cone diameter increases.

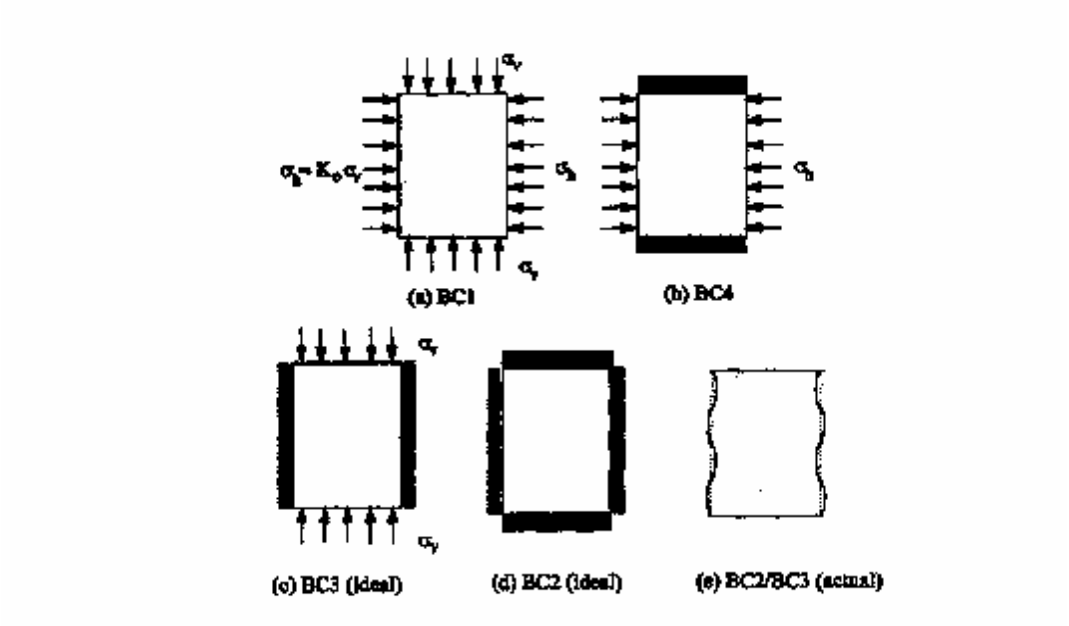


| Boundary conditions | Top and bottom boundary | | Lateral boundary | |
|---|---|---|---|---|
| | Stress | Strain | Stress | Strain |
| B1 | Constant | – | Constant | – |
| B2 | – | 0 | – | 0 |
| B3 | Constant | – | – | 0 |
| B4 | – | 0 | Constant | – |
| B5 | Constant | – | Servo–controlled | |

BC5 – Simulator Field Condition (Huang & Hsu, 2004 & 2005)

**Figure 2.10** Types of boundary conditions in calibration chamber tests

### 2.4.2 Review of the history of calibration chambers

The calibration chamber tests used in geotechnical practice over the last two decades differ in a number of ways, including dimensions; stiffness and nature of lateral, top, and bottom boundaries; sample deposition procedures; and form of control of boundary conditions (Ghionna and Jamiolkowski, 1991). The characteristics of various chambers used worldwide are listed in Table 2.2. These chambers all have flexible lateral boundaries. The first calibration chamber used for geotechnical engineering purposes was built in 1969 by the Country Roads Board (CRB) in Melbourne, Australia to evaluate the performance of a full-size cone penetrometer under conditions of controlled stress, strain, and soil properties (Holden, 1971). The sample in the chamber was 0.75 m in diameter and 0.90 m in height. The base piston was inflated by water from an air/water cylinder, with deformations being derived from water level observations. Sample formation was achieved by means of a traveling sand spreader (following the principle of Kolbuszewski and Jones, 1961), and the results of this investigation were reported by Veismanis (1974).

Subsequent developments of calibration chamber occurred in various countries, with progressive development in technology. A chamber for samples 1.2m by 1.2m was built at the University of Florida in 1970, essentially similar to its predecessor but intended to accommodate a larger cone (Holden, 1971; Laier et al., 1975). Further developments from the Florida design, and the need for increased travel, led to the construction of a 1.2m diameter by 1.8m high chamber at Monash Univesity (Australia), with traveling spreader (Chapman, 1974), followed soon after by a 1.2m by 1.5m chamber at the Norwegian Geotechnical Institute (NGI), Olso (Parkin et al., 1982). Both of these chambers had air inflation under the base piston, with a transducer provided for the measurement of piston movement. Because of the difficulty of achieving sample uniformity, due to the large air currents created by traveling sand spreaders, the latter project also introduced a new static sand rainer (Holden, 1977), developed in association with Jacobsen, at the University of Aalborg (Jacobsen, 1976).

The subsequent developments of calibration chambers including that at the Italian Electricity Board (ENEL), Milan (1977) have the same size as the NGI chamber, and use similar sand spreaders.

**Table 2.2** Large diameter calibration chambers used in geotechnical investigations (after Ghionna and Jamiolkowski, 1991)

| Test Cell Owner/Location | Specimen Diameter (m) | Specimen Height (m) | Boundary Conditions | | |
|---|---|---|---|---|---|
| | | | Radial | Bottom | Top |
| Country Roads Bureau, Australia | 0.76 | 0.91 | Flexible | Cushion | Rigid |
| University of Florida, USA | 1.2 | 1.2 | Flexible | Cushion | Rigid |
| Monash University, Australia | 1.2 | 1.8 | Flexible | Cushion | Rigid |
| Norwegian Geotechnical Institute | 1.20 | 1.50 | Flexible | Cushion | Rigid |
| ENEL-CRIS, Milano, Italy | 1.20 | 1.50 | Flexible | Cushion | Rigid |
| ISMES, Bergamo, Italy | 1.20 | 1.50 | Flexible | Cushion | Rigid |
| University of California, Berkeley, USA | 0.76 | 0.80 | Flexible | Rigid | Rigid |
| University of Texas at Austin, USA | cube 2.1x2.1x2.1 m | | All flexible | | |
| University of Houston, USA | 0.76 | 2.54 | Flexible | Cushion | Cushion |
| North Carolina State University, USA | 0.94 | 1.00 | Flexible | Rigid | Rigid |
| Luisiana State University, USA | 0.55 | 0.80 | Flexible | Flexible | Rigid |
| Golder Associates, Calgary, Canada | 1.40 | 1.00 | Flexible | Rigid | Cushion |
| Virginia Polytechnic Institute and State University, USA | 1.5 | 1.5 | Flexible | Rigid | Rigid |
| University of Grenoble, France | 1.2 | 1.5 | Flexible | Cushion | Cushion |
| Oxford University, UK | 0.90 | 1.10 | Flexible | Cushion | Rigid |
| University of Tokyo, Japan | 0.90 | 1.10 | Flexible | Rigid | Rigid |
| University of Clarkson, USA | 0.51 | 0.76 | Flexible | Rigid | Rigid |
| University of Sheffield, UK | 0.79 | 1.00 | Flexible | Rigid | Flexible |
| Cornell University, USA | 2.1 | 2.9 | Flexible | Rigid | Rigid |

### 2.4.3 Basic description of typical calibration chamber

***Country Roads Board (CRB) type***

In the case of the ENEL chamber (Bellotti et al., 1982), significant developments were made in the incorporation of a precision servo-controlled mechanical device for the penetrometer by replacing the hydraulic ram with a highly sensitive device for volume change measurement. Figure 2.11 shows the general set-up of CC testing used by ENEL (Bellotti et al., 1982 and Bellotti et al., 1988).

In the ENEL system, the entire system consists of a flexible cavity wall chamber, a sand rainer and a loading frame. The sand specimen is enclosed at the side and the base by rubber membranes; the side membrane is sealed around an aluminum plate which forms the top boundary of the specimen and transfers the thrust of the chamber piston from the sand to the lid.

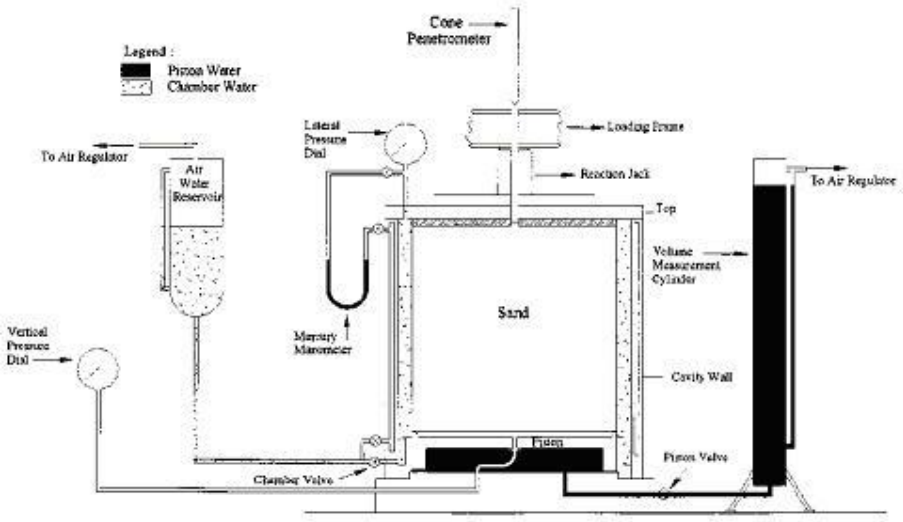


**Figure 2.11** Schematic of ENEL calibration chamber (from Bellotti et al., 1988)

During the test, the vertical stress is applied to the specimen via the based chamber piston raised by pressurized water and the lateral stress is applied by a water-filled annular space surrounding the specimen. A hole in the centre of the lid allows the pushing of in-situ tests of different sizes into the chamber. The samples are general prepared by pluvial deposition in the air or by vacuum.

A detailed account of above equipment and the procedures used were given by Bellotti et al. (1982). Although dry sand is usually used, the ENEL chamber can accommodate saturated samples as outlined by Bellotti et al. (1988).

***Golder Associates calibration chamber***

Been et al. (1987) conducted a series calibration chamber tests involving the penetration of a cone in sand dredged from the Erkdsk borrow pit in the Beaufort Sea. This sample in the chamber was 1m in height and 1.4m in diameter. This diameter, choose in part as a result of practical size limitations, provided a chamber to standard cone diameter ratio of 38. The construction of the Golder Associates chamber is illustrated in Figure 2.12.

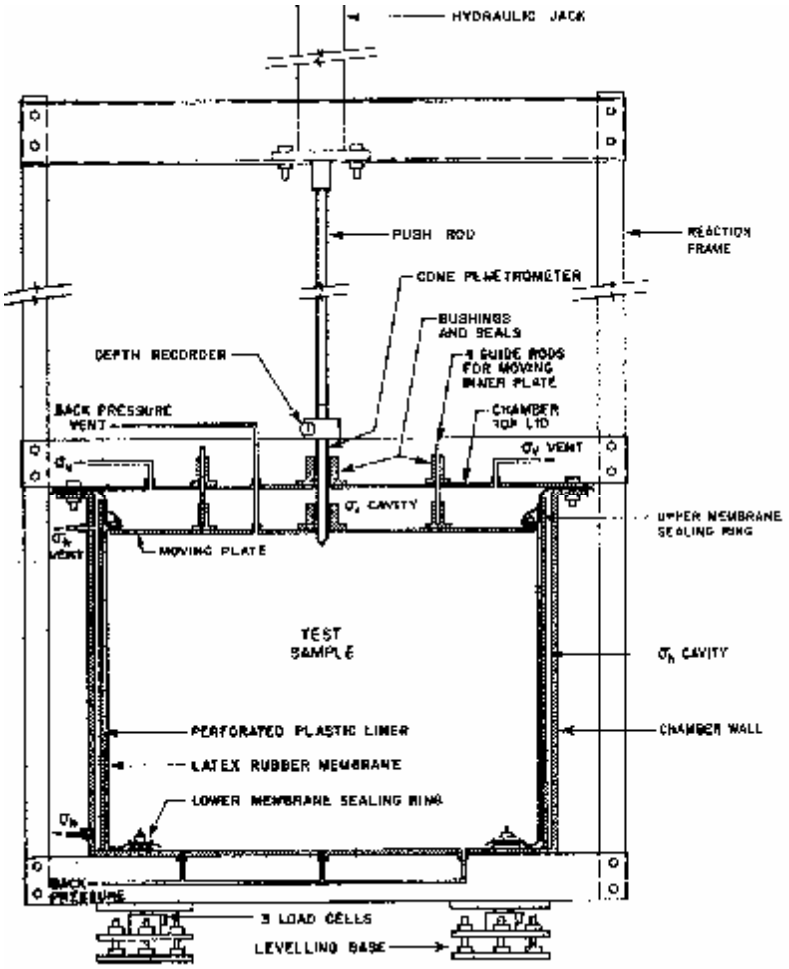


**Figure 2.12** Schematic of Golder Associates calibration chamber (after Been et al., 1987)

An important design feature of the Golden Associates chamber is its rigid base plate. This is in contrast to the flexible membrane-sand interfaces usually used in other chambers. A zero-strain base boundary is considered to be more representative of in-situ conditions, where sand displacement in front of the cone tip is restrained by underlying strata. Principal stress of up 1000 kPa are applied independently through a circumferential ( $s_h$ ) and upper ( $s_v$ ) cavity as shown in Figure 2.12. A back pressure can also be applied directly to the sand sample. A manually controlled system, fed by a pressurized air supply is used to impose a variety of stress conditions on the chamber sample using 130 L capacity air-over-water cells (one cell each for $s_v$, $s_h$ and back pressure). Constant stress is achieved by pressure regulators. In this

design, the horizontal stress is transmitted to the sample through a latex rubber membrane, as in triaxial testing, while the vertical stress is applied through a steel plate. A four-channel electric cone penetrometer, a standard 10 $cm^2$, 60°, and a right cylindrical cone were used.

The penetration resistance and state parameter relationship derived from the data obtained by a series of calibration chamber tests in Erksak sand confirmed the applicability of previously used corrections for Erksak sand. More importantly, strong confirmation of the use of the slope of the steady state line to characterize the material properties controlling penetration resistance in sands was provided. In order to determine the in-situ state of sands from penetration resistance measurements, Been et al. (1987) concluded that it is necessary to know the in-situ stress conditions and the steady state line.

***Virginia Polytechnic Institute (VPI) calibration chamber***

The calibration chamber at Virginia Polytechnic Institute was built by Sweeney and Clough (1990) as part of a project involving the evaluation of the liquefaction potential of soil deposits using a miniature cone penetrometer. The chamber was modeled after the original CRB chamber designed by Holden (1971), and is very similar to other chambers around the world. The Virginia Tech calibration chamber is a conceptually simple, low-cost chamber for calibration of cone penetrmeters and other in-situ tests. The chamber was designed to allow lateral and vertical pressures to be applied independently to the sand specimen. A schematic of the Virginia Tech calibration chamber is presented as Figure 2.13, with the major components outlined in the following section.

The Virginia Tech calibration chamber shell has an outside diameter of 1.6 m, a wall thickness of 29mm, and is 1.7 m in height. Flanges are located at both the top and bottom of the shell to allow the shell to be bolted to the lid and the chamber base plate. The chamber incorporates a number of concepts which are different from other chambers. These include a self-equilibrating structural design, automated specimen preparation and testing procedures, an innovative specimen forming jacket which is removed after the chamber is assembled, and the possibility for multiple penetrations with the in-situ testing probe. The chamber contains a large soil specimen with a

diameter and height of 1.5 m. This specimen size is one of the largest in the world at that time for a CC and it minimizes the effects of boundary constraints. The chamber permits testing under a range of vertical and lateral stress conditions.

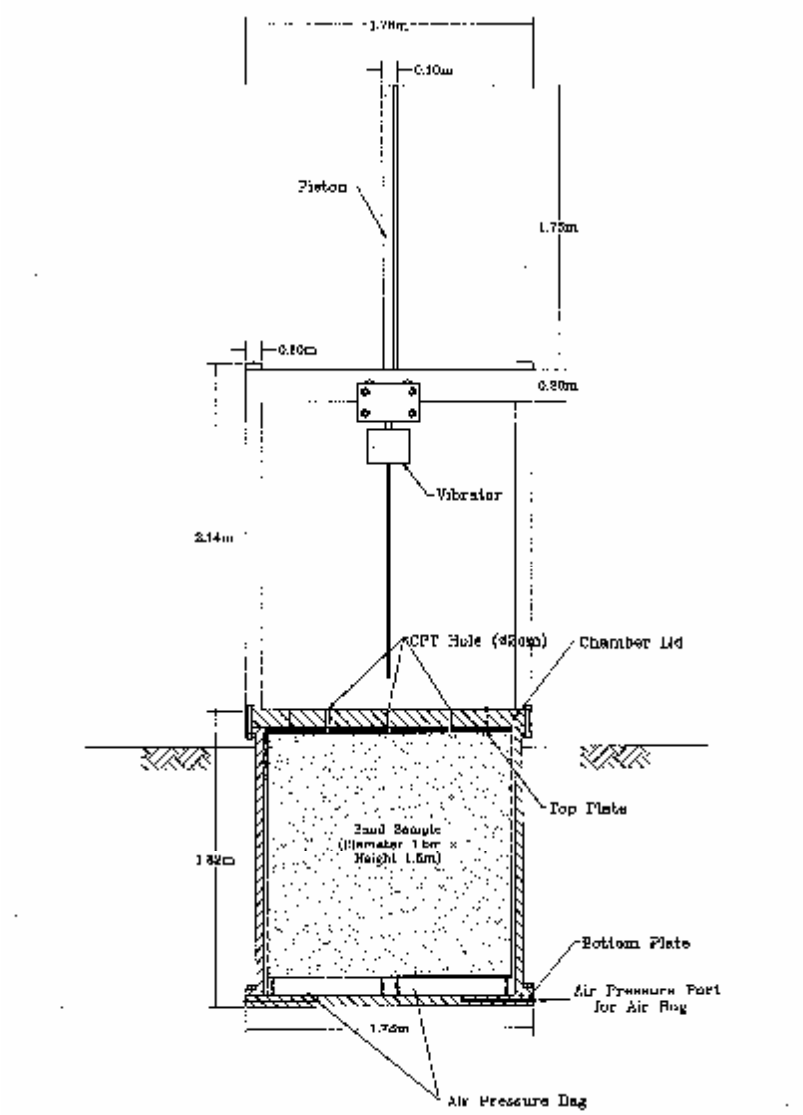


**Figure 2.13** Schematic of Virginia Tech Calibration Chamber (after Sweeney and Clough, 1990)

The vertical stress is applied to the soil sample through three airstroke actuators (Figure 2.14). These actuators are attached to the base plate of the chamber through a steel ring that contains an o-ring groove.

The sample is pluviated into the chamber using the pluviation apparatus. The sand is leveled and the final height of the sample is measured so that the arranged density of the soil could be calculated. The sample is then overlain by a 25mm thick by 1.5m diameter steel top plate. The membranes are wrapped over the top plate and a 12.7mm diameter rubber o-ring is placed above the membranes in a groove located near the perimeter of the top plate. The purpose of the o-ring is to provide a seal so that the air pressure applied to the lateral boundary of the sample does not infiltrate into the sample.

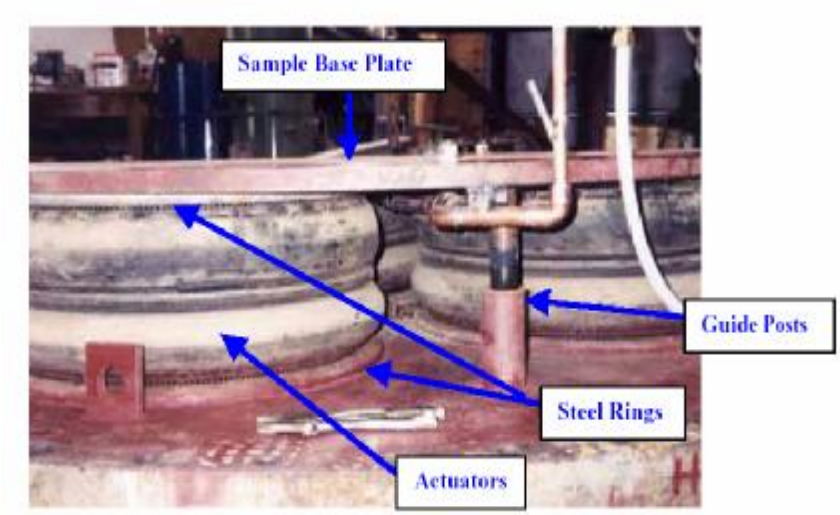


**Figure 2.14** Firestone airstroke actuators

The Virginia Tech calibration chamber testing program was successful in producing high quality data consistent with that obtained in other more sophisticated devices. The Virginia Tech CC test results from the chamber tests are plotted in Fig. 2.15 to allow a comparison to trends developed from CC tests performed by others. This figure presents correlations between tip resistance, relative density, and vertical effective stress as reported from CC tests with different sands by Schmertmann (1978), Villet and Mitchell (1981) and Balidi et al. (1982). Of the correlations shown, those of Villet and Mitchell are thought to be the most appropriate for comparison with the results of this testing program since they developed their relationship from experiments in Monterey No.0 sand, a very similar material to Monterey No. 0/30 sand. The other CC tests were conducted on more compressible sands than the Monterey materials. As can be seen in Figure 2.15, the measured $q_c$ values follow

the suggested trends. For the lower relative densities, the $q_c$ values from VPI tests are in close agreement with those from the Berkeley tests, while for the higher relative densities, the VPI $q_c$ values are about 50% above those from the Berkeley tests. This agreement of the findings is felt to support the approach taken in the VPI chamber design and testing.

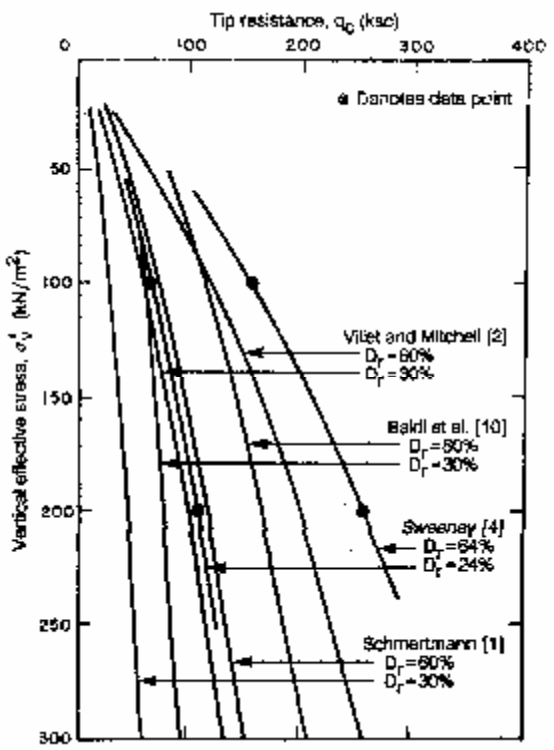


**Figure 2.15** Cone tip resistance as a function of relative density and vertical effective stress (Sweeney and Clough, 1990)

### 2.4.4 Limitations of conventional calibration chambers and new trend in the development of CC testing

***Limitations of conventional CC tests***

Been et al. (1987) and Ghionna and Jamiolkowski (1991) have critically reviewed the advantages and disadvantages of the calibration chamber approach. They have listed the following factors as very important when considering how applicable CC tests may be to the field condition:

1) Sample age
2) Types of sand tested
3) Chamber size and boundary effects

Among the three factors, the principal uncertainty that relates to the effect of sample size and boundary condition on the cone readings is generally considered the most significant.

Parkin and Lunne (1982) illustrated the influence of chamber size on cone resistance (Figure 2.16). Figure 2.16 shows the results of tests on Hokksund sand with the chamber diameter to cone diameter ratio between 21 and 50. Form these tests, it was concluded that for loose sand, chamber size and boundary conditions do not have a significant effect on the cone resistance. For dense sands on the other hand the effects are considerable.

Based on Figure 2.16, Lunne and Christophersen (1983) proposed that the CC results on Hokksund sand should be corrected to represent the field conditions. It was assumed that a chamber/diameter ratio $R_d$ of 50 is sufficient for eliminating the boundary effect.

Jamiolkowsli et al. (1985) adopted more or less the same approach and proposed the following formulation for both Ticino and Hokksund sand:

$$q_{c(\,field)} = q_{c(CC)}\left(\frac{1+0.2(D_r\,\%-30)}{60}\right) \tag{2.18}$$

This equation is valid for a $10\,\mathrm{cm}^2$ cone penetrometer in a 1.2 m diameter chamber.

Kulhawy and Mayne (1990) assumed that the size effect is no longer important when the value of chamber/cone diameter ratio $R_d$ reaches 70, regardless of the initial relative density and stress state.

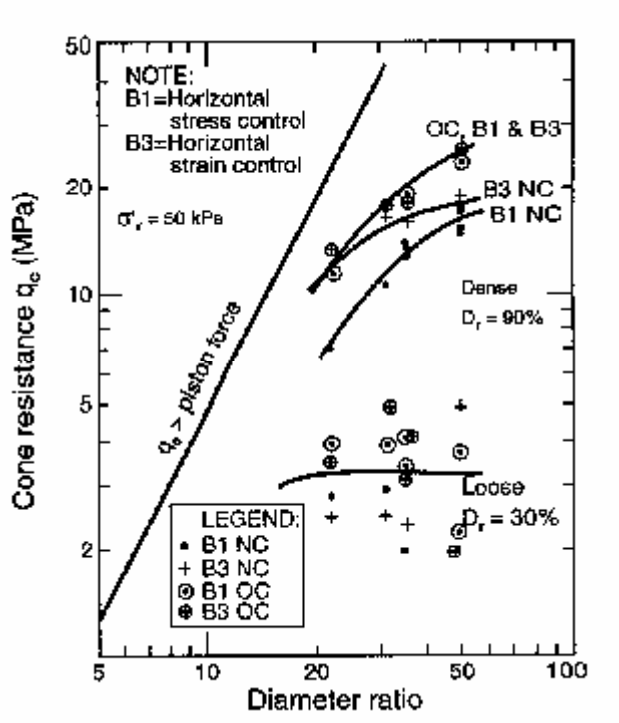


**Figure 2.16** Effect of chamber size on the CPT for Hokksund sand (after Parkin and Lunne, 1982)

Ghionna and Jamiolkowski (1992) showed that for relatively compressible sand, like the Toyura sand, chamber/cone diameter ratio and boundary conditions are very important, as illustrated in Figures 2.17 and 2.18.

Salgado et al. (1998) quantified the chamber size effect using penetration-resistance theory (Salgado et al. 1997). A parametric study using the theory shows how sand properties and the initial stress state affect the magnitude of the observed chamber size effect for BC1-BC4. The most important factors identified include the relative density $D_r$, the stress state, the intrinsic parameters $C_g$ and $e_g$ (Salgado et al., 1997 ) that describe the small-strain shear modulus $G_o$, and Bolton's $Q$ parameter (Bolton 1986). The size effect increase as $D_r$, $C_g$, $e_g$, and $Q$ increase and as the confining stress decreases. For existing calibration chambers and diameters of cones that have been used in research and practice, the diameter ratio lies in the range of approximately 25-120. Salgado et al. (1998) concluded that the ratio of chamber to field penetration resistance in this range will vary between approximately 0.5 and 0.9 for heavily dilatant samples of Ticino sand, a typical silica sand. For compressive

samples the ratio of chamber to field penetration resistance will lie in the range of 0.8-0.98 for values of the chamber/cone diameter ratio $R_d$ of between 25 and 120. Differences of these magnitudes indicate that CPT correlations developed by calibration chamber tests need to be corrected if they are intended for use in field applications.

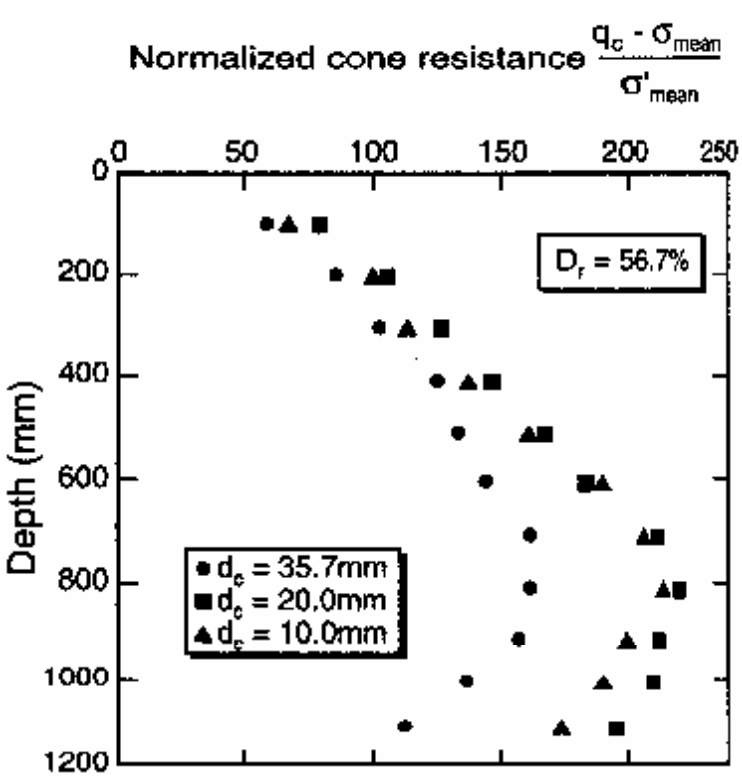


| Test no. | | 363 | 366 | 364 |
|---|---|---|---|---|
| BC | (-) | 1 | 1 | 1 |
| $D_r$ | (%) | 56.7 | 56.5 | 57.0 |
| $\sigma'_{vp}$ | (kPa) | 60.0 | 61.0 | 61.0 |
| $\sigma'_{hp}$ | (kPa) | 27.8 | 28.2 | 30.0 |
| OCR | (-) | 1 | 1 | 1 |
| $d_c$ | (mm) | 35.7 | 20.0 | 10.0 |

**Figure 2.17** Influence of cone size on cone resistance of Toyoura sand (after Ghionna and Jamiolkowski, 1992)

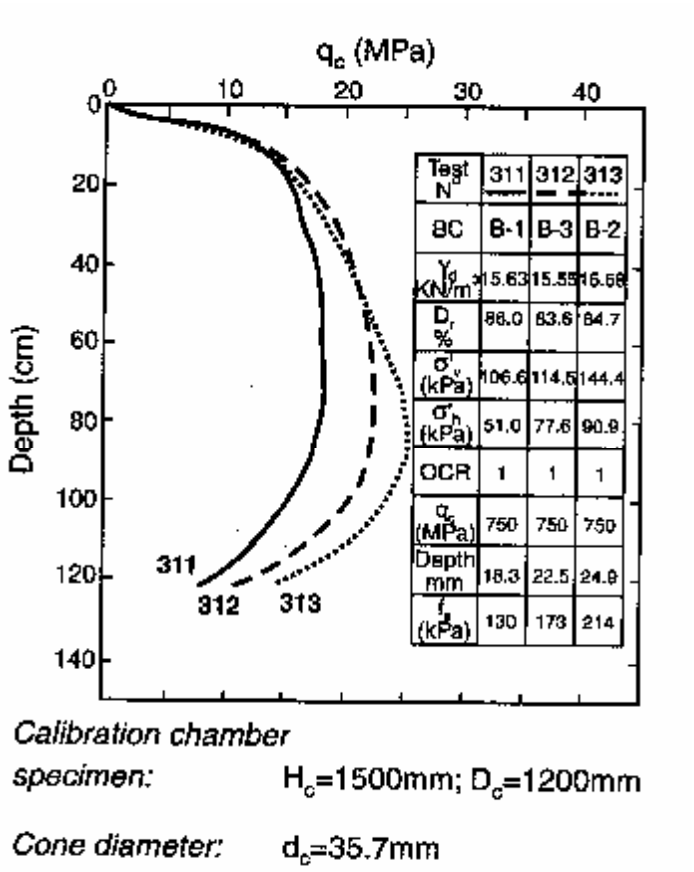


**Figure 2.18** Influence of boundary conditions on cone resistance of Toyoura sand (after Ghionna and Jamiolkowski, 1992)

In contrast to the common opinion that it is the constraint from the chamber walls that cause the normal $q_c$ to deviate from the field value, Wesley (2002) suggested that it may be the change in vertical stress arising from the downward force of the peneteometer that provides the best explanation for changes in cone resistance with chamber size. In field situation, the vertical stress above the cone remains essentially constant (equal to the overburden pressure), while that below the cone increases by an amount dependent on the cone force and the properties of the soil (Figure 2.19 (a)). In contrast, the vertical stress in the chamber is applied using a loading piston at the base of sample. The base boundary condition can be either constant pressure or zero volume change in the base piston compartment, as illustrated in Figure 2.19 (b).

The relationship between $s_v$, $s_b$, $q_c$ can be derived from the equilibrium equation of the soil sample in chamber as follows:

$$s_v = s_b - \frac{q_c}{(R_d)^2} \tag{2.19}$$

This means that during a test the stresses in front of the cone are limited by the applied pressure at the base or the rigidity of the base, and the vertical stresses above the cone is reduced (Figure2.19 (b)). This tends to lead a reduction in confinement around the cone penetrometer and therefore cause the $q_c$ value to decrease. It can be concluded that the average value of $s_v$ above the tip of the cone will always be less than the applied pressure at the base, by amount depending on $q_c$ and the chamber/cone diameter ratio $R_d$. This finding suggests that some change may be desirable in the way tests are carried out to prevent the change in vertical stress, and thus more closely replicate the stress situation in the field.

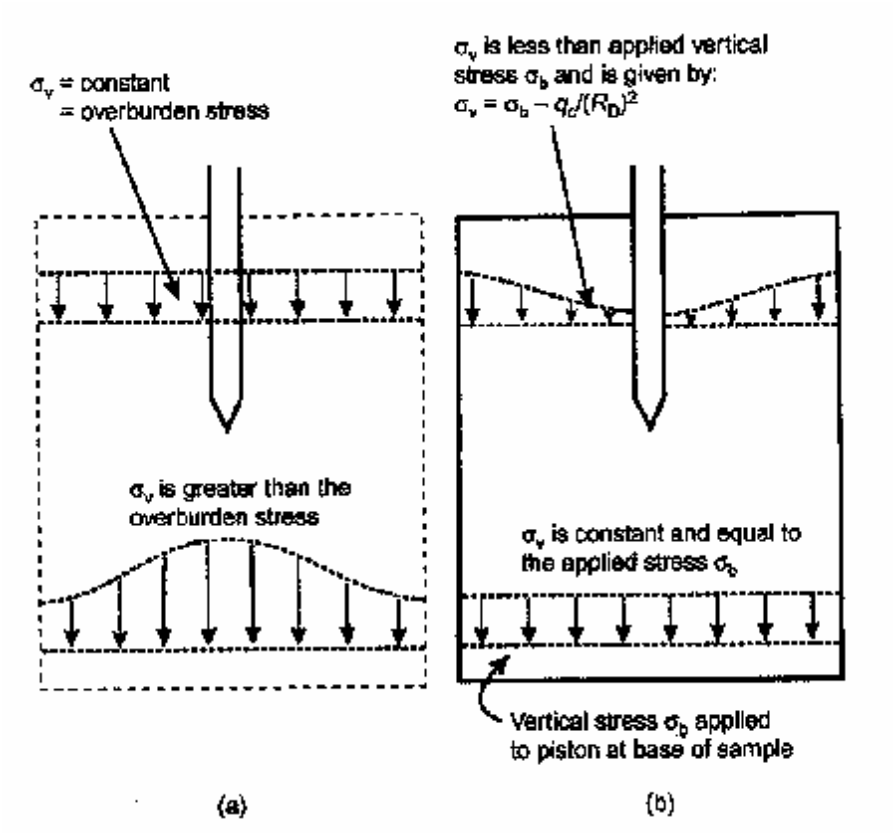


**Figure 2.19** Stress states in (a) field and (b) chamber (after from Been et al., 1988)

***New trend in calibration chamber design***

A field simulator developed by Hsu and Huang (1998) appears to be an ideal chamber that can practically eliminate the chamber lateral boundary effects.

Huang and Ma (1994) used the distinct element method (DEM) coupled with the boundary element method (BEM) to simulate CPT in a granular material with infinite boundary conditions. Results obtained by Huang and Ma (1994) have indicated the effectiveness of minimizing boundary effects by incorporating BEM simulations in the test. The success and experience gained in earlier attempts inspired the development of an axisymmetric field simulator in which CPT calibration tests could be conducted under substantially reduced boundary effects (Hsu and Huang, 1998).

The field simulator system developed at National Chiao-Tong University (NCTU), Taiwan, consists of a sand rainer, chamber rings, an electronic data logging and control unit, a pneumatic system, a reaction frame system, and a hydraulic system. Figure 2.20 shows a schematic diagram of the fully assembled calibration chamber system. The diameter and height of the sand specimen are 790 mm and 1600 mm, respectively. The lateral boundary of the field simulation consists of a stack of rings. This is the main difference between the conventional chambers and the new simulator. The simulator rings are lined with an inflatable silicone rubber membrane on the inside to facilitate boundary displacement measurement and stress control. The vertical stress is applied through four airstroke actuators attached to the reaction frame. Four air bellows inflated at constant pressure are placed at the bottom of the ring stack. This system, similar to the concept of a floating ring in an oedometer, reduces frictional forces between sand and rubber membranes.

A sand rainer similar to that described by Rad and Tumay (1987) is used to prepare the specimen. The specimen is prepared by pluviation from a hopper through a perforated plate and two diffuser meshes. The uniformity and density can be properly controlled by means of this arrangement and by controlling the diameter of the holes in the perforated plate. The lateral boundary is set to be rigid, simulating $K_0$ conditions, during sand pluviation.

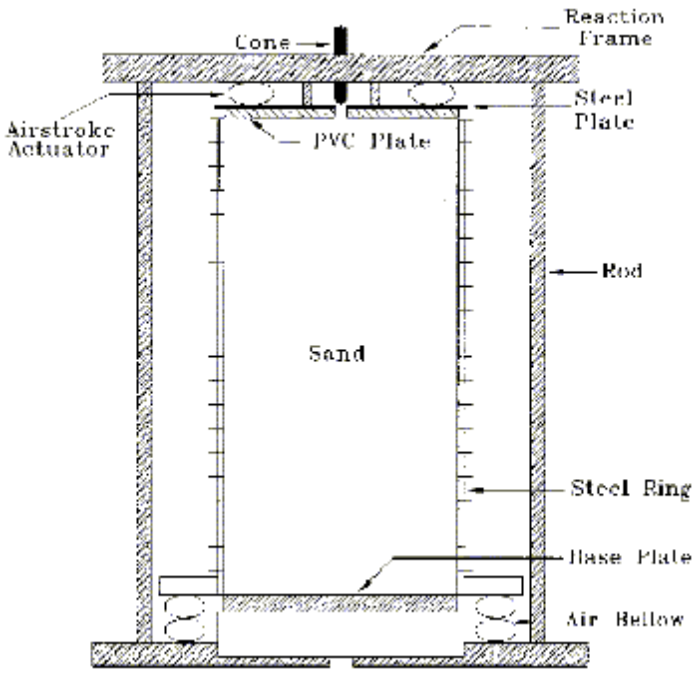


**Figure 2.20** Physical/numerical coupling of the simulator (after Hsu and Huang, 1998)

The membrane expansion measuring system consists of a wax lubricated, heavy duty fishing line wrapped around the membrane. The ends of the fishing line are attached to a piece of delrin chain and then to a spring loaded extensometer. The extensometer, instrumented with full bridged strain gauges, tightens the fishing line and senses the circumferential displacement of the rubber membrane. Figure 2.21 shows a schematic and cross sectional view of the simulator ring and its membrane.

The field simulation involves of a physical cylindrical specimen and a numerically simulated soil mass that extends laterally from the physical boundary to infinity. Numerical simulation of the soil mass is conducted based on the cylindrical cavity expansion theory. The stress-strain relationship of the sand specimen is directly measured by means of a lateral compression test on the specimen. The relationship between stress ( $p_{ro}$ ) and radial strain ( $e_{ro}$ ) at the physical-simulated interface is then derived by means of integration from the physical boundary to infinity, expressed as follows:

$$p_{ro} = p_0 + \int_0^{e_{ro}} \frac{f(e_r)}{2e_r} de_r \qquad (2.20)$$

where $f(e_r)$ is the stress strain relationship measured by means of a lateral compression test on the sand specimen and $e_r$ is the strain in the radial direction.

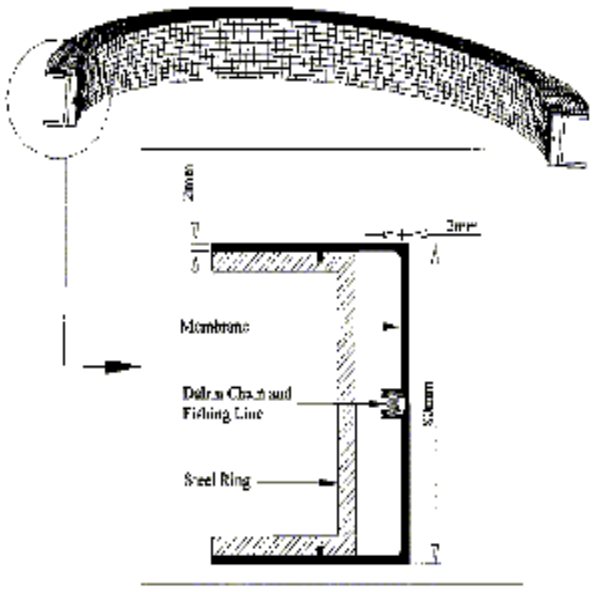


**Figure 2.21** Cross-sectional view of a simulator ring (after Hsu and Huang, 1998)

During cone penetration, the boundary displacements and stresses are measured and individually controlled at each ring level. The circumferential displacement at the boundary of each ring level, $\Delta C$, is converted to $e_{ro}$

$$e_{ro} = \frac{\Delta C}{pD}$$

where $D$ is the diameter of the physical specimen.

The value $p_{ro}$ in response to $e_{ro}$ under simulated field conditions is determined in accordance with the pre-recorded $p_{ro} - e_{ro}$ relationship. Figure 2.22 shows the $f(e_r)$ value obtained from the lateral compression test and the corresponding $p_{ro} - e_{ro}$ curve. During penetration, $p_{ro}$ for each ring level is adjusted pneumatically and continuously updated with the measured value of $\Delta C$

A hydraulic piston equipped with a proportional valve, capable of accurate speed control, is used for the advancement of the cone penetrometer. The cone penetration rate is set at a constant value of 2.0 mm/second. The slow penetration rate is necessary to allow the reaction of lateral air pressure to reach an equilibrium condition in all the stress control units.

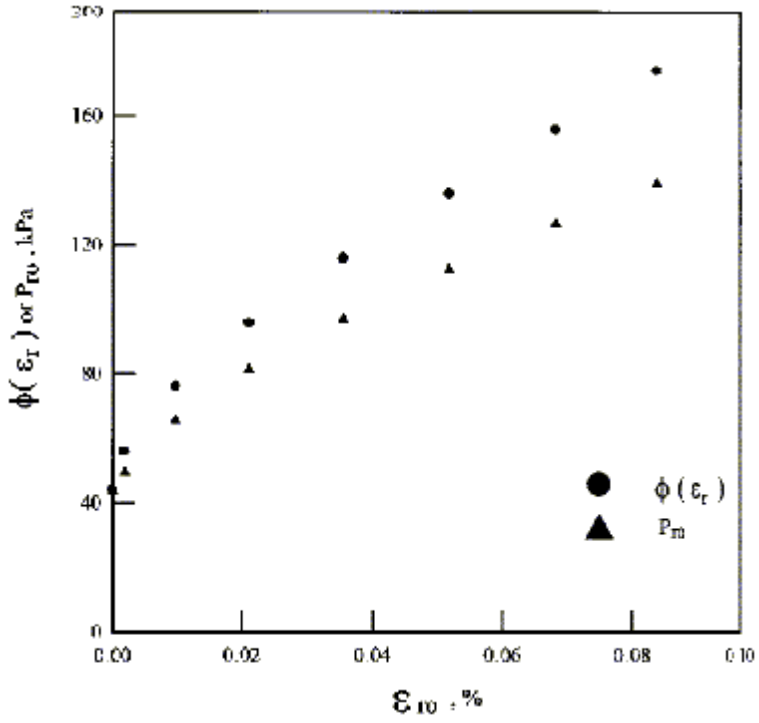


**Figure 2.22** $f(e_r)$ obtained from the lateral compression test (after Hsu and Huang, 1998)

A series of cone penetration tests was performed in Da Nang sand, a clean uniformly graded quartz sand from Vietnam, using the simulator. Figure 2.23 shows the $q_c$ profiles under the simulated field condition, where $s'_{vo}$ =43.7 kPa and $s'_{ho}$=22 kPa, with chamber-cone diameter ratio $R_d$ values of 18 and 22 and $D_r$ values of 65% and 84%. The average of the $q_c$ values at depths from 600 to 1200 mm was taken as the representative value. Results show that $q_c$ at two $R_d$ values agree within 6.9% for $D_r$ of 65% and within 0.1% for $D_r$ of 84% sand. The similarity of $q_c$ under two different $R_d$ values indicates that the boundary effects were substantially reduced with the use of the field simulation.

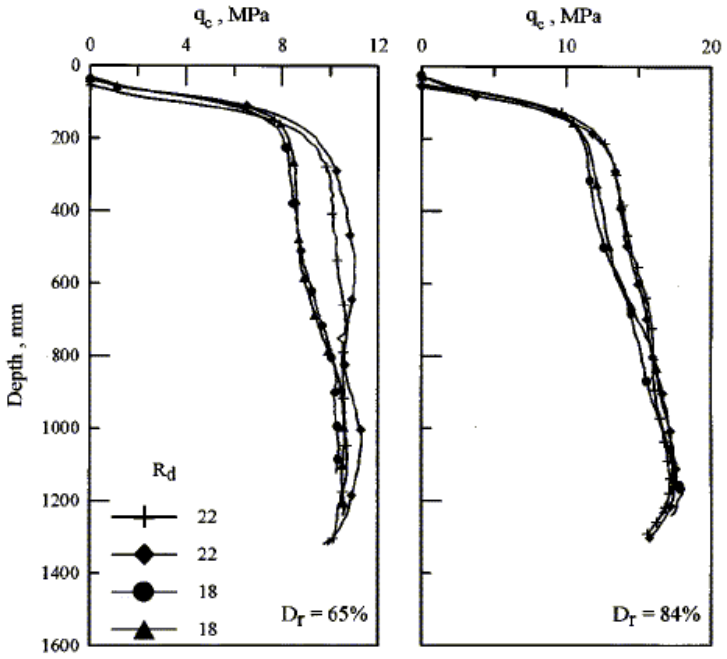


**Figure 2.23** $q_c$ profiles under simulated field condition (after Hsu and Huang, 1998)

Available CPT tests in the simulator have indicated that the simulator is capable of duplicating field conditions where the lateral boundary extends to infinity. Because of the capability of physically reducing the boundary effects to a minimal, it would seem unnecessary to use a correction factor for CPT calibration tests in the future. However, the limitation of this simulator is that its construction is too sophisticated to be suitable for normal engineering applications. Another potentially practical way of reducing and minimizing the boundary effects that one may consider is to use a rigid wall chamber that incorporates an elastic and compressible layer as a buffer between the sand mass and the rigid boundary (Chang and Cao, 2001). The design of such a new chamber will be described in a later chapter.

# CHAPTER 3 CAVITY EXPANSION ANALYSIS IN INFINITE SAND MASS

## 3.1 Introduction

It is commonly understood that the advancement of penetrometer in soil can be modeled as an expansion of cavity expansion in an elastic-plastic medium. Prior to the investigation of soil response to penetration in a semi-confined or restrained space, as in a calibration chamber, one needs to be able to analyze the distribution of stresses and associated strains around an expanding cavity in a semi-infinite half space.

The problem of expansion of spherical or cylindrical cavities in an infinite medium has been dealt with by many investigators in the last 50 years, in connection with its potential application to a number of practical problems in both mechanical and civil engineering. Its theoretical appeal has always been the simplicity of its geometry, which has made it possible to obtain relatively simple closed-form solutions in different materials. Most of these solutions follow the conventional applied mechanics approach: after satisfying the compatibility and equilibrium relations, and introducing a simplified form of describing the stress–strain and strength characteristics of the material, the state of stress and strain in the medium around the cavity are determined by solving the equations. In the case of soils, the usual assumptions on the material behavior include the validity of a linear Mohr-Coulomb strength envelope and a simplified form of stress–strain response, with some allowance for variation in the accompanied volumetric strain (e. g., Gibson and Anderson, 1961; Vesic, 1972; Ladanyi et al., 1974; Carter and Yeung, 1985; Carter et al., 1986; Collins et al., 1992).

In the subsequent section of this chapter, new solutions for the stress, strain and displacement distribution of expansion of cylindrical cavities in sands are proposed.

## 3.2 Cavity expansion analysis in infinite sand mass

Cavity expansion theory consists of determining the cavity pressure required for the expansion a cavity in a material medium by a certain radial distance. The cavity pressure in a cavity created in the soil is equal to the limit or steady-state cavity pressure when the cavity radius approaches infinity. In this cavity expansion analysis, the sand is assumed to be homogeneous and subjected to an initial stress $p_0$ throughout the whole body of sand. Using a cylindrical polar coordinate system, the initial position of a soil element around a cylindrical cavity can be described as $(r_0, q, z)$. A plane strain condition is assumed for the cylindrical cavity. The cavity with an initial radius $a_0$ is assumed to expand under a uniformly distributed internal pressure and the cavity radius increases to $a$ as the internal cavity pressure increase from $p_0$ to $p$. An element initially located at the radial position $r_0$ from the centre of the cavity will move to a new position $r$ with the expansion of the cavity. The corresponding displacement of the element is $u = r - r_0$. A region of sand around the cavity will deform plastically if the internal pressure in the cavity exceeds the yield pressure described by Mohr-Coulomb criterion. The sand will remain in a state of elastic equilibrium outside the plastic region. The radius of the elastic-plastic interface can be denoted as $b$, as illustrated schematically in Figure 3.1.

### 3.2.1 Elastic response

The stress-strain response of the sand is assumed to follow a nonlinear relationship until the onset of yielding. The shear stress, shear strain and volumetric strain of sand can be expressed respectively as follows (Teh et. al., 2001):

$$t = \frac{s_r - s_q}{2} \tag{3.1}$$

$$g = e_r - e_q \tag{3.2}$$

$$e_v = e_r + e_q \tag{3.3}$$

where $s_r$ and $s_q$, $e_r$ and $e_q$ are the radial stress and circumferential stress, radial strain and circumferential strain, respectively. In the analysis the convention is

adopted that compressive stresses and strains are positive, as is usually done in soil mechanics.

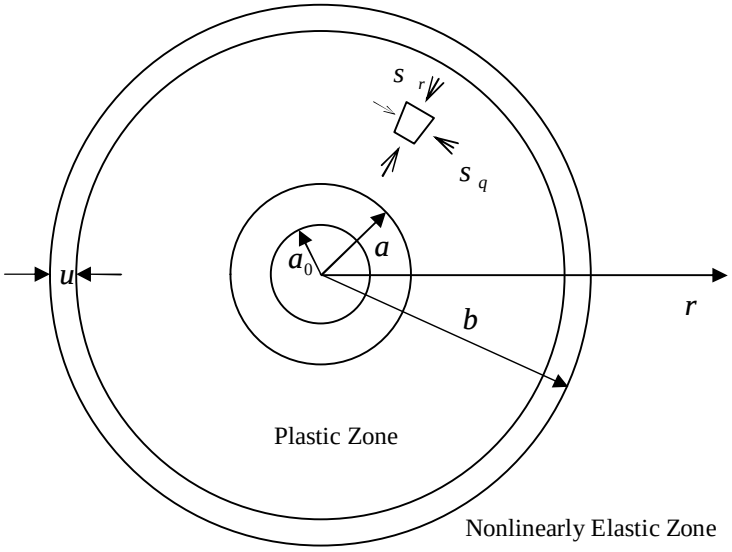


**Figure 3.1** Expansion of a cavity

The sand stress-strain behavior is nonlinear except for very small strain. The change in stiffness with strain can be represented by a power-law function. The power law function relationship of shear stress with strain is shown in Figure 3.2 and can be expressed as

$$t = a g^{b} \tag{3.4}$$

where $a$ and $b$ are the stiffness constant and elastic exponent ( $0 < b \leq 1$ ), respectively. The two parameters $a$ and $b$ can be determined from the stress-strain curve, plotted in log scales,

The secant shear modulus $G_s$ is given by

$$G_s = a g^{b-1} = a^{1/b} t^{(b-1)/b} \tag{3.5}$$

Note that when $b = 1$, the parameter $a$ is equal to the shear modulus of a linear elastic material.

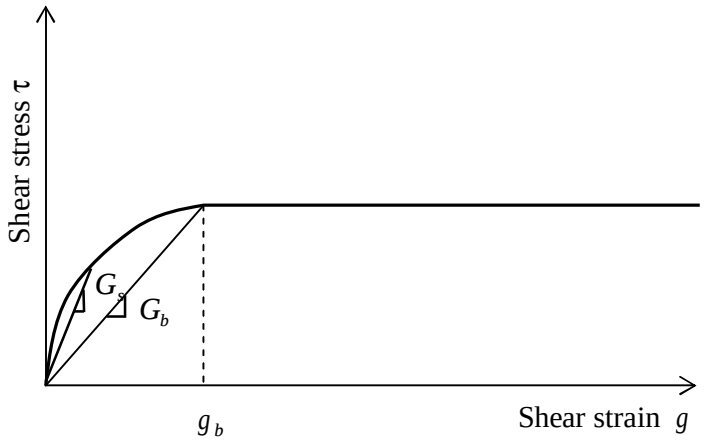


**Figure 3.2** Shear stress vs shear strain for ideal nonlinear elastic/perfectly plastic soil

### 3.2.2 Plastic response

After the initial yielding at the cavity wall, the position of the sand extending from the cavity wall to the radial distance $b$ (elastic-plastic boundary) will be in plastic state as the cavity pressure continues to increase. Yielding of the sand is described by the Mohr-Coulomb yield criterion given by:

$$s_r - s_q = (s_r + s_q)\sin f \tag{3.6}$$

in which $f$ is the internal friction angle of the sand.

From Equations (3.1), (3.4) and (3.5) the secant shear modulus at the onset of yielding based on the power-law function can be expressed as:

$$G_b = a^{\frac{1}{b}} \left(\frac{s_{rb} - s_{qb}}{2}\right)^{\frac{b-1}{b}} \tag{3.7}$$

Note that $s_{rb}$ and $s_{qb}$ are the radial stress and circumferential stress at elastic-plastic boundary. Equation (3.7) indicates that $G_b$ is depended on the nonlinear parameters $a$ and $b$, and the shear stress $t$ at yield condition.

Considering an element at a radical distance $r$ from the centre of cavity subjected to a radical stress $s_r$ and a circumferential stress $s_q$, the differential equation of equilibrium can be expressed as:

$$\frac{ds_r}{dr} + \frac{s_r - s_q}{r} = 0 \tag{3.8}$$

If the volume change of sand is assumed to be zero in the elastic region (Hsu and Huang, 1998), the radical displacement can be related to the cavity expansion as:

$$r^2 - r_0^2 = a^2 - a_0^2 \tag{3.9}$$

The radical displacement increment can be expressed by the differential in radius:

$$du = dr = (\frac{a}{r})da \tag{3.10}$$

The radical and the circumferential strain increments can then be expressed as:

$$de_r = -\frac{d(du)}{dr} = (\frac{a}{r^2})da = \frac{dr}{r} \tag{3.11}$$

$$de_q = -\frac{da}{r} = -(\frac{a}{r^2})da = -\frac{dr}{r} \tag{3.12}$$

From Equations (3.2), (3.11) and (3.12), the shear strain increment is:

$$dg = de_r - de_q = (\frac{2a}{r^2})da = \frac{2dr}{r} \tag{3.13}$$

For a soil element initially at $r_0$, Equation (3.13) can be integrated to give the finite logarithmic shear strain:

$$g = 2\ln(\frac{r}{r_0}) \tag{3.14}$$

By combining Equations (3.9) and (3.14), the relationship for condition associated with the particle originally at $r_0$ can be rewritten in terms of $r$, and $r_0$ is eliminated.

The distribution of shear strain around the cavity of radius $a$ can be obtained as follows:

$$g = 2\ln(\frac{r}{r_0}) = -\ln(\frac{r_0}{r})^2 = -\ln(1-\frac{a^2-a_0^2}{r^2}) \tag{3.15}$$

Equation (3.8) can be expressed in terms of the relationship between the stress and the shear strain by using Equations (3.1) and (3.15) as follows

$$\frac{ds_r}{dr}+\frac{s_r-s_q}{r}=\frac{ds_r}{dg}\frac{dg}{dr}+\frac{2t}{r}=\frac{ds_r}{dg}-\frac{t}{\exp(g)-1}=0 \tag{3.16}$$

the following two boundary conditions exist :

$$s_r = p \quad \text{when} \quad r=a \quad \text{or} \quad g_a = 2\ln(a/a_0) \tag{3.17}$$

$$s_r = p_0 \quad \text{when} \quad r\to\infty \quad \text{or} \quad g=0 \tag{3.18}$$

## 3.3 Elastic analysis

As the internal pressure in the cavity increase from initial pressure $p_0$, the deformation of the sand around the cavity is at first in the elastic state. Only when the cavity radius approaches infinity does the cavity pressure reach a limit or steady-state pressure. The sand body outside the plastic zone ($r > b$) is governed by nonlinear elasticity. In the subsequent analysis, the elastic stress-strain relationship in the derivation for the cavity expansion process is described by a power-law function.

Integrating equation (3.16) from$g=0$, which corresponds to $r\to\infty$, the following is obtained:

$$s_r = a\int \frac{g^b}{\exp(g)-1}dg + p_0 \tag{3.19}$$

Equation (3.19) is equally applicable to large strain problem because there is no assumption made regarding strain in the analysis. Definitely, no closed-form solution to Equation (3.19) can be obtained and only an approximate solution is possible.

### 3.3.1 Approximate large strain solution

In order to integrate Equation (3.19) for the solution of large strain problems, an approximate solution may be introduced by expressing:

$$\exp(g) = 1 + g + \frac{1}{2!}g^2 + \mathbf{L} + \frac{1}{n!}g^n + \mathbf{L} \tag{3.20}$$

By ignoring terms of $g$ of the third power and higher oders, the solution of Equation (3.19) may be approximated as:

$$s_r = \frac{ag^b}{b(1+0.5g)}(1+G) + p_0 \tag{3.21}$$

in which the $\Gamma = \frac{g}{2(1+b)(1+0.5g)} + \frac{g^2}{2(1+b)(2+b)(1+0.5g)^2}$

and $g$ is related to the cavity radius $r$ by using Equation (3.15).

The circumferential stress also can be derived from Equation (3.4) and Equation (3.21) as:

$$s_q = \frac{ag^b}{b(1+0.5g)}(1+G) - 2ag^b + p_0 \tag{3.22}$$

### 3.3.2 Small strain solution

In small strain conditions, the terms involving the shear strains of power of two and above are very small. It is possible to ignore terms of $g$ of order two and above, the radial stress $s_r$ and circumferential stress $s_q$ can be expressed as:

$$s_r = \frac{ag^b}{b} + p_0 \tag{3.23}$$

$$s_q = \frac{ag^b}{b} - 2ag^b + p_0 \tag{3.24}$$

It is useful to compare the large and small strain solutions in the nonlinear elastic region. The cavity pressure is normalized by the stiffness constant $a$ and elastic exponent $b$. Cao et al. (2002) suggested that it is difficult to differentiate the small strain solution from the large strain solution even at very large elastic strain levels (shear strain > 1%) for both nonlinear elasticity and linear elasticity. Because of this reason, the use of large strain solution is not strictly necessary in the analysis of elastic cavity expansion problems. The small strain solution is adopted for the nonlinear elastic region in the subsequent analysis.

## 3.4 Plastic analysis

### 3.4.1 Stress and strain at the elastic-plastic boundary

Based on the definition of $t$ in Equation (3.1) and the power-law in Equation (3.4), the radial stress $s_{rb}$ and circumferential stress $s_{qb}$ at the elastic-plastic boundary can be expressed using the small strain solutions in Equations (3.23) and (3.24) as:

$$s_{rb} = \frac{s_{rb} - s_{qb}}{2b} + p_0 \tag{3.25}$$

$$s_{qb} = \frac{s_{rb} - s_{qb}}{2b} - (s_{rb} - s_{qb}) + p_0 \tag{3.26}$$

From Equation (3.1), the shear strain $g_b$ at the elastic-plastic boundary $(r = b)$ can be related to the shear stress $t_b$ and the secant shear modulus at the onset of yielding $G_b$, as defined in Equation (3.7), and expressed as:

$$g_b = \frac{s_{rb} - s_{qb}}{2G_b} \tag{3.27}$$

Based on the selected yielding criterion in Equation (3.6), the relationship between the radical and circumferential stresses in the elastic-plastic boundary is given by:

$$s_{rb} - s_{qb} = (s_{rb} + s_{qb})\sin f \tag{3.28}$$

Combining Equations (3.25), (3.26) and (3.28), the resulting equation is as follows:

$$s_{rb} + s_{qb} = \frac{2p_0}{(1+\sin f - \frac{\sin f}{b})} \tag{3.29}$$

Substituting Equations (3.7), (3.27) and (3.29) into Equation (3.27), the shear strain in the elastic-plastic boundary can be expressed as:

$$g_b = \left\{ \frac{p_0 b \sin f}{a[(1+\sin f)b - \sin f]} \right\}^{1/b} \tag{3.30}$$

The radius of elastic-plastic boundary can be obtained from Equation (3.15) and expressed as:

$$b^2 = \frac{a^2 - a_0^2}{1 - \exp(-g_b)} \tag{3.31}$$

Substituting Equation (3.30) in to Equation (3.31), the radius of the elastic-plastic boundary is:

$$b^2 = \frac{a^2 - a_0^2}{1 - \exp\left\{ - \left\{ \frac{p_0 b \sin f}{a[(1+\sin f)b - \sin f]} \right\}^{1/b} \right\}} \tag{3.32}$$

### 3.4.2 Elastic-plastic stress analysis

After initial yielding at the cavity wall, a plastic region will form within the range as described by $a < r < b$ around the inner wall of the cavity with the increase of the cavity pressure $p$.

***<u>The plastic region</u>*** ***($a < r < b$)***

The stress components which satisfy the equilibrium Equation (3.8) and yield condition in Equation (3.6) can be obtained, through integration, as follows:

$$s_r = Ar^{(-\frac{2\sin f}{1+\sin f})} \qquad (\frac{ds_r}{dr} + \frac{\frac{2\sin f}{1+\sin f}s_r}{r} = 0) \tag{3.33}$$

$$s_q = \frac{1-\sin f}{1+\sin f} Ar^{(-\frac{2\sin f}{1+\sin f})} \tag{3.34}$$

where $A$ is a constant of integration.

Considering the boundary conditions at the elastic-plastic boundary, $s_{rb}$ (elastic) = $s_{rb}$ (plastic) and $s_{qb}$ (elastic) = $s_{qb}$ (plastic), and using the small strain solutions in Equations (3.23) and (3.24), the stress distribution in elastic-plastic boundary can be written as:

$$s_{rb} = \frac{ag_b^{\ b}}{b} + p_0 \tag{3.35}$$

$$s_{qb} = \frac{ag_b^{\ b}}{b} - 2ag_b^{\ b} + p_0 \tag{3.36}$$

and the constant $A$ in Equations (3.33) and (3.34) can be calculated as follows:

$$A = (ag_b^{\ b}/b + p_0)/b^{\frac{-2\sin f}{1+\sin f}} \tag{3.37}$$

or

$$A = [(1/b - 2)ag_b^{\ b} + p_0]\cdot(1+\sin f)/[(1-\sin f)b^{\frac{-2\sin f}{1+\sin f}}] \tag{3.38}$$

Substituting Equation (3.30) into Equations (3.37) and (3.38), the different expression of constant $A$ in Equations (3.37) and (3.38) can be expressed in the same formulation as follows:

$$A = [\frac{p_0(1+\sin f)b}{(1+\sin f)b - \sin f}]/b^{\frac{-2\sin f}{1+\sin f}} \tag{3.39}$$

Combining Equation (3.15) and Equation (3.32), the shear strain $g$ can be related to the radius $r$ and expressed as:

$$g = -\ln\left[1-[1-\exp(-g_b)]\left(\frac{b}{r}\right)^2\right] \tag{3.40}$$

***The elastic region*** *(* $r \geq b$ *)*

Substituting Equation (3.40) into Equations (3.23) and (3.24), the stress components in the elastic zone may be expressed as follows:

$$s_r = \frac{a\left\{-\ln\left[1-[1-\exp(-g_b)]\left(\frac{b}{r}\right)^2\right]\right\}^b}{b} + p_0 \tag{3.41}$$

$$s_q = (1/b-2)a\left\{-\ln\left[1-[1-\exp(-g_b)]\left(\frac{b}{r}\right)^2\right]\right\}^b + p_0 \tag{3.42}$$

Note that $g_b$ is defined in Equation (3.30). The stresses are defined in terms of material properties, initial stress state, nonlinear parameters, radial coordinates and the radius of the elastic-plastic boundary $b$ . Because the value of $b$ is generally unknown, results obtained from Equations (3.41) and (3.42) can not be used to calculate the distribution of stress until the displacement field is known.

## 3.5 Elastic-plastic displacement analysis

During the cylindrical cavity expansion, the radial displacement $u$ in the soil, is expressed as the difference between the initial position of a generic material point $r_0$ and its position at the deformed state $r$ . That is:

$$u = r - r_0 \tag{3.43}$$

The strains in an elastic medium, based on the small strain theory, for the initial phase of elastic loading are:

$$e_r = -\frac{du}{dr} \tag{3.44}$$

$$e_q = -\frac{u}{r} \tag{3.45}$$

It is assumed earlier that the volume change of sand in the elastic region can be taken as zero. The relationship between radial strain $e_r$ and circumferential strain $e_q$ can be described as follows:

$$e_v = e_r + e_q = 0, e_r = -e_q \tag{3.46}$$

The elastic stress-strain relationship defined by power-law function relationship can be shown as follows by Combining Equations (3.44), (3.1), (3.2) and (3.4),

$$e_r^e = \frac{1}{2}\left(\frac{s_r - s_q}{2a}\right)^{1/b} \tag{3.47}$$

$$e_q^e = -\frac{1}{2}\left(\frac{s_r - s_q}{2a}\right)^{1/b} \tag{3.48}$$

where superscript $e$ denote the elastic components of the total strain.

On substituting Equations (3.41) and (3.42) into Equation (3.48), the displacement in the elastic region ( $r > b$ ) can be shown to be

$$u = -\frac{1}{2}\ln\left[1-[1-\exp(-g_b)]\left(\frac{b}{r}\right)^2\right]r \tag{3.49}$$

It is also possible to express the relationship between the position of the elastic-plastic boundary $b$ and the cavity radius $a$ during the plastic phase. Acknowledging that the cavity pressure is $p$ when the radius of cavity reaches $a$, it is possible to define the expression of $b/a$ in terms of the current cavity pressure $p$ and initial cavity pressure $p_o$, by Combining Equations (3.17) and (3.33), as follows:

$$\frac{b}{a} = \left\{\left[1-\frac{\sin f}{(1+\sin f)b}\right]\frac{p}{p_0}\right\}^{\frac{1+\sin f}{2\sin f}} \tag{3.50}$$

where $\left[1-\frac{\sin f}{(1+\sin f)b}\right]\frac{p}{p_0}$ is denoted as $R$.

Considering compression stresses as positive and accounting for effects of large strains, the principal strains may be defined in Eulerian coordinate.

The radial strain is denoted as:

$$e_r = -\ln\left(\frac{dr}{dr_0}\right) \tag{3.51}$$

The circumferential strain is denoted as:

$$e_q = -\ln\left(\frac{r}{r_0}\right) \tag{3.52}$$

The stress-dilatancy theory can be used to describe the relationship between the friction angle and dilation angle. The basic features associated with stress-dilation behaviour have been established following the pioneering work of Taylor (1948), Rowe (1962) and Bolton (1986). Rowe (1962) proposed that there was an analogy between irregular packing of soil particles and regular assemblies of spheres. Bolton (1986) drew the same conclusion after investigating of a large database from triaxial and plane strain tests. The concepts introduced by Rowe were applied by Hughes et al. (1977) to relate the total various train increments. Later, Houlsby et al. (1988), Yu and Houlsby (1991) defined the flow rule in terms of plastic strain components in cylindrical cavity expansion formulations.

The determination of the displacement in the plastic region requires the use of a plastic flow rule which describes the relative magnitude of plastic strain increments in different directions. It is assumed that while yield is occurring, the total strain increment is decomposed into additive elastic and plastic components. Following Davis (1969), the soil is assumed to dilate plastically at a constant rate during the plastic flow. This non-associated flow rule with Mohr-Coulomb yield criterion is well established for modeling dilatant soil behavior.

The plastic flow rule can be written as follows:

$$\frac{d\varepsilon_r^p}{d\varepsilon_q^p} = -\frac{1-\sin y}{1+\sin y} = -\frac{1}{h} \tag{3.53}$$

where $d\varepsilon_r^p$ and $d\varepsilon_r^p$ are the plastic components of the radial and circumferential strain increments, $y$ is the dilation angle of sand and $\frac{1+\sin y}{1-\sin y}$ is denoted as $h$.

A mathematical simplification is assumed in this approach by ignoring the contribution of elastic strains within the plastically deforming region.

In order to express the pressure-expansion relationship during the plastic phase of the expansion, it is necessary to incorporate the displacement field of the plastic region around the cavity as follows (Yu et al., 1991):

$$hd\varepsilon_r + d\varepsilon_q = hd\varepsilon_r^e + d\varepsilon_q^e + hd\varepsilon_r^p + d\varepsilon_q^p = hd\varepsilon_r^e + d\varepsilon_q^e \tag{3.54}$$

For a cavity from initial condition to current condition Substituting Equations (3.47) and (3.48) into Equation (3.54) results in:

$$hd\varepsilon_r + d\varepsilon_q = \frac{1}{2b}(h-1)\left(\frac{s_r - s_q}{2a}\right)^{\frac{1}{b}-1}\left(\frac{ds_r - ds_q}{2a}\right) \tag{3.55}$$

For a cavity increment increasing from $p_0$ to $p$, The above expression can be lead to

$$he_r + e_q = \frac{1}{2b}(h-1)\left(\frac{s_r - s_q}{2a}\right)^{\frac{1}{b}} \tag{3.56}$$

Substituting Equations (3.51), (3.52), (3.33), (3.34) and (3.39) into Equation (3.56) leads to:

$$\ln\left[\left(\frac{r}{r_0}\right)^{1/h}\cdot\frac{dr}{dr_0}\right] = \frac{1}{2b}\left(1-\frac{1}{h}\right)\left[\frac{p_0 b\sin f}{a[(1+\sin f)b-\sin f]}\right]^{1/b}\left(\frac{b}{r}\right)^{\frac{2\sin f}{b(1+\sin f)}} \tag{3.57}$$

Denote

$$k = \frac{1}{2b}\left(1-\frac{1}{h}\right)\left[\frac{p_0 b\sin f}{a((1+\sin f)b-\sin f)}\right]^{1/b} \tag{3.58}$$

Equations (3.57) can be rewritten as

$$\left(\frac{r_0}{r}\right)^{1/h} \cdot \frac{dr_0}{dr} = \exp\left[k\left(\frac{b}{r}\right)^{\frac{2\sin f}{b(1+\sin f)}}\right] \tag{3.59}$$

Let

$$r = \left(\frac{b}{r}\right)^{\frac{2\sin f}{b(1+\sin f)}} \tag{3.60}$$

Equation (3.59) becomes:

$$\frac{-2\sin f}{b(1+\sin f)}\left(\frac{r_0}{b}\right)^{\frac{1}{h}} d\left(\frac{r_0}{b}\right) = \exp(kr)\, r^{-\frac{b(1+\sin f)(1+h)}{2h\sin f}-1} dr \tag{3.61}$$

Using Equation (3.49) to obtain the displacement at the elastic-plastic boundary, Equation (3.61) can be integrated over the interval $[b, r]$ and the resulting equation is:

$$\frac{2h\sin f}{b(1+\sin f)(1+h)}\left\{\left[1-\frac{1}{2}g_b\right]^{\frac{1}{h}+1} - \left(\frac{r_0}{b}\right)^{\frac{1}{h}+1}\right\}$$

$$= \int_1^{(b/r)^{\frac{2\sin f}{b(1+\sin f)}}} \exp(kr)\, r^{-\frac{b(1+\sin f)(1+h)}{2h\sin f}-1} dr \tag{3.62}$$

Assuming $r_0 = a_0$, $r = a$ and making use of Equation (3.50), Equation (3.62) becomes:

$$\frac{2h\sin f}{b(1+\sin f)(1+h)}\left\{\left[1-\frac{1}{2}g_b\right]^{\frac{1}{h}+1} - R^{-\frac{(1+\sin f)(1+h)}{2h\sin f}}\left(\frac{a_0}{a}\right)^{\frac{1}{h}+1}\right\}$$

$$= \int_1^{R^{\frac{1}{b}}} \exp(kr)\, r^{-\frac{b(1+\sin f)(1+h)}{2h\sin f}-1} dr \tag{3.63}$$

By defining $h = \dfrac{b(1+\sin f)(1+h)}{2h\sin f}$, Equation (3.63) can be expressed as:

$$\frac{1}{h}\left\{\left[1-\frac{1}{2}g_b\right]^{\frac{1}{h}+1}-R^{-\frac{h}{b}}\left(\frac{a_0}{a}\right)^{\frac{1}{h}+1}\right\}=\int_1^{R^{\frac{1}{b}}}\exp(kr)\,r^{-h-1}dr \tag{3.64}$$

where $1-\frac{1}{2}g_b$ can be denoted as $l$.

Obviously Equation (3.64) can not be integrated and solved directly. However, it is possible to solve Equation (3.64) by introducing the infinite series expansion:

$$\exp(kr)=\sum_{n=0}^{\infty}\frac{(kr)^n}{n!} \tag{3.65}$$

Using Equation (3.62), the following explicit expression for the pressure-expansion relationship of cavity expansion can be deduced from Equation (3.64):

$$\frac{a}{a_0}=\left\{\frac{R^{-\frac{h}{b}}}{l^{\frac{1}{h}+1}-h\wedge_1(R^{\frac{1}{b}},k)}\right\}^{\frac{h}{1+h}} \tag{3.66}$$

in which

$$\wedge_1(R^{\frac{1}{b}},k)=\sum_{n=0}^{\infty}A_n^1 \tag{3.67}$$

and

$$A_n^1=\begin{cases}\dfrac{k^n}{n!}\ln R^{\frac{1}{b}} & \text{if} \quad n=h\\ \dfrac{k^n}{n!(n-h)}[(R^{\frac{1}{b}})^{n-h}-1] & \text{otherwise}\end{cases} \tag{3.68}$$

The first condition in Equation (3.66) is rarely encountered since $h$ is unlikely to take an integer number. Having note that $k$ is a small value with the same order as $l$, it is easily to prove that the series defined by Equation (3.67) converges very rapidly for all different values of parameters such as $f$, $y$, $a$ and $b$ from sand. In the general case, the addition of first few terms in the series of expansion of Equation (3.67) may be sufficient to give satisfactory results.

All the necessary information is now available to construct the complete cavity pressure-expansion curve, but it can not be expressed in terms of a single equation. The proposed procedure for constructing the curve is as follows:

(a) Choose input parameters $f$ , $y$ , $a$ , $b$ and $p_0$.

(b) Calculate the derived parameters $h$ , $k$ , $h$ and $l$ from Equations (3.53), (3.58), (3.63) and (3.64), respectively.

(c) Evaluate $a/a_0$ from Equation (3.66) and construct the pressure-expansion curve.

When a cavity is expanded in a plastically deforming material, the pressure does not increase in definitely, but a limit cavity pressure $p_l$ is approached. By letting $(a/a_0) \to \infty$ in Equation (3.64), the limit cavity pressure $p_l$ may be obtained by finding $(R^{\frac{1}{b}})_\infty$ from:

$$\wedge_1\left((R^{\frac{1}{b}})_\infty, k\right) = \frac{l^{\frac{1}{h}+1}}{h} \tag{3.69}$$

where

$$(R^{\frac{1}{b}})_\infty = \left[(1 - \frac{\sin f}{(1+\sin f)b})\frac{p_l}{p_0}\right]^{\frac{1}{b}} \tag{3.70}$$

The limit cavity pressure depends strongly on both the angle of friction and the angle of the dilation, as well as the stiffness properties and the initial stress state of the soils.

## 3.6 Sample pressure expansion and stress distribution curves

Example sets of pressure expansion curves can be generated to investigate the effect of the various parameters on the behaviour of cavity expansion. Pressure-expansion relationships were derived from the procedure described above for sands ranging from loose to very dense in compaction with varying internal friction angles, dilation angles and nonlinear parameters. The input parameters of these different sands are summarized in Table 3.1.

Figures 3.3, 3.4 and 3.5 show the pressure-expansion curves for the sand at different densities with properties as described in Table3.1 (Na, 2002). The pressure-expansion curves are expressed non-dimensionally with the cavity pressure $p$ normalized by the initial cavity pressure $p_0$.

The stiffness of the response is increasing with the increasing compactness and dilation angle as shown in Figures 3.3, 3.4 and 3.5. Limit cavity pressure is reached when the cavity radius increases to 3 to 5 times of the initial radius $a_o$. The limit cavity pressure is seen to depend strongly on the angle of dilation, as a higher angle of dilation results in a more extensive plastically deforming zone. For sand of similar compactness, the differences in the pressure-expansion curve and the limit cavity pressure are mainly due to the effect of the different nonlinear parameters.

The stress calculated around an expanding cylindrical cavity at the ultimate state, as defined by Equations (3.33) and (3.34), (3.41) and (3.42) for the sands with properties as described in Table 3.1 are shown in Figures 3.6 to 3.8. The variable on the horizontal axis is $r/a_u$. These figures show that the radial and circumferential stresses which are the largest close to the cavity wall decrease rapidly as the radial distance increases. The rate of decrease is more rapid in the radial stress than in the circumferential stress.

**Table 3.1** Typical engineering parameters of Changi sand (Na, 2002)

| Soil type | | $f$ (°) | $y$ (°) | $a$ (MPa) | $b$ | Initial $p_0$ (kPa) |
|---|---|---|---|---|---|---|
| 1 | Loose sand | 35.3 | 2.8 | 1.06 | 0.597 | 29.3 |
| 2 | Loose sand | 37.9 | 5.9 | 5.59 | 0.673 | 83.8 |
| 3 | M. dense sand | 42.5 | 12.0 | 5.35 | 0.685 | 86.7 |
| 4 | M. dense sand | 43.5 | 13.3 | 9.84 | 0.748 | 65 |
| 5 | Dense sand | 48.5 | 20.1 | 7.48 | 0.692 | 93.3 |
| 6 | Dense sand | 48.9 | 20.7 | 4.29 | 0.659 | 52.0 |

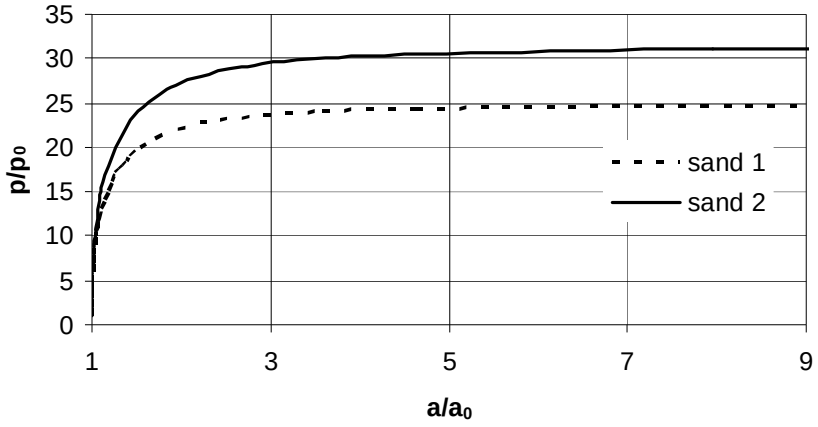


**Figure 3.3** Pressure-expansion curves for cylindrical cavities in loose sand

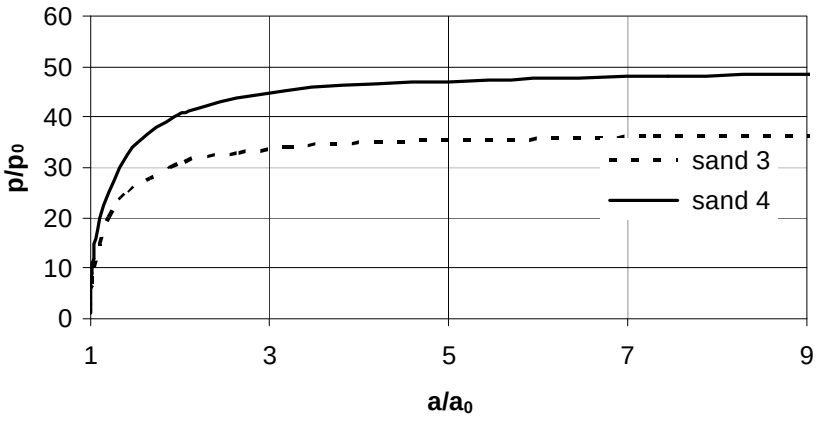


**Figure 3.4** Pressure-expansion curves for cylindrical cavities in medium dense sand

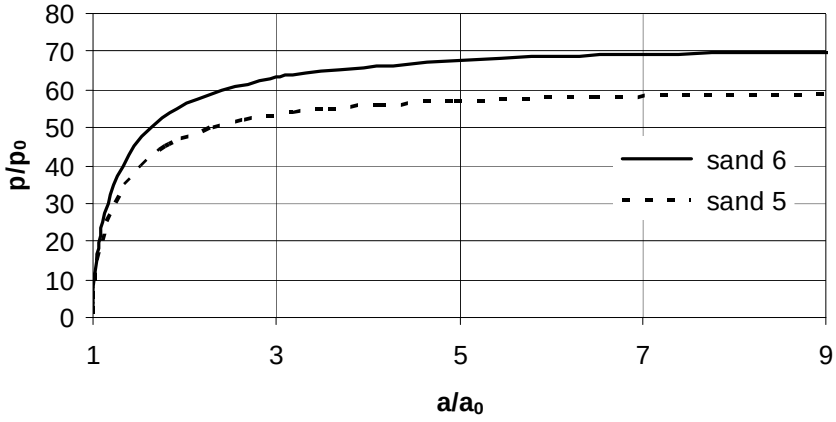


**Figure 3.5** Pressure-expansion curves for cylindrical cavities in dense sand

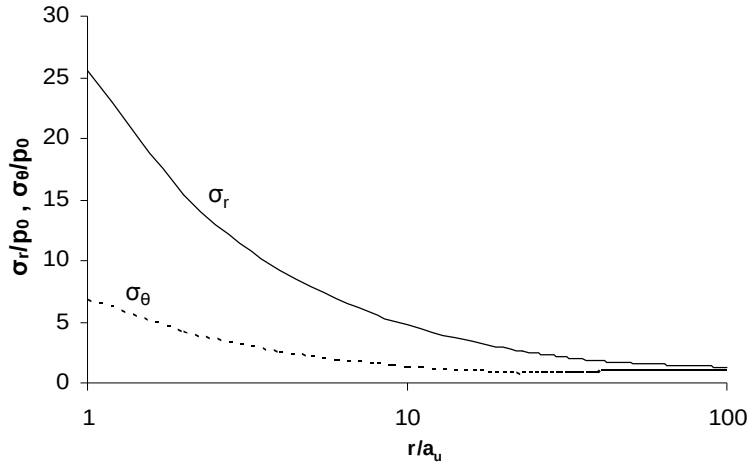


(a) Sand 1

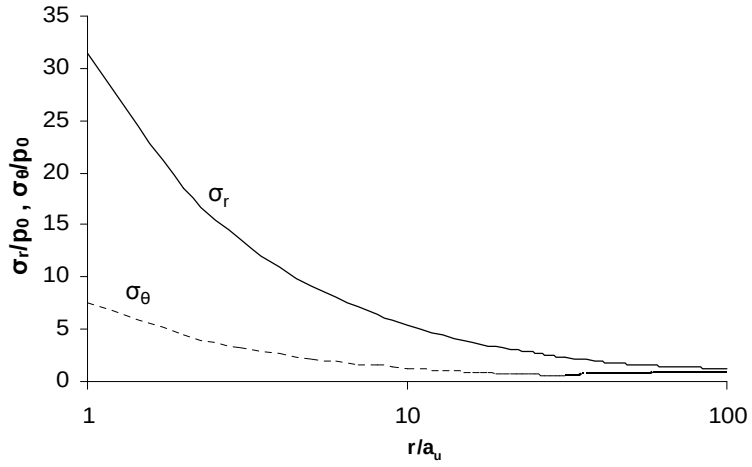


(b) Sand 2

**Figure 3.6** Stress distributions around a cavity for loose sand

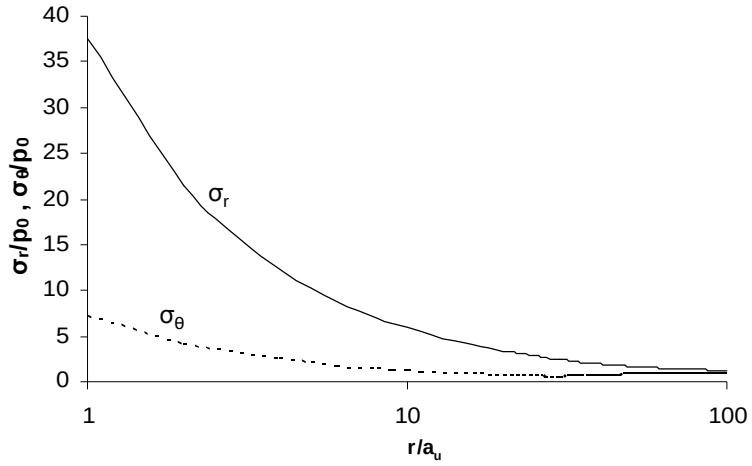


(a) Sand 3

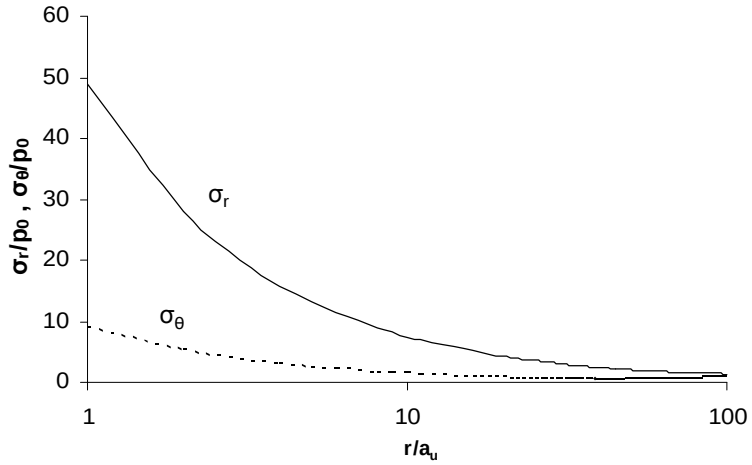


(b) Sand 4

**Figure 3.7** Stress distributions around a cavity for medium dense sand

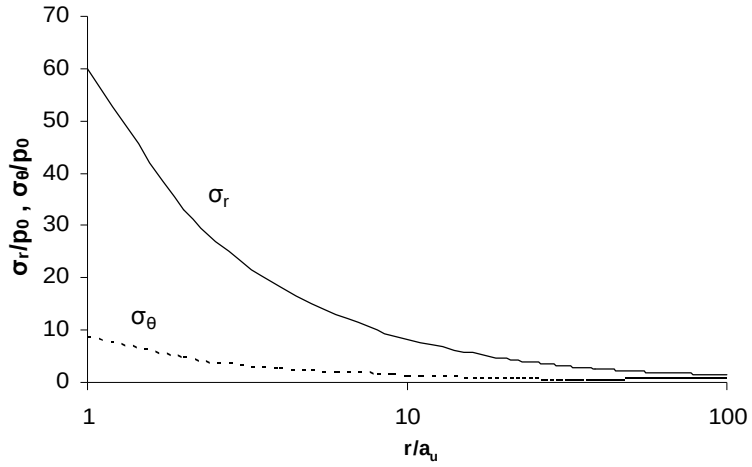


(a) Sand 5

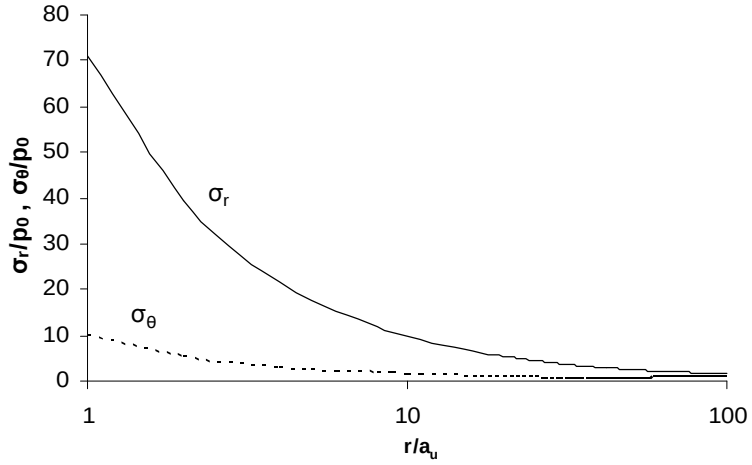


(b) Sand 6

**Figure 3.8** Stress distributions around a cavity for dense sand

# CHAPTER 4 CAVITY EXPANSION ANALYSIS IN CONFINED SAND MASS

## 4.1 General

The analogy between cavity expansion and the cone penetration process has been recognized by a number of researchers. Various correlations have been proposed between the cone resistance and the limit cavity pressure in the expansion of spherical/cylindrical cavity. Due to the approximate nature of these correlations, it is impossible to determine which one would suit better than the others. Based on cavity expansion and stress rotation analyses, the cone resistance $q_{cc}$ in a confined cylindrical sample of sand may be generally expressed as (Salgado et al., 1997):

$$q_{cc} = F\, p_{lc} \tag{4.1}$$

where $p_{lc}$ is the limit pressure in the expansion of a cylindrical cavity from the zero radius to the radius of a cone $a$ in a confined cylindrical sample, and $F$ is the function of soil parameters. Since $F$ is a factor that is related purely to stress rotation (Salgado, 1997), the cone resistance in an unbounded medium of sand $q_c$ may be related to the limit pressure that is required for the expansion of a cylindrical cavity in an unbounded medium $p_l$ as follows:

$$q_c = F\, p_l \tag{4.2}$$

From Equations (4.1) and (4.2), one obtains

$$\frac{q_c}{q_{cc}} = \frac{p_l}{p_{lc}} \tag{4.3}$$

Conceptually, if one makes $p_{lc}$ and $p_l$ the same by choosing a suitable boundary condition in calibration chamber, the cone resistance measured in a calibration

chamber will be the same to that measured in field. The schematic illustration of the expansion of cavity by cone penetration in the calibration chamber of this analysis is shown in Figure 4.1.

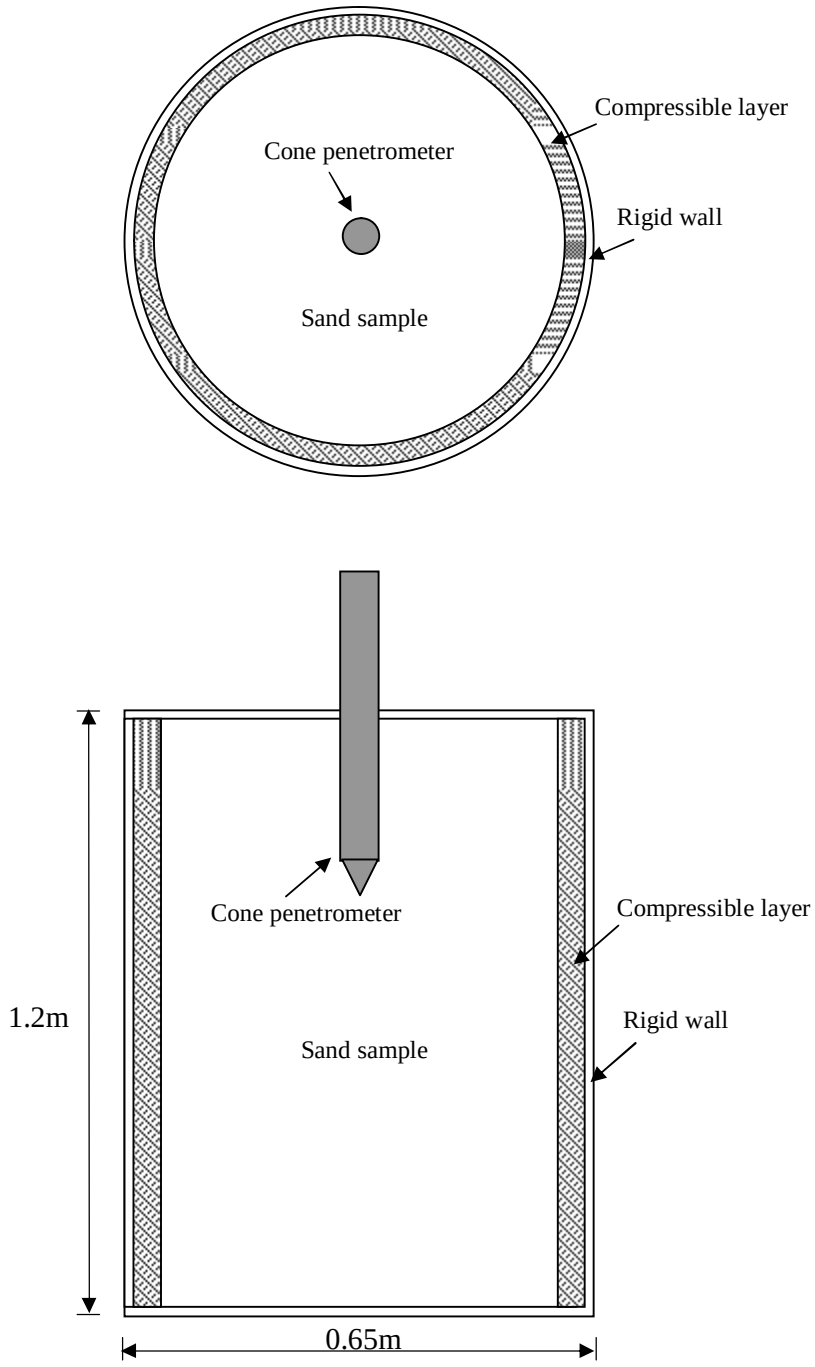


**Figure 4.1** Expansion of cavity by cone penetration in a calibration chamber:
(a) Plane view; (b) Section view

## 4.2 Stress and displacement around an expanded cylindrical cavity in an unbounded medium

For an unbounded medium of dilative nonlinear elastic plastic sand described by power-law function and Mohr-Coulomb yield criterion with a non-associated flow rule, a closed form solution for radial stress and displacement disturbance around a expanding cylindrical cavity is proposed in Chapter 3. The solution is briefly summarized in the subsequent paragraphs.

The limit cavity pressure $p_l$ can be calculated from Equation (3.69) and rewrite as follows:

$$\frac{1}{h} l^{\frac{1}{h}+1} = \sum_{n=0}^{\infty} \frac{k^n}{n!(n-h)} \left\{ \left[ (1 - \frac{\sin f}{(1+\sin f)b}) \frac{p_l}{p_0} \right]^{\frac{n-h}{b}} - 1 \right\} \tag{4.5}$$

where $$h = \frac{1+\sin y}{1-\sin y} \tag{4.6}$$

$$h = \frac{b(1+\sin f)(1+h)}{2h \sin f} \tag{4.7}$$

$$l = 1 - \frac{1}{2} g_b \tag{4.8}$$

$$k = \frac{(1-\frac{1}{h})}{2} \left[ \frac{p_0 b \sin f}{a((1+\sin f)b - \sin f)} \right]^{1/b} \tag{4.9}$$

$$g_b = [\frac{p_0 b \sin f}{a((1+\sin f)b - \sin f)}]^{1/b} \tag{4.10}$$

and $p_0$ is the initial cavity pressure in the soil, $a$ and $b$ are the elastic parameters and $0 < b \leq 1$, $f$ is the friction angle , $y$ is the dilation angle and $g_b$ is the shear strain in the elastic-plastic boundary. Note that Equation (4.5) is not a close-form solution. It can be solved using Microsoft Excel tool “solver”.

In the limit state, the location of elastic-plastic boundary at a radial distance $b$ can be related to $p_l$ and the ultimate cavity radius $a_u$ based on Equation (3.50):

$$\frac{b}{a_u} = \left( (1 - \frac{\sin f}{(1+\sin f)b}) \frac{p_l}{p_0} \right)^{\frac{1+\sin f}{2\sin f}} \tag{4.11}$$

Meanwhile, a material point moves from $r_{co}$ to $r_c$, the material between $b$ and $r_c$ will be in the elastic state. The displacement $u_c$ defined as $(r_c - r_{co})$ can be calculated from Equation (3.49):

$$u_c = -\frac{1}{2} \ln[1 - (1 - \exp(-g_b))(\frac{b}{r_c})^2] r_c \tag{4.12}$$

The corresponding radial stress is:

$$s_{rc} = \frac{a[-\ln(1 - \frac{b^2(1-\exp(-g_b))}{r_c^2}]^b}{b} + p_0 \tag{4.13}$$

If $b$ is large than $r_c$, the material at $r_c$ will be in the plastic state. Based on the Equation (3.64), the location of $r_c$ can be calculated from the original location $r_{co}$ using the following equation

$$\frac{1}{h}\left[ l^{\frac{1}{h}+1} - \left( \frac{r_{co}}{b} \right)^{\frac{1}{h}+1} \right] = \sum_{n=0}^{\infty} \frac{k^n}{n!(n-h)} \left\{ \left( \frac{b}{r_c} \right)^{\frac{2n\sin f}{b(1+\sin f)} - \frac{h+1}{h}} - 1 \right\} \tag{4.14}$$

Note that Equation (4.14) is also not a close-form solution. It can be solved using Microsoft Excel tool "solver".

The radial stress at location $r_c$ is:

$$s_{rc} = \left( \frac{a g_b^b}{b} + p_0 \right) \left( \frac{b}{r_c} \right)^{\frac{2\sin f}{1+\sin f}} \tag{4.15}$$

Equations (4.12) to (4.15) provide the radial stress and displacement at $r_c$ induced by the limit cavity pressure $p_l$. In other words, if the displacement and the radial stress at the interface between the soil and the compressible layer is equal to $u_c$ and $s_{rc}$ calculated from Equations (4.12) to (4.15), respectively, the limit cavity pressure $p_{lc}$ in a calibration chamber will be equal to $p_l$.

## 4.3 Stress and displacement on the chamber wall

Based on practical considerations, the modified calibration chamber should consist of a wall with two layers, with a compressible layer attached to the inside face of the rigid layer. Assuming the materials of the both layers are elastic, the radial stress $s_r$ and displacement $u$ for a material point during cylindrical cavity expansion can be expressed as (Cao, 1997):

$$s_r = -\frac{E}{(1+n)(1-2n)}[c_1 + (2n-1)\frac{c_2}{r^2}] \tag{4.16}$$

$$u = c_1 r + \frac{c_2}{r^2} \tag{4.17}$$

where $c_1$ and $c_2$ are constants that can be determined from the boundary condition.

For the rigid wall, the boundary conditions are:

$s_r = 0$ when $r = r_{ow}$

$s_r = s_{rw}$ when $r = r_{iw}$

For the compressible layer, the boundary conditions are:

$s_r = s_{rw}$ when $r = r_{iw}$

$s_r = s_{rc}$ when $r = r_c$

Substituting the boundary conditions of the compressible layer into Equation (4.16), the displacement at $r_c$ can be expressed as:

$$u_c = \frac{(1+n_c)r_c}{E_c(r_{iw}^2 - r_c^2)}[(1-2n_c)(s_{rc}r_c^2 - s_{rw}r_{iw}^2) + (s_{rc} - s_{rw})r_{iw}^2] \tag{4.18}$$

where $E_c$ and $n_c$ are Young's modulus and Poisson's ratio of the compressible layer, respectively. The displacement at $r_{iw}$ can be expressed as:

$$u_{iw} = \frac{(1+n_c)r_{iw}}{E_c(r_{iw}^2 - r_c^2)}[(1-2n_c)(s_{rc}r_c^2 - s_{rw}r_{iw}^2) + (s_{rc} - s_{rw})r_c^2] \tag{4.19}$$

Substituting the boundary conditions of the rigid wall into Equation (4.16), the displacement at $r_{iw}$ can be expressed as:

$$u_{iw} = \frac{(1+n_w)r_{iw}s_{rw}}{E_w(r_{ow}^2 - r_{iw}^2)}[(1-2n_w)r_{iw}^2 + r_{ow}^2] \tag{4.20}$$

where $E_w$ and $n_w$ are Young's modulus and Poisson's ratio of the rigid wall, respectively.

Note that $u_c$ and $s_{rc}$ that appear in Equations (4.18) to (4.20) can be calculated from Equations (4.12) to (4.15). If the elastic properties of the rigid wall, $E_w$ and $n_w$, and either $E_c$ or $n_c$ of the compressible layer are known, the other property of the compressible layer, $n_c$ or $E_c$, can be calculated from Equations (4.18) to (4.20).

## 4.4 Selection of the stiffness of chamber wall

As discussed in the previous sections, it is possible to simulate the field infinite boundary condition in a calibration chamber with a proper design of the calibration chamber wall. In this section, the development of a criterion for selecting suitable materials for the construction of such a calibration chamber is presented.

Like conventional calibration chamber, the rigid wall is generally made of steel. In this analysis, the steel's Young's modulus $E_w$ and Poisson's ratio can be taken as

$2\times10^8$ kPa and 0.3, respectively. The required elastic properties of the compressible layer depend on the elastic properties, the initial stress and the shear characteristics of the soil to be calibrated.

The stiffness of sand depends mainly on its dry density and the prevailing stress level. The nonlinear elasticity of sand in this analysis is represented by a power-law function in Equation (3.4), the nonlinear parameters $a$ and $b$ play significantly roles in determining the behavirour of sand. These two soil parameters are required to implement the solution, both of them are general obtained from pressuremeter tests incorporating cycles of unloading and reloading or from plane strain tests with small strain in the laboratory.

In the subsequent analysis, parameters of sand as described in Table 3.1 are adopted. With the knowledge of $a$ , $b$ , $f$ , $y$ and $p_0$ for a given sand, one can take the following steps to determine the required stiffness of the compressible wall:

(1) Calculate the limit cavity pressure $p_l$ from Equation (4.5). Note that Equation (4.5) is not a close-form solution. It can be solved using Microsoft Excel tool "solver".

(2) Calculate the location of elastic-plastic boundary $b$ in sand sample using Equation (4.11).

(3) Calculate the displacement $u_c$ and the radial stress $s_{rc}$ at the inside wall using Equations (4.12) and (4.13) if $r_c > b$ , or Equations (4.14) and (4.15) if $r_c < b$. Note that Microsoft Excel tool "solver" is needed for solving Equation (4.14).

(4) Calculate Young's modulus of the compressible layer $E_c$ using Equations (4.18), (4.19) and (4.20) with an assumed value of $n_c$ and given values of $r_{ow}$ and $r_{iw}$ on the basis of the detailed chamber design.

The sketch in Figure 4.1 shows a steel cylindrical tank in the Geotechnic Workshop at Nanyang Technological University (NTU). The outer radius of the rigid wall $r_{ow}$ of

this tank is 0.33m and the thickness ($r_{ow} - r_{iw}$) is 0.005m, the value of $E_C$ can be calculated based on the parameters shown in Table 3.1. Figure 4.2 to 4.4 show the variation of $E_c$ with the thickness of the compressible layer ($r_{iw} - r_c$) for different sands with different initial stresses. A material with higher Young's modulus is needed with an increased thickness of the compressible layer. Thus, for different sands, one can vary the thickness of the compressible layer to suit the selection criterion, while maintaining the same material.

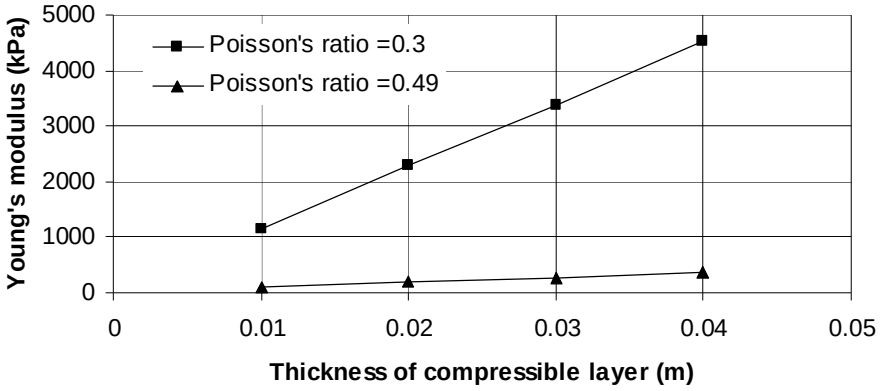


(a) Sand 1

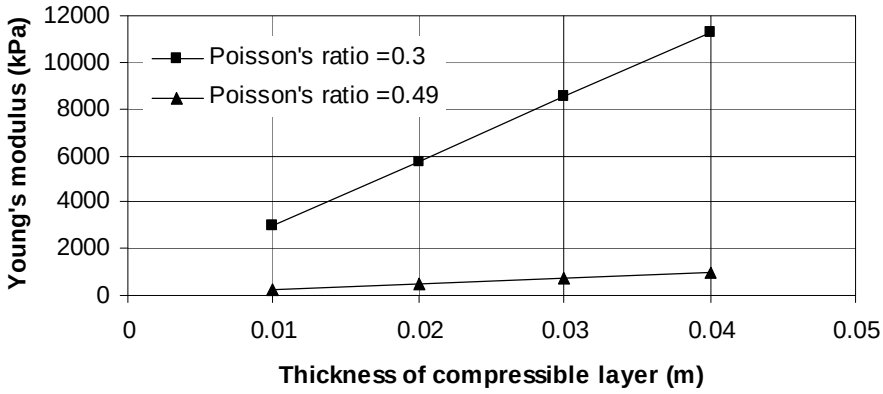


(b) Sand 2

**Figure 4.2** Required Young's modulus versus required thickness of the compressible layer for loose sand

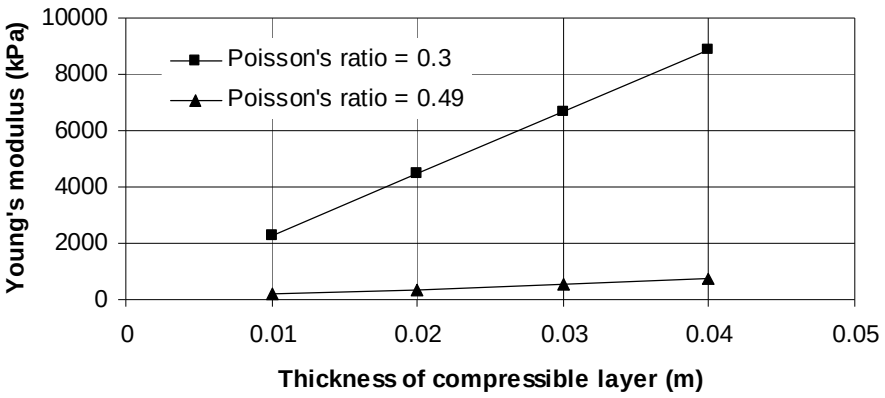


(a) Sand 3

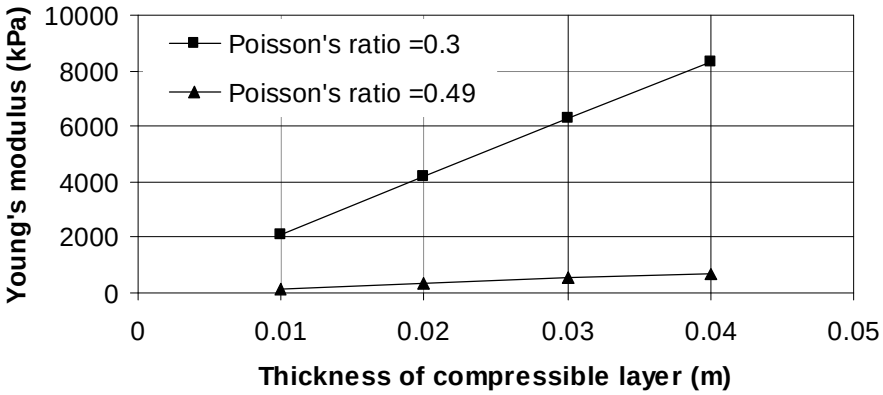


(b) Sand 4

**Figure 4.3** Required Young's modulus versus required thickness of the compressible layer for medium dense sand

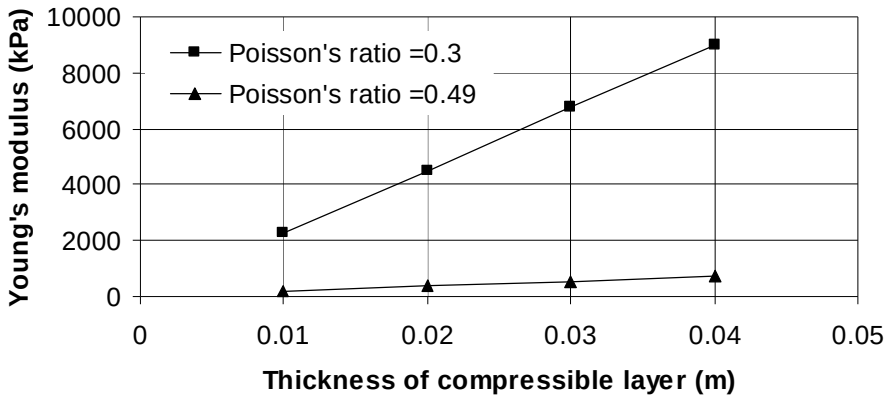


(a) Sand 5

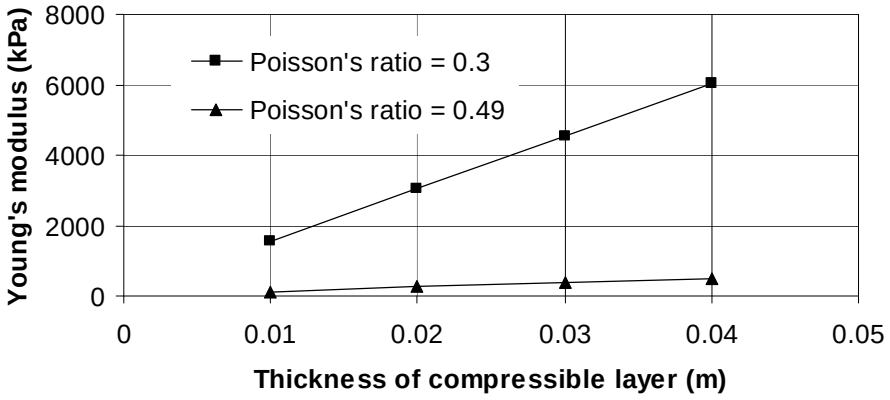


(b) Sand 6

**Figure 4.4** Required Young's modulus versus required thickness of the compressible layer for dense sand

# CHAPTER 5 LABORATORY CHARACTERIZATION OF CHANGI SAND

## 5.1 Introduction

The experimental work in this study consists of both laboratory and large scale calibration chamber (CC) tests. For assessment of basic index soil properties and stress-strain characteristics of the Changi sand tested in calibration chamber, various supplemental tests were conducted in laboratory. The descriptions of these tests are shown as follows in Table 5.1.

**Table 5.1** Tests of characterization of Changi sand

| Test | Target Soil Property |
|---|---|
| Specific gravity test | Specific gravity $G_S$ |
| Particle size distribution test | Grain size distribution |
| Relative density test | Minimum dry density $r_{min}$<br>Maximum dry density $r_{max}$ |
| Triaxial test | Stress-Strain relationship |

## 5.2 Determination of basic properties

The sand tested in this CC test is a granular fill material obtained from the Changi land reclamation project in Singapore, named as Changi sand. This material was dredged from seabed and therefore it contained some marine substances such as shells.

Observation from the scanning electron microscopy (SEM) revealed that the shell particles are flaky and generally much larger than the sand particles, as shown in Figure

5.1. It can be also seen from this figure that the individual grains of the Changi sand are mainly sub-angular in shape.

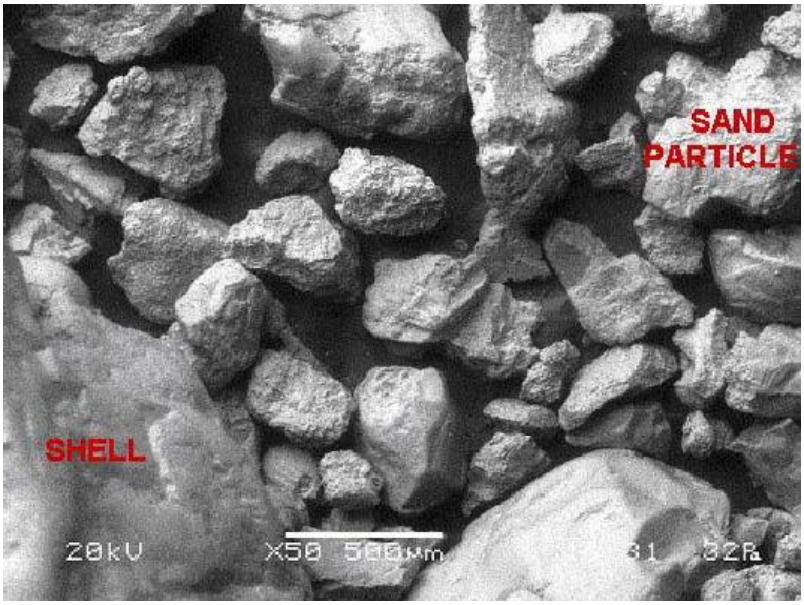


**Figure 5.1** The microscope photograph of Changi sand (Gan, 2002)

### 5.2.1 Specific gravity test (BS 1377: Part 2: 1990)

The density bottle method is used to determine the specific gravity $G_S$ of sand, defined as follows:

$$G_S = \frac{Mass\ of\ dry\ solid}{Mass\ of\ distilled\ water\ of\ the\ same\ volume}$$

$$= \frac{W_2 - W_1}{(W_4 - W_1) - (W_3 - W_2)} \qquad (5.1)$$

where $W_1$ = Mass of density bottle; $W_2$ = Mass of soil + density bottle; $W_3$ = Mass of soil + density bottle + distilled water; and $W_4$ = Mass of distilled water + density bottle.

The specific gravity $G_S$ of the Changi sand for CC test determined by the specific gravity test is show in Table 5.2 as follows,

**Table 5.2** Results of specific gravity test of Changi sand

| Sample No. | Test No. | M1 | M2 | M3 | M4 | Gs | Average Gs | |
|---|---|---|---|---|---|---|---|---|
| **1** | 1 | 42.938 | 56.218 | 151.855 | 143.565 | 2.661323 | 2.660 | **2.657** |
| | 2 | 42.22 | 54.158 | 151.052 | 143.609 | 2.65584 | | |
| | 3 | 41.346 | 54.127 | 149.923 | 141.943 | 2.662154 | | |
| **2** | 4 | 42.951 | 56.424 | 152.039 | 143.635 | 2.657921 | 2.656 | |
| | 5 | 42.913 | 56.847 | 152.394 | 143.72 | 2.649049 | | |
| | 6 | 42.577 | 56.769 | 151.852 | 142.994 | 2.660667 | | |
| **3** | 7 | 41.846 | 54.058 | 150.32 | 142.73 | 2.642146 | 2.654 | |
| | 8 | 42.229 | 56.228 | 151.753 | 143.035 | 2.650824 | | |
| | 9 | 42.921 | 55.312 | 152.246 | 144.496 | 2.669899 | | |

### 5.2.2 Particle size distribution test (BS 1377: Part 2: 1990)

The particle size distribution curve or the grading curve of the sand was obtained from the particle size distribution test. The dry sieving procedure was used.

Figure 5.2 shows the results if the particle size distribution analyses of the sand. The gravel content is about 6 to 7% and 93-94% sand.

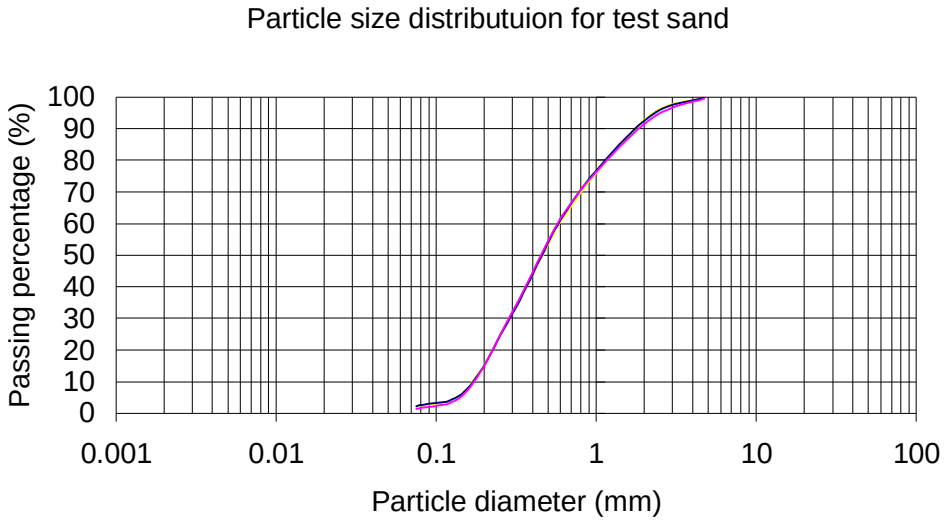


**Figure 5.2** Particle size distributions for Changi sand

The uniformity coefficient ($C_U$):

$$\frac{D_{60}}{D_{10}} = \frac{0.6}{0.18} = 3.33 \qquad (5.2)$$

### 5.2.3 Relative density test (ASTM 4253 & ASTM 4254)

It is necessary to determine the minimum and maximum dry density of the sand in order that samples can be prepared to the required relative density. A 2830 $cm^3$ ASTM standard mould was used for the minimum and maxi mum dry density test. The minimum dry density test is usually conducted by filling the soil sample loosely into the mould. The minimum dry density of the sand is the ratio of mass of loose sand over the volume of mould. As for the maximum dry density test, a surcharge is usually applied on top of the sand in the mould followed by 10 minutes of vibration on a 50 Hz vertically vibrating table. The height of sample after vibration is measured enabling the respective volume and the density of the sand to be found. The relative density $D_r$ of the soil sample can be found using the following relationship:

$$D_r = \frac{r_{max}(r - r_{min})}{r\ (r_{max} - r_{min})} \times 100\% \qquad (5.3)$$

where $r$ = dry density of soil sample; $r_{max}$ = maximum dry density of soil sample; and $r_{min}$ = minimum dry density of soil sample.

The summary of minimum and maximum dry density of the sand is shown as shown in table 5.3,

**Table 5.3** Minimum and maximum dry density of Changi sand

| **Sample** | **Minimum dry density ($Mg/m^3$)** | | **Maximum dry density ($Mg/m^3$)** | |
|---|---|---|---|---|
| 1 | 1.475 | Average | 1.781 | Average |
| 2 | 1.478 | **1.4757** | 1.790 | **1.7887** |
| 3 | 1.474 | | 1.795 | |

## 5.3 Triaxial tests

To investigate the stress-strain characteristics of the Changi sand in calibration chamber tests, CD triaxial tests have been performed in the laboratory.

The triaxial test is considered the proper laboratory test to investigate the stress-strain behaviour and to provide the reliable soil parameters. The data obtained from triaxial tests is used to characterize the stress-strain behaviour of Changi sand.

### 5.3.1 Setup and sample preparation

The triaxial equipments are schematically shown in Figure 5.3. Two different preparation methods are commonly used in the preparation of cohesionless specimens for compression tests: the moist tamping (MT). The sand sample was formed in metal split metal mould. The height of sand sample is about 200mm and the diameter is 100mm. The sand sample is 100mm in diameter and 200mm in height. The cell pressure and back pressure were applied by GDS. The axial load was measured by a 10 kN capacity internal load cell. The volume change of the sand sample was measured by volume change transducer. The pore water pressure was measured by a pore water pressure transducer at the bottom of the sand samples. The vertical displacement instrumentation used in the apparatus consists of one external Linear Variable Differential Transducer (LVDT). The external LVDT with a maximum range of 50 mm is installed on top of cell chamber to serve as default axial strain measuring device. The difference between cell pressure and back pressure was controlled to be equivalent to a soil suction measured in laboratory during the whole saturation procedure. A rate of applying the cell and back pressures was kept slow enough to avoid a local failure form irregular distribution of pore pressure.

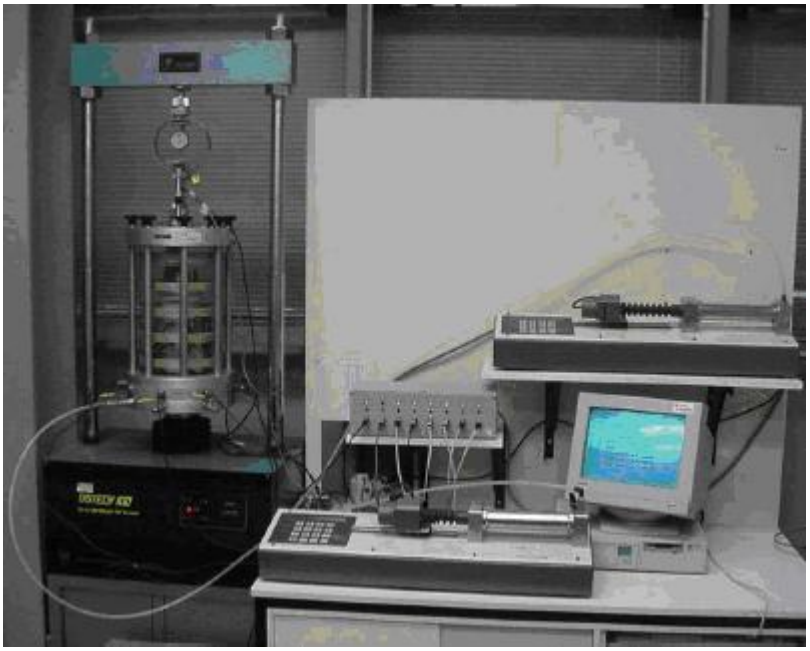

**Figure 5.3** Triaxial testing equipments

### 5.3.2 Tests and results

The description of the triaxial tests is shown in Table 5.4.

**Table 5.4** Triaxial test carried in laboratory

| Test | Relative density (%) | Consolidation pressure (kPa) | Test type |
|---|---|---|---|
| 1 | ~35 | 100 | CD |
| 2 | ~60 | 100 | CD |
| 3 | ~75 | 100 | CD |

The stress-strain curves of Changi sand from the triaxial tests are shown in Figures 5.4 to 5.6 as follows.

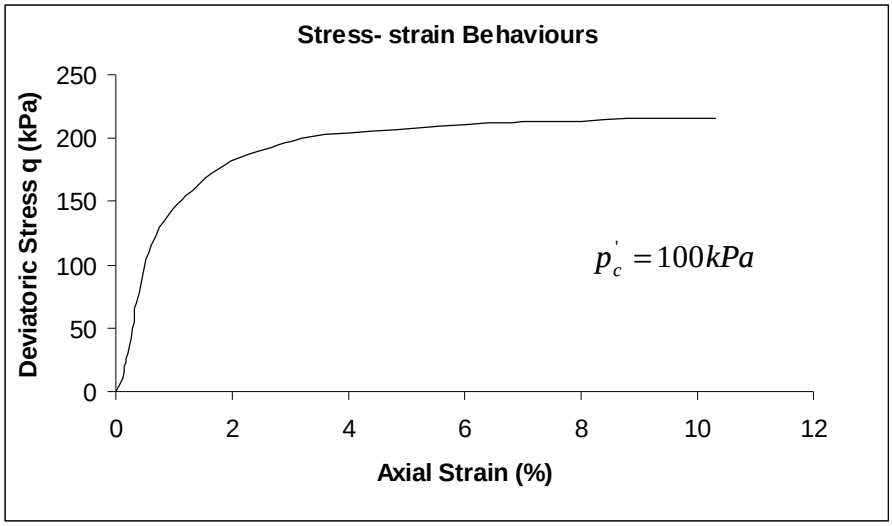


**Figure 5.4** Stress-strain behaviours for loose sand sample (Dr = 35%)

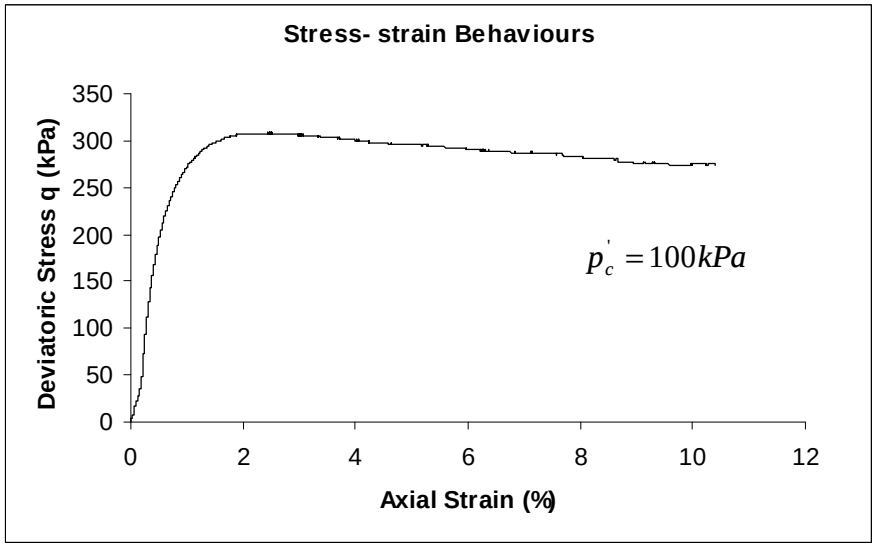


**Figure 5.5** Stress-strain behaviours for medium dense sand sample (Dr = 60%)

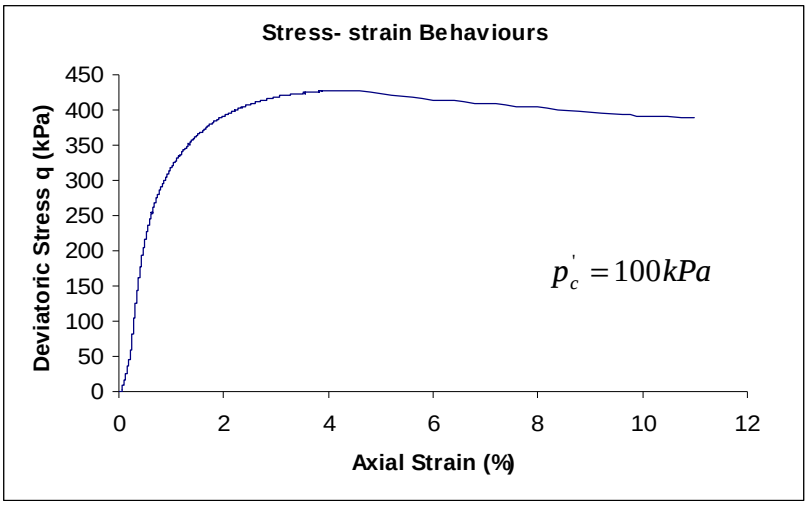


**Figure 5.6** Stress-strain behaviours for dense sand sample (Dr = 75%)

It can be seen from the figures above that the stress-strain relationship is nonlinear even in small strain range. The shear strength parameters of sand are expressed in terms of the internal friction angle at failure. Failure can be defined as the condition corresponding to the maximum deviator stress $(s_1 - s_3)_{max}$. The internal friction angle and dilation angle of sand can be deduced from the equation as follows,

$$\frac{q}{p'} = \frac{6\sin f'}{3-\sin f'} \tag{5.4}$$

$$y = -0.11 + 0.59D_r - 0.11D_r \ln(p'/p_a) \text{ (Houlsby, 1991)} \tag{5.5}$$

Where $p' = (s_1' + 2s_3')/3$, $q = (s_1' - s_3')$

The parameters of the Changi sand are summarized in Table 5.5.

**Table 5.5** Soil parameters of Changi sand

| Sand sample | Relative density (%) | Internal friction angle $f$ (deg) | dilation angle $y$ (deg) | $a$ (MPa) | $b$ |
|---|---|---|---|---|---|
| 1 | ~35 | 31.1 | 4.3 | 3.78 | 0.52 |
| 2 | ~60 | 37.4 | 11.3 | 4.74 | 0.68 |
| 3 | ~75 | 42.8 | 14.9 | 4.81 | 0.84 |

# CHAPTER 6 LABORATORY CHARACTERIZATION OF BUFFER MATERIAL

## 6.1 Introduction

The basic idea of the design of the new calibration chamber is to incorporate an elastic compressible layer between the sand sample and the steel rigid wall. Elastic materials, such as elastomer (rubber), foam and sponge were considered. Elastomers can perhaps best be defined as materials capable of large or fairly large elastic deformations, which are suitable for the construction of the chamber wall. In this study, sponge rubber sheets with different thickness are adopted as the buffer layers of the chamber wall which is commercially available in Singapore.

Two elastic moduli, Young's modulus $E$ and Poisson's ratio$n$ , are used in the proposed theoretical analysis based on the Hooke's law. Young's modulus is the ratio of tensile or compressive stress to corresponding strain below proportional limit of the material. The value of Young's modulus is a material property useful in design for compliance of structural materials that follow Hooke's law when subjected to uniaxial loading (that is, the strain is proportional to the applied force). Poisson's ratio is the ratio of the transverse (lateral) strain to the axial strain of the material. Poisson's ratio is used for the design of structures in which all dimensional changes resulting from the application of the force need to be taken into account and in the application of the generalized theory of elasticity to structural analysis.

During the cone penetration test in calibration chamber, the buffer layer is compressed due to the cavity expansion in the sand. Since the buffer layer in chamber test is under compressive condition, compression stress-strain tests on buffer samples are required in NTU Geotechnics Lab to obtain the elastic moduli under the same loading condition of the buffer layer in chamber tests.

Typical stress-strain curve for determining the elastic modulus of material is shown in Figure 6.1. The slope of the initial straight line portion of the curve is the Young's modulus of the material which defined as follows:

$$E = \frac{ds}{de} \tag{6.1}$$

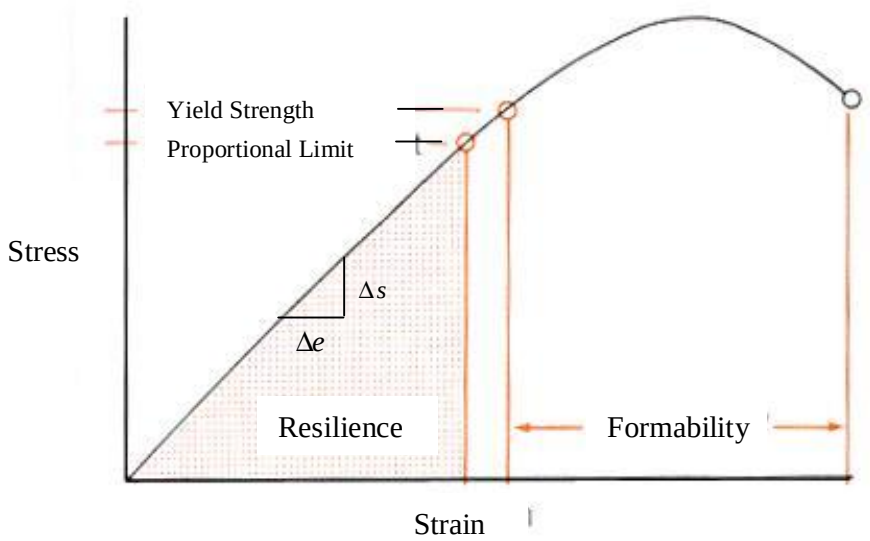


**Figure 6.1** Typical stress-strain curves for elastic materials

Poisson's ratio $n$ also can be obtained from compression stress-strain tests. This test method covers the determination of Poisson's ratio of buffer materials. Poisson's ratio is defined as the absolute value of the ratio of transverse (lateral) strain to the corresponding axial strain resulting from uniformly axial stress below the proportional limit of the material:

$$n = \frac{-e_t}{e_a} \tag{6.2}$$

$e_a$ is the axial strain while $e_t$ is the transverse strain.

## 6.2 Apparatus

The compression testing machine has a loading frame and a stationary head and a moveable base each with horizontal steel plate. Buffer samples are installed between two parallel steel plates so that the direction of load applied to the specimen is coincident with the longitudinal axis of the specimen. The sketch of the compression machine is shown in Figure 6.2. The force and axial strain were measured by the loading dial and LVDT, respectively.

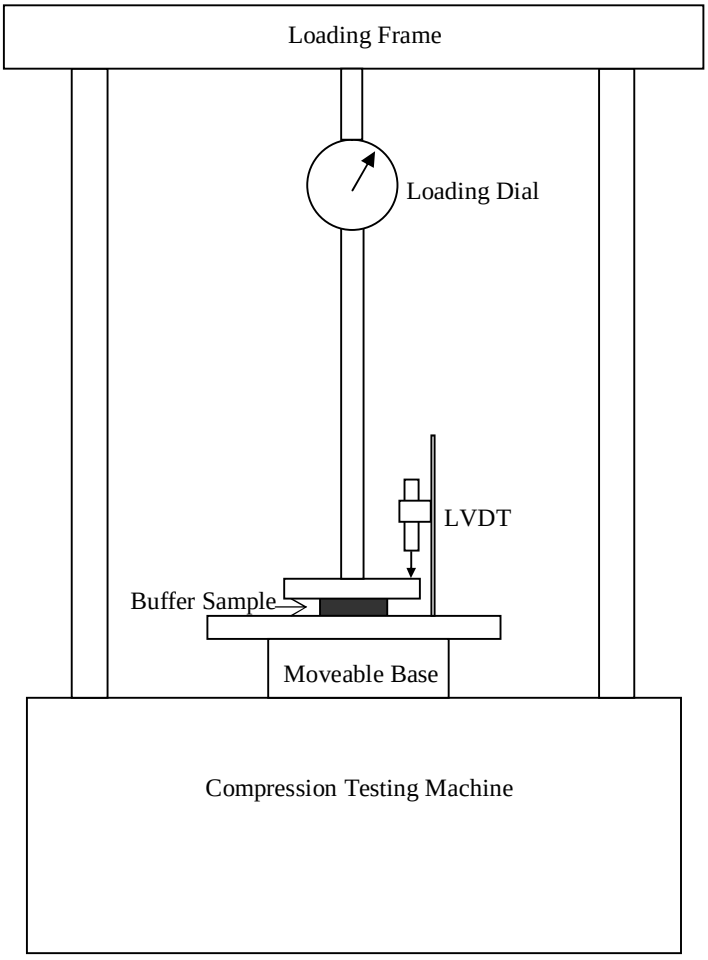


**Figure 6.2** Sketch of Compression Testing Machine

## 6.3 Test specimen

Sponge rubber sheets with three different thicknesses (10mm, 20mm & 38mm) were adopted as buffer layer in this study. Three different sizes of small square samples were cut from these sheets for the compression tests to get the elastic moduli of the buffer material. The sizes of the square samples are 40mm*40mm, 50mm*50mm and 70mm*70mm for each sponge rubber sheet of three thicknesses.

## 6.4 Test procedure

The test procedure of the compression test is summarized as follows:

1) Install the square sample to the compression machine between the two parallel horizontal plates.

2) Mark a 1 cm color horizontal line on the side surface of the buffer sample for the measuring of the lateral strain during the compression.

3) Apply small force to get the initial reading to eliminate the setting error.

4) Run the compression test and record the force, axial and lateral strain.

## 6.5 Evaluation of data

**Young's modulus *E***

If a plot of load-versus-extension is obtained by means of an autographic recorder, the value for Young's modulus may be obtained by determining the slope of the line for loads less than the load corresponding to the proportional limit. Young's modulus is calculated from the load increment and corresponding extension increment, between two points on the line as far apart as possible, by use of the following equation:

The precision of the value obtained for Young's modulus is depend upon the precision of each of the values used in the calculation.

The test results of Young's modulus for the buffer samples are shown in Figure 6.3 – 6.5 as follows:

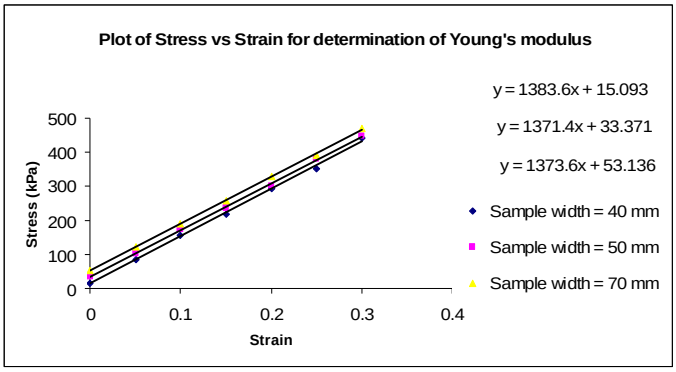


**Figure 6.3** Stress- Strain curve for sponge rubber sheet of 10 mm thickness

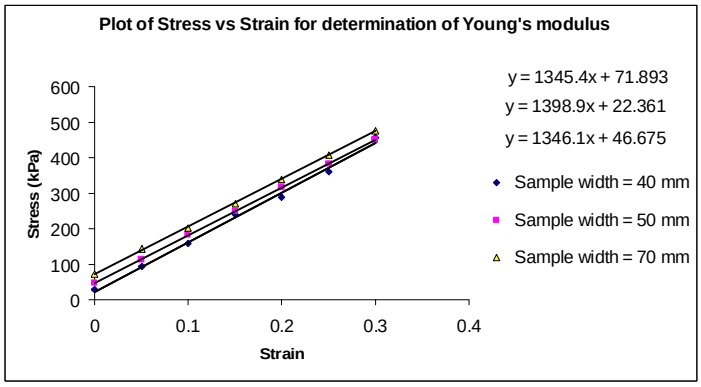


**Figure 6.4** Stress- Strain curve for sponge rubber sheet of 20 mm thickness

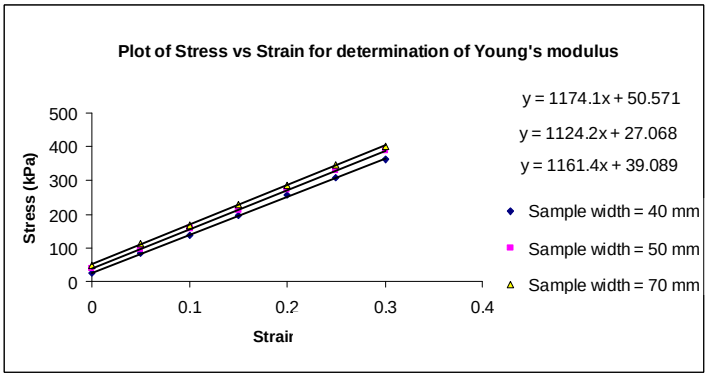


**Figure 6.5** Stress- Strain curve for sponge rubber sheet of 38 mm thickness

**Poisson's ratio** *n*

The accuracy of the determination of Poisson's ratio is usually limited by the accuracy of the transverse strain measurements because the percentage errors in these measurements are usually greater than in the axial strain measurement.

The test results of Poisson's ratio for the buffer samples are shown in Figures 6.6 – 6.8 as follows:

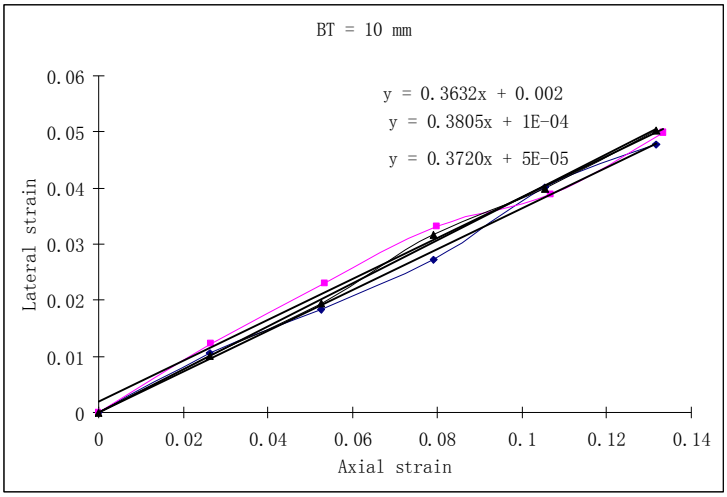


**Figure 6.6** Poisson's ratio for sponge rubber sheet of 10 mm thickness

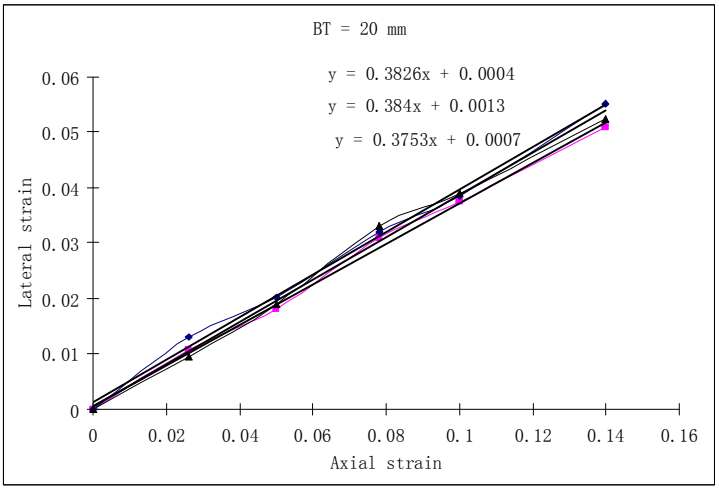


**Figure 6.7** Poisson's ratio for sponge rubber sheet of 20 mm thickness

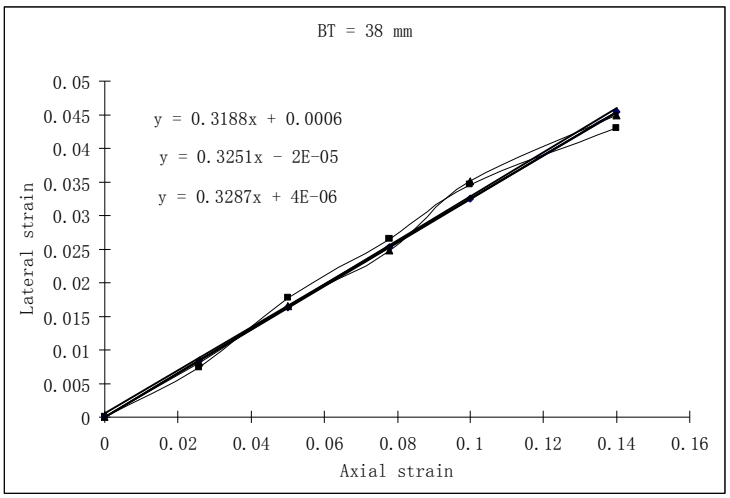


**Figure 6.8** Poisson's ratio for sponge rubber sheet of 38 mm thickness

The Young's modulus and Poisson's ratio of the sponge rubber sheets are summarized in Table 6.1 as follows:

**Table 6.1** Summary of elastic parameters of sponge rubber

| Sponge Rubber Thickness (mm) | Average Young's Modulus (kPa) | Average Poisson's ratio |
|---|---|---|
| 10 | 1376.2 | 0.372 |
| 20 | 1363.5 | 0.381 |
| 38 | 1153.2 | 0.325 |

# CHAPTER 7 CONE PENETRATION TESTS IN CALIBRATION CHAMBER

## 7.1 Introduction

In this chapter, the apparatus and setup for the new calibration chamber (CC) and the procedure of the chamber tests are described.

The construction of calibration chamber was conducted in the Geotechnics Workshop of Nanyang Technological University (NTU). Based on practical considerations, the new calibration chamber consists of a double-wall system, with a compressible layer attached to the inner face of the rigid wall.

A series of cone penetration test (CPT) were carried in the new chamber on dry samples of Changi sand with different relative densities prepared by the pluviation method.

## 7.2 Apparatus setup

The proposed chamber testing system consists of a 5 ton electric cone penetrometer, a sand pluviation device, the chamber, an electronic data logger and control unit, a pneumatic system for the supply of air pressure, and a hydraulic system to push the cone penetrometer etc.

### 7.2.1 Hydraulic actuator

A 100-ton hydraulic actuator, reacting against the loading frame as shown in Figure 7.1 is used to provide the vertical pushing force. It consists of a 100-ton capacity hydraulic power actuator that mounted on top of a steel frame. The steel frame, constructed of H beams, stiffeners and columns, is powered by a hydraulic power pack and its operation is controlled by an automated controller panel. The actuator can move up and down 400 mm vertically from the neutral position. The reaction system that includes the hydraulic actuator and the loading frame, was used to push the cone penetrometer steadily at a constant speed into the prepared sand sample in the chamber. The movement rate of the

hydraulic actuator can be set at a penetration rate of 2 cm/sec that is commonly adopted in a standard CPT test.

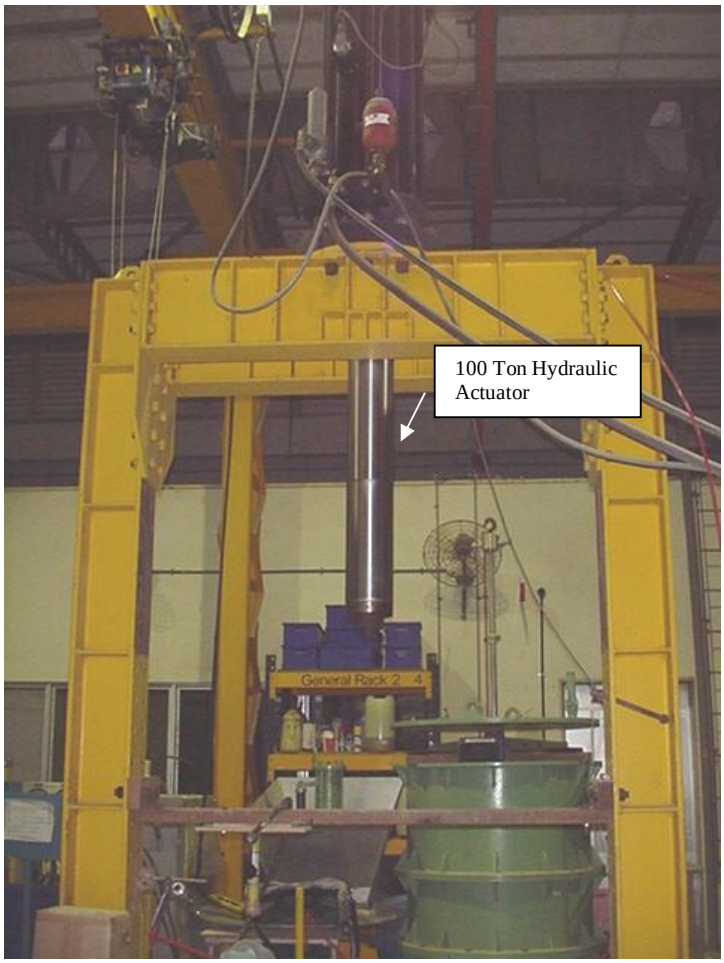


**Figure 7.1** 100- ton hydraulic actuator and the loading frame

### 7.2.2 Sand pluvial deposition system

Pluvial method may be the best one to obtain reasonably homogeneous reconstituted sand sample in laboratory to simulate the natural sand deposits (Jacobsen, 1976). A pluvial deposition method following the basic system described by Jacobsen (1976) was used in this investigation for the preparation of sand sample in the chamber.

The pluvial deposition devices (sand rainer devices), as shown and sketched in Figures 7.2 (a) and 7.2 (b) are usually used to discharge the sand at certain height and rate in

order to achieve the required relative density. The diameter of the sand container is as same as the diameter of the chamber (diameter: 650mm). Three shutter plates with different sieve patterns were used to achieve different relative density (Dr) of sand samples. Calibration of the sand rainer was carried to determine the range of relative density that can be produced by this pluvial deposition.

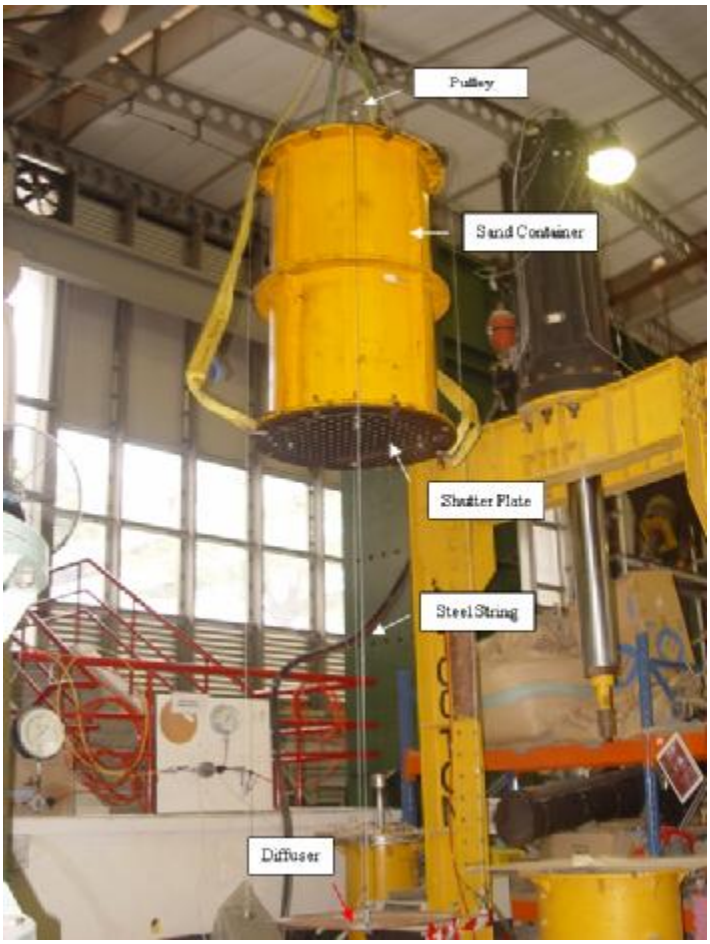


**Figure 7.2(a)** Pluvial deposition devices for sand sample preparation

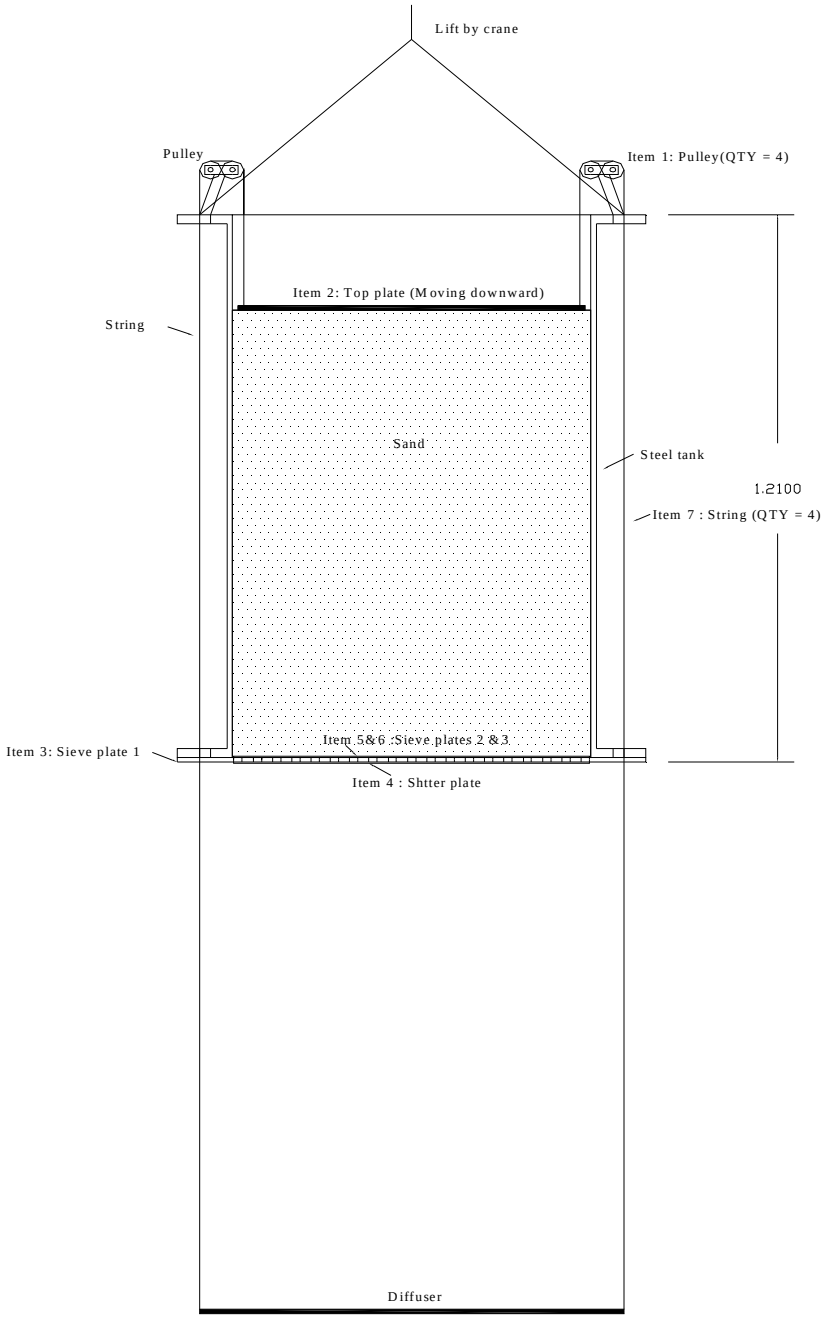


**Figure 7.2(b)** Pluvial deposition devices for sand sample preparation

The drop height is one of the factors to control the sand density. This drop height could be kept a constant value during sand pluviation. The diffuser and top plate of sand in the overhead sand rainer are connected by four steel strings. As the diffuser is moving

upward, the top plate of sand in sand rainer is moving downward at the same rate in the mean time, when the sand is being deposited into the chamber underneath. The main factor that controls the relative density of the sand sample is the spacing in the shutter plate at the bottom of the sand rainer. Three different sieve patterns as described in Table 7.1 were used.

The relative density of the sand sample was determined by using a plastic box with known volume placed below the diffuser. It is very important to ensure the uniformity and homogeneity at the different depth of the sand sample. If one can control the drop height at a constant value with a given shutter plate, it is believed that the sand sample would be uniform.

In this study, the drop height is kept about one meter for all cases. Two methods were used to check sample uniformity described as follows:

***Method 1: Small tin:***

1) Put several small plastic tins (height = 9cm, diameter = 7cm) at the different levels of the chamber, bottom, middle and top during the sand pluviation.

2) When the sample is prepared, remove sand mass layer by layer in the chamber and take out these tins full of deposited sand with great care.

3) Measure the weight of the sand in the tins to check the relative density of the sand sample at different levels.

This method was not successful due to the error and disturbance to the sample when removing the sand mass surrounding the tins. The small change in volume of sand due to the soil disturbance led to a significant change in relative density calculated as the total volume of each tin was small. As a result, the relative density calculated by this method was highly scattered and not indicative of sand uniformity.

***Method 2: Bigger Plastic box***

As the small tin method did not work, bigger plastic boxes were used to check the uniformity of the sand sample prepared by sand pluviation system. The dimension of the

plastic box is 20cm (L) x15 cm (W) x15 cm (H). The basic idea is the same as the small tin method. Three plastic boxes were placed in bottom, middle and top of the chamber during sample preparation. The error due to soil disturbance during removing of sand is small and negligible compared to the large volume of sand in the plastic box. The scatter of the relative densities calculated from the weight of the sand in plastic boxes was insignificant for each shutter plate. The results show a good uniformity at different depth of sand sample prepared by this sand pluviation system.

Results of the calibration of the sand rainer by method 2 are summarized in Table 7.1

**Table 7.1** Summary of the calibration of sand rainer

| Falling height (m) | Hole diameter of Shutter plate (mm) | Center to center distance of shutter holes (mm) | Average relative density Dr (%) |
|---|---|---|---|
| 1 | 15 | 40 | ~35 |
| 1 | 15 | 60 | ~60 |
| 1 | 15 | 80 | ~75 |

The mechanism of the sand pluvial deposition system and sand sample preparation procedure are briefly described as follows:

1) Fill up the steel container with sand and level the surface of sand.

2) Place the moveable top plate of sand rainer on the sand surface and connect to the diffuser by four steel strings.

3) Uplift the sand rainer over the chamber to a fixed drop height.

4) Open the shutter plate, the sand drops into the chamber through the diffuser and the volume of sand in the container decrease. The top plate moves downwards and the diffuser moves upwards. The falling height of sand (from diffuser to the increasing top level of sand in chamber) keeps constant.

5) Close the shutter plate and remove the sand rainer from the top of the chamber when the chamber is fully fill up with sand and then level the sand surface in the chamber with great care.

6) Place and install the top plate of chamber.

### 7.2.3 Chamber design and model setup

A steel cylindrical steel tank (Figure 7.3) available in the NTU Geotechnics Workshop was used in the investigation for the construction of the calibration chamber. The cylindrical tank, as sketched in Figure 7.4, is 0.66 m in outside diameter, and 1.2 m in height. The thickness of the tank wall is 5 mm, giving an inside tank diameter of 650 mm.

**Figure 7.3** Cylindrical steel tank in Geotechnics Workshop, NTU

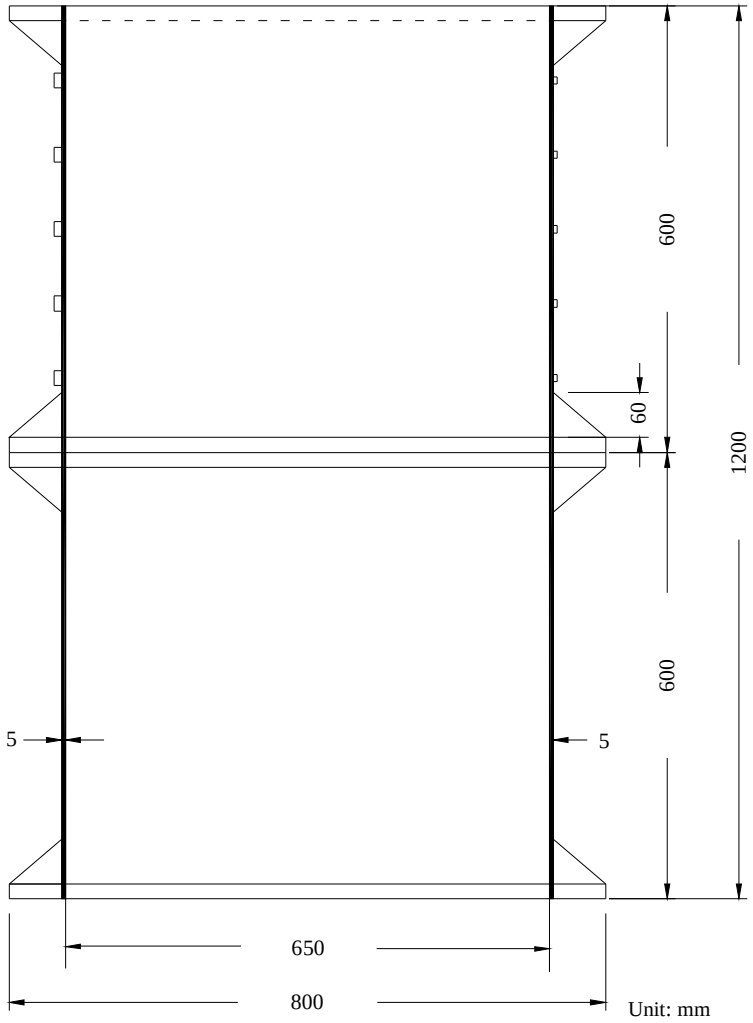


**Figure 7.4** Schematic diagram of the cylindrical steel tank

Figure 7.5 shows the cross section view of the design of the chamber. The chamber consists mainly of the cylindrical steel tank, top and bottom steel plates, air bellow, compressible layer and total pressure cells. Figure 7.6 shows the schematic illustration of the experimental setup.

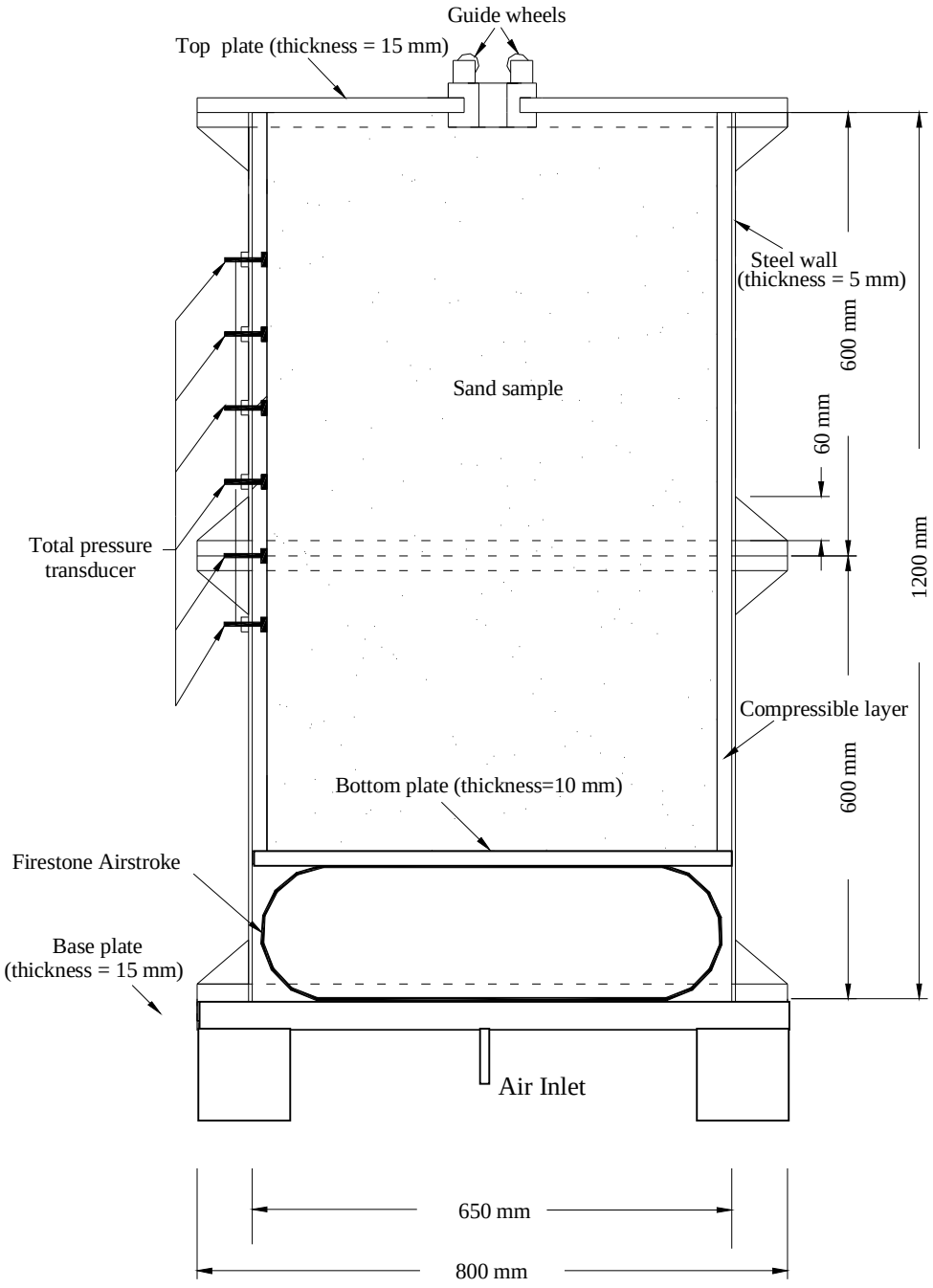


**Figure 7.5** Design of calibration chamber

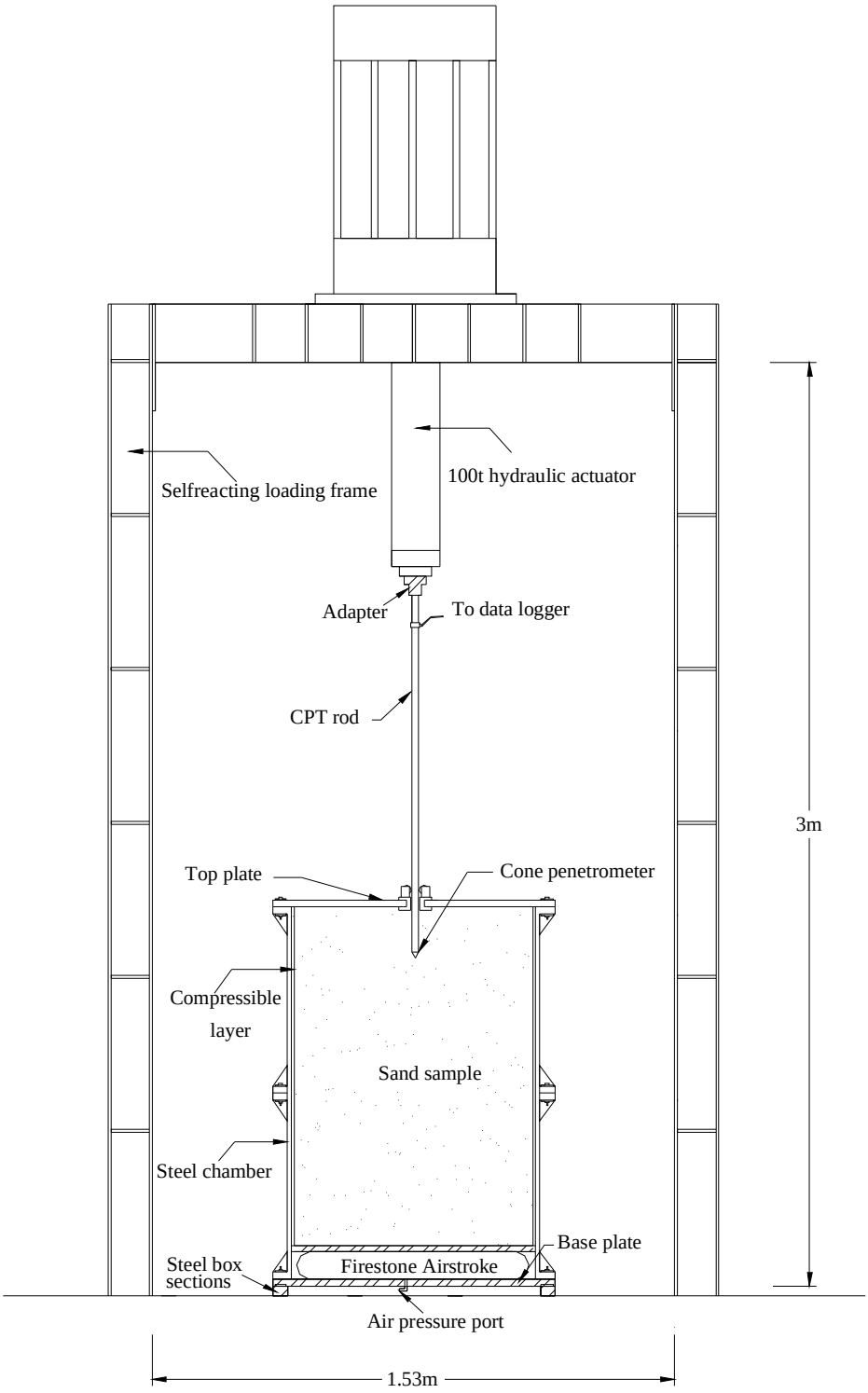


**Figure 7.6** Experimental setup

***Stress application***

The chamber was designed to apply vertical pressure to the sand sample from the bottom of the chamber using an air bellow and the lateral pressure increase with the increase of the vertical pressure. The air bellow of single convolution style manufactured by Firestone Industrial Products was adopted for the chamber. The specific type of air bellow is selected to optimize the vertical force delivered and to fit in the allotted space. Total pressure cells were mounted on the chamber wall to measure the lateral pressure at the interface between the soil and the compressible layer.

***Compressible layer***

The main idea of this study is to reduce and eliminate the boundary effects of the calibration chamber by incorporating a compressible material as buffer between the soil mass and the rigid steel wall. The material of compressible layer considered is sponge rubber with good elastic properties and can be easily attached onto the inner face of the rigid wall. Three sponge sheets of different thickness were proposed. Detailed methods of characterization of the buffer materials have been discussed in Chapter 6. Based on the theoretical analysis in previous chapters, one needs to use a buffer layer with specific thickness of a selected material for one sand sample in the chamber for a corresponding initial condition of sand.

It was difficult to obtain ideal buffer material from the market that can perfectly match the elastic properties that were derived from theoretical analysis for the buffer layer. In this study, the sponge rubber sheets bought from Singapore's market were adopted as the buffer layers. The Young's modulus and Poisson's ratio of the sponge rubber are characterized in Chapter 6.

Results presented in Figures 4.2 to 4.4 are summarized in Figure 7.7 and plotted with the properties of the sponge rubber sheets from Table 6.1. The black round points shown in Figure 7.7 indicate the elastic properties of the sponge rubber sheets of thickness of 10mm (BT=10mm), 20mm (BT=20mm) and 38mm (BT=38mm) as summarized in Table 6.1, respectively.

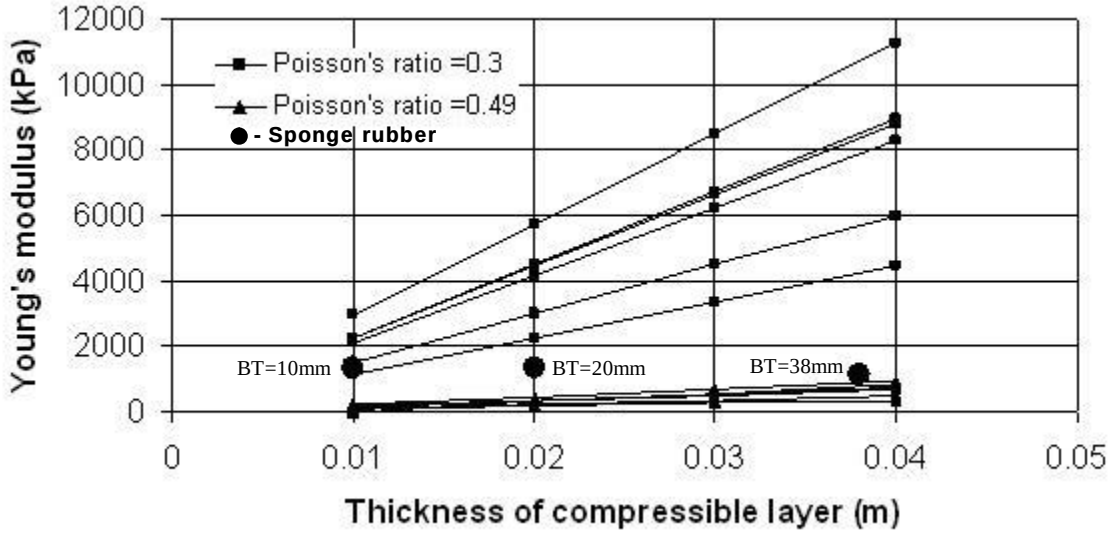


**Figure 7.7** Summary of Figures 4.2 to 4.4 and the elastic properties of sponge rubber of Table 6.1

Though the elastic properties of the selected sponge rubber may not match the selection criterion of the buffer layers described in Chapter 4 perfectly due to the reason mentioned above, the Young's modulus and Poisson's ratio of the sponge rubber are within the range of the requirements of the material properties as shown in Figure 7.7. Therefore, the sponge rubber can be adopted as the buffer layer of the chamber wall in this study.

***Top and bottom chamber plate***

The top and base plates will be 0.8 m in diameter and 15 cm in thickness. A hole in the center of the top plate will allow the passage of the cone penetrometer. Vertical pressure is to be applied by compressed air through an airport contained in the bottom plate. An assembly guide wheels will be incorporated in the top steel cover in order to ensure the verticality of the cone penetrometer during penetration.

***Electric cone penetrometer and adapter to loading frame***

An electric cone penetrometer will be used in this investigation. In the chamber testing, the signals from the inner load cell of cone penetrometer is transmitted to the data logger through a cable inside the hollow penetrometer drill rods and the signals will be processed by computer to obtain the cone tip resistance $q_c$ and the unit sleeve friction $f_s$. The available 5 ton capacity electric cone penetrometer in the NTU Geotechnics Workshop is shown in Figure 7.8.

**Figure 7.8** 5 Ton Electric cone penetrometer in NTU Geotechnics Workshop

## 7.3 CPT tests in the chamber

Twelve successful CPT tests have been performed in the developed calibration chamber. The detailed information for each test is described in Table 7.2 as follows,

**Table 7.2** Cone penetration tests conducted in the calibration chamber

| Test No. | Sand relative density ($D_r$ %) | Thickness of Buffer layer (mm) | $p_0$ (kPa) |
|---|---|---|---|
| **1** | 35 | 0 (Rigid boundary) | 100 |
| **2** | 60 | 0 (Rigid boundary) | 100 |
| **3** | 75 | 0 (Rigid boundary) | 100 |
| **4** | 35 | 10 | 100 |
| **5** | 60 | 10 | 100 |
| **6** | 75 | 10 | 100 |
| **7** | 35 | 20 | 100 |
| **8** | 60 | 20 | 100 |
| **9** | 75 | 20 | 100 |
| **10** | 35 | 38 | 100 |
| **11** | 60 | 38 | 100 |
| **12** | 75 | 38 | 100 |

The verification and interpretation of the chamber test results will be discussed and described in the next chapter.

# CHAPTER 8 VERIFICATION AND INTERPRETATION OF CALIBRATION CHAMBER TESTS

## 8.1 Introduction

The reliability of the cone penetration test in calibration chamber is mainly depended on the boundary condition of the calibration chamber. A series of CPT tests in Changi sand by using standard 36mm cone were carried in the developed calibration chamber in NTU Geotechnics Workshop as described in Chapter 7. In this chapter, the results of these CC tests are interpreted to verify that the performance of the new chamber wall design is capable of reducing and minimizing the boundary effect of the calibration chamber.

## 8.2 Boundary effect of loose sand samples

The results of 4 CPT tests in the calibration chamber with buffer layers of different thickness (0, 10, 20 and 38mm, respectively) on loose sample (Dr = ~35%) are shown in Figure 8.1 as follows. (Please refer to Table 7.2 for the description of Test No.)

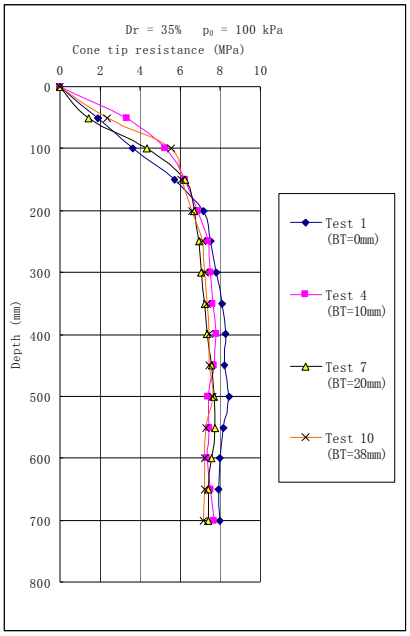


**Figure 8.1** $q_c$ of chamber tests in loose sand samples (Dr = ~35%)

The relationship between the measured $q_c$ at the middle depth of the sand sample and the thickness of buffer layers on loose sand samples are shown in Figure 8.2:

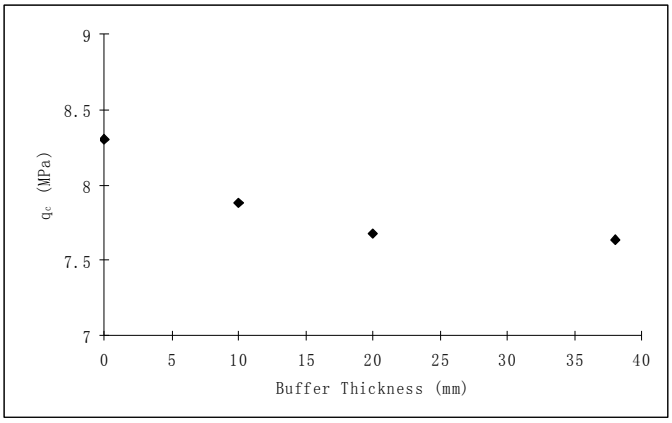


**Figure 8.2** $q_c$ vs buffer thickness for loose sand samples (Dr = ~35%)

The relationship between the ratio of $q_c/q_{c,R}$ and the thickness of the buffer layers for loose sand samples are shown in Figure 8.3, where $q_{c,R}$ is the cone tip resistance measured in rigid wall condition (without buffer layer).

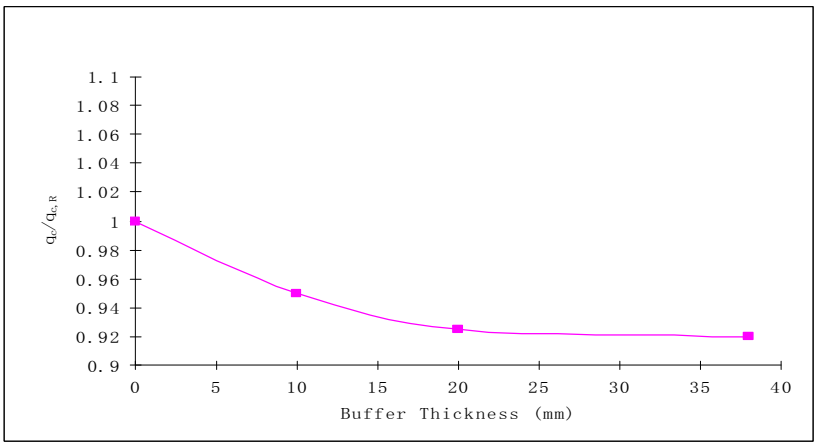


**Figure 8.3** $q_c/q_{c,R}$ vs buffer thickness for loose sand samples (Dr = ~35%)

It can be seen in Figure 8.3 that even for loose sand samples the boundary effect of the chamber wall still exists although the magnitude is small and can probably be neglected for very loose sand. This is consistent with the conclusion made by Parkin

(1988) that the $q_c$ results of calibration chamber tests on the loose sample are almost independent of boundary conditions.

## 8.3 Boundary effect of medium dense sand samples

The results of 4 CPT tests in the calibration chamber with buffer layers of different thickness (0, 10, 20 and 38mm, respectively) on medium dense sand samples (Dr = ~60%) are shown in Figure 8.4 as follows,

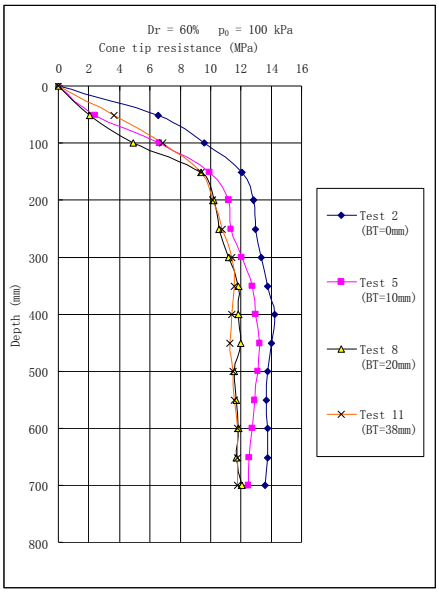


**Figure 8.4** $q_c$ of chamber tests in medium dense samples (Dr = ~60%)

The relationship between $q_c$ and buffer thickness on medium dense sand samples are shown in Figure 8.5:

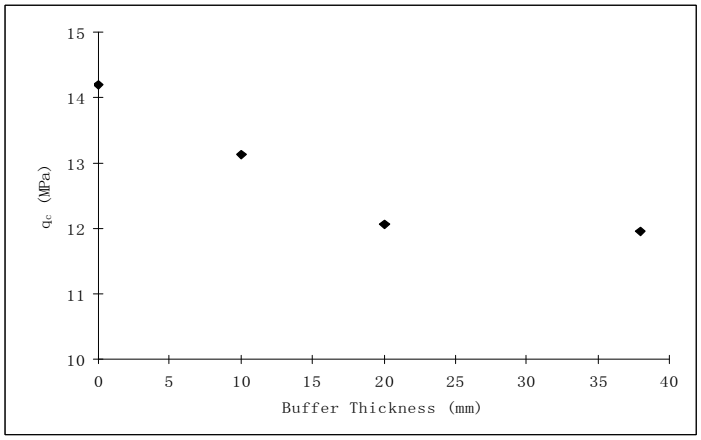


**Figure 8.5** $q_c$ vs buffer thickness for medium dense samples (Dr = ~60%)

The relationship between the ratio of $q_c/q_{c,R}$ and the thickness of the buffer layer for medium dense samples are shown in Figure 8.6, where $q_{c,R}$ is the cone tip resistance measured in rigid wall condition (without buffer layer).

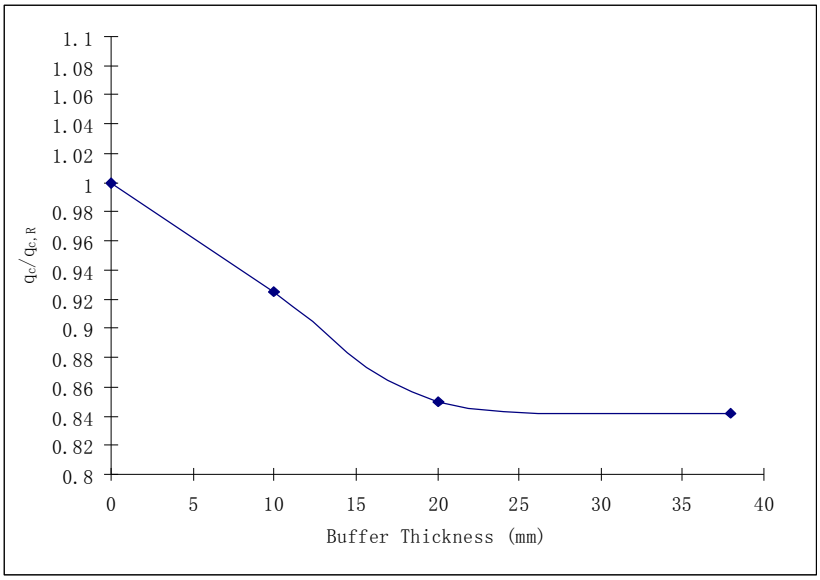


**Figure 8.6** $q_c/q_{c,R}$ vs buffer thickness for medium dense samples (Dr = ~60%)

It shows that the $q_c$ value decreases when the thickness of buffer layer increases. The $q_c$ converged when the thickness of buffer layer was increased to between 20mm and 38mm. The boundary effect of the chamber can therefore be reduced and minimized by the buffer material. The ratio of the converged $q_c$ to the $q_{c,R}$ of rigid boundary condition for medium dense sand sample is about 86%.

## 8.4 Boundary effect of dense sand samples

The results of 4 CPT tests in the calibration chamber with buffer layers of different thickness (0, 10, 20 and 38mm, respectively) on dense sand samples (Dr = ~75%) are shown in Figure 8.7 as follows,

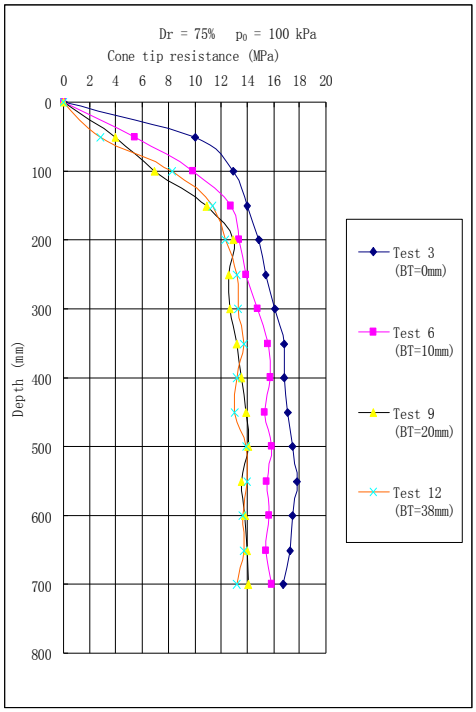


**Figure 8.7** $q_c$ of chamber tests in dense sand samples (Dr = ~75%)

The relationship between $q_c$ and buffer thickness on dense sand samples are shown in Figure 8.8:

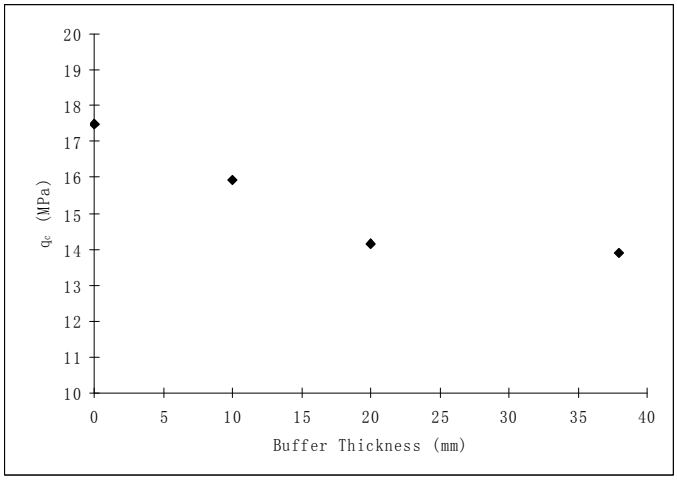


**Figure 8.8** $q_c$ vs buffer thickness for dense sand samples (Dr = ~75%)

The relationship between the ratio of $q_c/q_{c,R}$ and the thickness of the buffer layers for dense samples are shown in Figure 8.9, where $q_{c,R}$ is the cone tip resistance measured in rigid wall condition (without buffer layer).

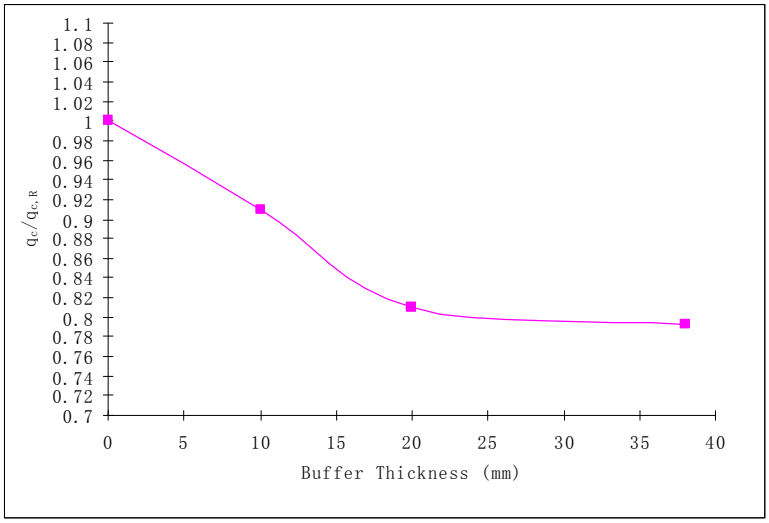


**Figure 8.9** $q_c/q_{c,R}$ vs buffer thickness for dense sand samples (Dr = ~75%)

It shows that the $q_c$ value decreases when the thickness of buffer layer increases. The $q_c$ converged when the thickness of buffer was increased to between 20mm and 38mm. Hence, the boundary effect of the chamber can be reduced and minimized by the buffer material. The ratio of the converged $q_c$ to the $q_{c,R}$ of rigid boundary condition is about 80%.

From the interpretations of the calibration chamber tests mentioned above, it can be concluded that the boundary effect of the calibration chamber with the rigid wall is obvious and significant for both medium dense and dense sand. For very loose sand, the boundary effect still exists but is small and can be neglected. This is consistent with the findings of previous researchers, such as by Parkin (1988) etc.

The $q_c$ measured in the rigid wall condition is higher than the $q_c$ measured in the boundary condition with buffer layer while other factors are kept the same. The CC

tests results shows that the boundary effect of the chamber can be reduced and minimized by increasing the thickness of the buffer layers to a certain value for a selected material. It also can be concluded from this investigation that the $q_c$ converged to a certain value and there is not much difference of $q_c$ measured for the two boundary conditions of 20mm and 38mm buffer layer for medium dense and dense sand samples.

Jamiolkowski et al. (1985) proposed using Equation (2.2) to obtain the correction factor $K_q$ for the chamber size effect (for 1.2m diameter chamber). The measured $q_{c,R}$ in the chamber needs be divided by $K_q$ ($q_c / q_{c,R} = 1/K_q$) to obtain in-situ $q_c$ value . The $q_c/q_{c,R}$ value mentioned in previous sections and $1/K_q$ are shown in Table 8.1

**Table 8.1** Comparison between $q_c/q_{c,R}$ of CC tests and $1/K_q$ derived from Equation (2.2)

| Dr of sand sample (%) | $q_c/q_{c,R}$ | $1/K_q$ |
|---|---|---|
| 35 | 0.93 | 0.98 |
| 60 | 0.86 | 0.90 |
| 75 | 0.80 | 0.86 |

It can be concluded that the boundary effect of the calibration chamber is reduced by the chamber buffer wall. The difference between $q_c/q_{c,R}$ of this study and $1/K_q$ derived from Equation (2.2) is probably because of the smaller diameter chamber (0.65m) used in this investigation. A larger boundary effect than the chamber of 1.2m diameter used by Jamiolkowski et al. (1985) is therefore expected.

## 8.5 $q_c$ vs Relative density

CPT tests were carried in calibration chamber on sand samples with different relative densities from loose to dense in this study. The relationship between cone tip resistance ($q_c$) and relative density (Dr) of sand is important for the interpretation of CPT results in the chamber.

Correlations for the relative density and cone tip resistance $q_c$ proposed by various researchers will be discussed as follows,

Jamiolkowski et al., (1985):

$$Dr = 66\log(q_c/(s'_{vo})^{0.5}) - 98 \qquad (8.1)$$

The correlation between $q_c$ and Dr proposed by Jamiolkowski et al., (1985) are plotted in Figure 8.10 and compared with the data measured in the calibration chamber of Changi sand.

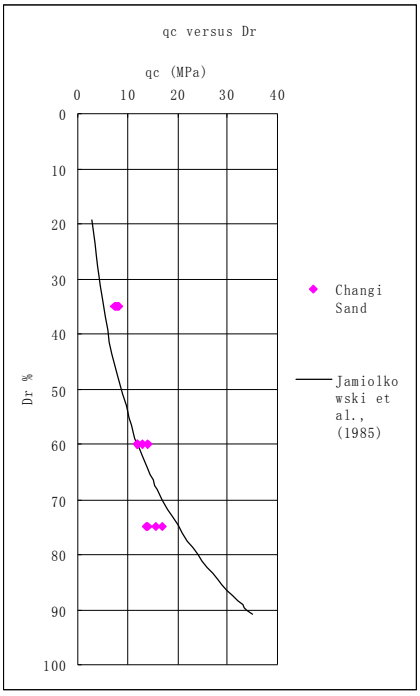


**Figure 8.10** Comparison of $q_c$ vs Dr relationship between Equation (8.1) and chamber test results of Changi sand

The real relative density of sand samples in chamber versus Dr derived from Equation (8.1) by using measured $q_c$ in chamber are plotted in Figure (8.11) as follows,

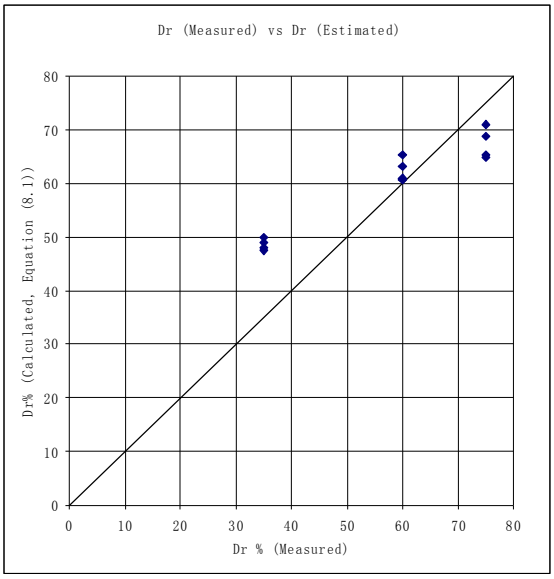


**Figure 8.11** Dr (real value) vs Dr (Derived from Equation (8.1))

Baldi et al. (1986) proposed the following correlation for Dr and $q_c$

$$D_r = \frac{1}{C_2} \cdot \ln\left( \frac{q_c}{C_o \left(s'\right)^{C_1}} \right) \tag{8.2}$$

where $C_o$, $C_1$ and $C_2$ are soil constants; $s'$ is effective stress in kPa, with $s'$ equal to either the mean effective stress $s'_m$ or the vertical effective stress $s'_{vo}$.

The correlation between $q_c$ and Dr proposed by Baldi et al. (1986) are plotted in Figure 8.12 and compared with the data measured in the calibration chamber of Changi sand.

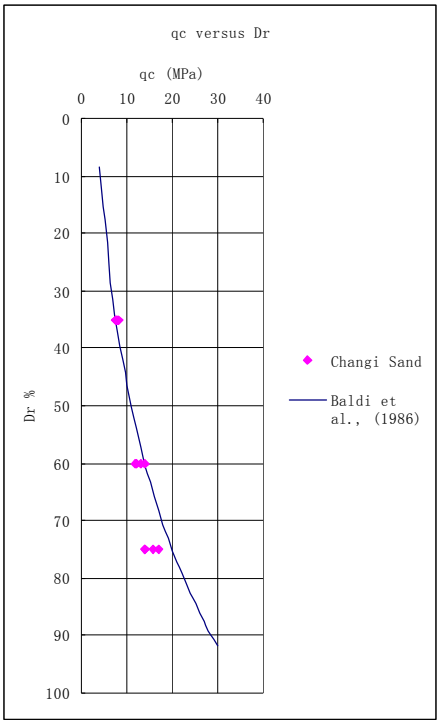


**Figure 8.12** Comparison of $q_c$ vs Dr relationship between Equation (8.2) and chamber test results of Changi sand

The real relative density of sand samples in chamber versus Dr derived from Equation (8.2) by using measured $q_c$ in chamber are plotted in Figure (8.13) as follows,

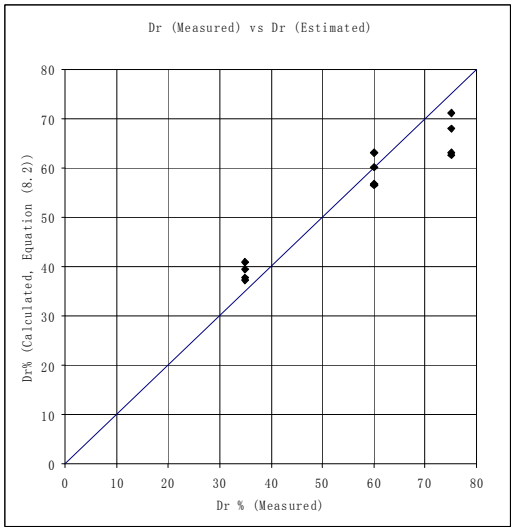


**Figure 8.13** Dr (real value) vs Dr (derived from Equation (8.2))

Kulhawy and Mayne (1990) proposed a simple formula for estimating relative density:

$$D_r^2 = \frac{q_{c1}}{305 Q_c \cdot Q_{OCR} \cdot Q_A} \qquad (8.3)$$

where

$q_{c1}$ = Dimensionless normalized cone resistance $= \dfrac{(q_c / p_a)}{(s'_v / p_a)^{0.5}}$

$p_a$ = Atmospheric pressure in same units as $q_c$

$Q_c$ = Compressibility factor $0.91 < Q_c < 1.09$

$Q_{OCR}$ = Overconsolidation factor

$Q_A$ = Ageing factor

The relative density for Changi sand derived from Equation (8.3) by using the $q_c$ values measured in the calibration chamber are shown as follows in Figure 8.14:

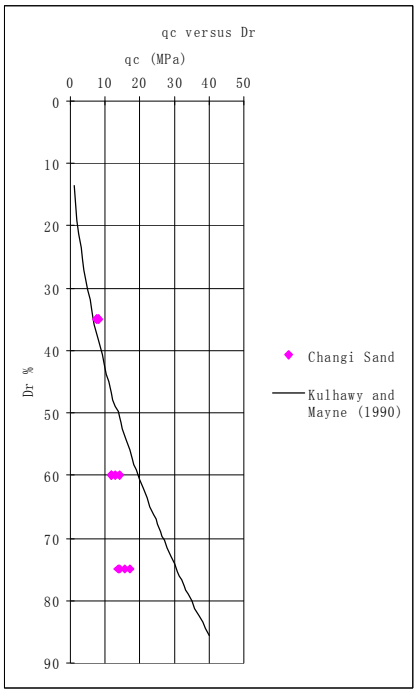


**Figure 8.14** Comparison of $q_c$ vs Dr relationship between Equation (8.3) and chamber test results of Changi sand

The real relative density of sand samples in chamber versus Dr derived from Equation (8.3) by using measured $q_c$ in chamber are plotted in Figure (8.15) as follows,

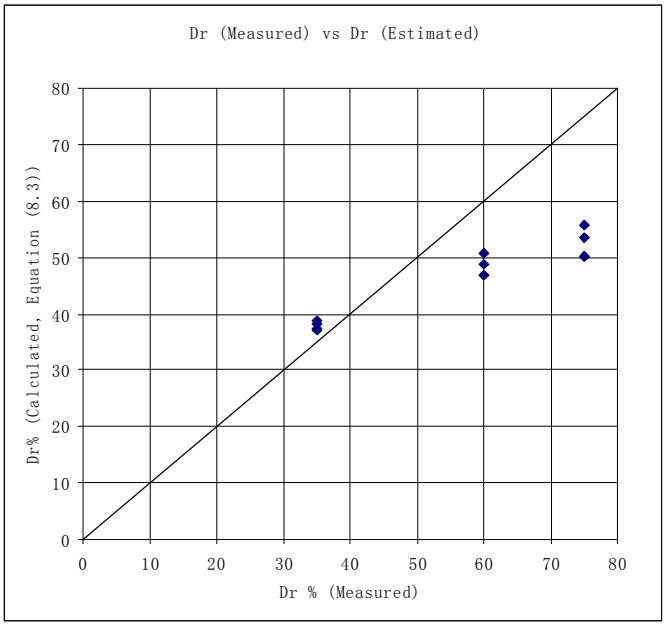


**Figure 8.15** Dr (real value) vs Dr (derived from Equation (8.3))

From the above figures it can be seen that the correlations between $q_c$ and Dr proposed by Jamiolkowski et al. (1985) and Baldi et al. (1986) are generally applicable for the Changi sand on $q_c$ values measured in the chamber tests. The correlation proposed by Kulhawy and Mayne (1990) are however not applicable for the Changi sand except in the case of loose sand.

## 8.6 Comparison with other CPT data

It is important to make a comparison between the CPT data of this study and CPT data in other sands. CPT data of other sands (Quiou sand, NC Ticnino sand, Toyoura sand and Hokksund sand) under the similar stress state of the sand samples of this study are plotted with the $q_c$-Dr correlations that mentioned in Section 8.5 in Figure 8.16 as follows,

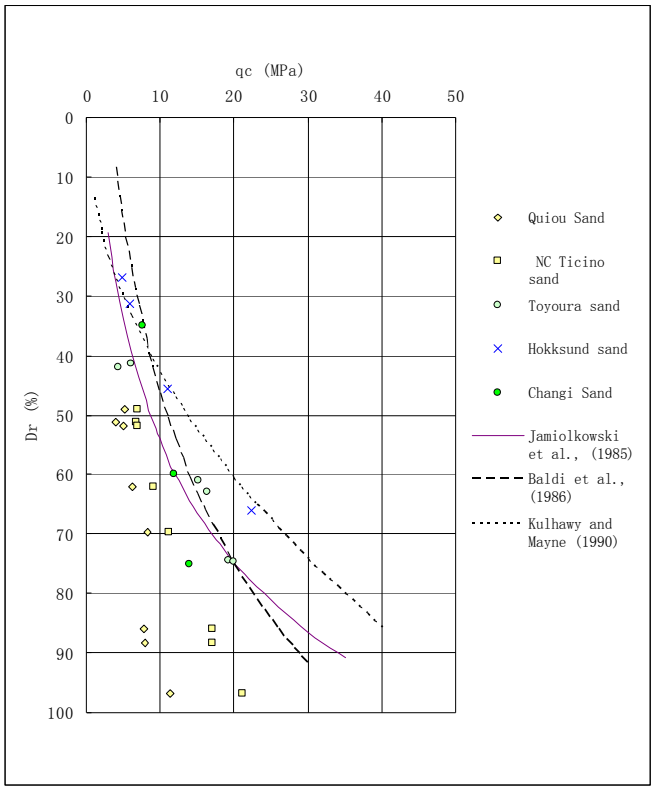


**Figure 8.16** Comparison of $q_c$-Dr relationship for different sands

From Figure 8.16, one can conclude that there is no universal $q_c$-Dr correlation that can be perfectly applicable to all sands. These correlations proposed by various researchers are empirical and site specific. The CPT data of Changi sand measured in the calibration chamber of this study are within the scatter of the CPT data of the various other sands mentioned above. Taking into consideration the site specific nature of all proposed $q_c$-Dr correlations, the $q_c$-Dr relationship obtained for the Changi sand in this study can therefore be considered to be reasonably probable.

## 8.7 Discussion

Salgado and Jamiolkowski (1998) pointed out that the difference between chamber and field $q_c$ values decrease as the ratio of the chamber size to cone diameter increases. This difference also depends on the type of boundary conditions.

Under BC1 ($\Delta s_h = 0$), $q_c$ is always lower than in the field, because a constant lateral stress during penetration underestimates the value that will develop during penetration

in the field. Ideal B3 ($\Delta e = 0$) conditions, with a perfectly rigid lateral wall, would always lead to higher $q_c$ values than those measured in the field.

Wesley (2002) made following points:

The surprising feature of the Figure 2.16 is that, for a given sand at constant relative density and applied stress state, the cone resistance $q_c$ increases as $R_d$ increases. This trend seems intuitively to be wrong: an increase in $R_d$ means a decrease in constraint from the chamber walls, and the cone resistance $q_c$ would be expected to become less, at least in those tests where lateral deformation is prevented. In contrast to the common opinion that it is the constraint from the chamber walls that cause the normal $q_c$ to deviate from the field value, Wesley (2002) suggested that it may be the change in vertical stress arising from the downward force of the penetrometer that provides the best explanation for changes in cone resistance with chamber size. In field situation, the vertical stress above the cone remains essentially constant (equal to the overburden pressure), while that below the cone increases by an amount dependent on the cone force and the properties of the soil (Figure 2.19 (a)). In contrast, the vertical stress in the chamber is applied using a loading piston at the base of sample. The base boundary condition can be either constant pressure or zero volume change in the base piston compartment, as illustrated in Figure 2.19 (b).

It can be seen from the literature that there were some contradictions in which boundary condition will result in the highest $q_c$ value. Is the highest $q_c$ under rigid boundary condition or field condition? The CPT test in a calibration chamber is a complex problem that is controlled by many factors. Interpretations of CPT by various authors contain significant difference in relating $q_c$ to soil parameters. The conflicting conclusion as to which are the main factor which affect $q_c$ could be due to difference in laboratory setups as well as analytical procedure (Huang and Hsu, 2004).

# CHAPTER 9 CONCLUSIONS AND RECOMMENDATIONS

## 9.1 Conclusions

A theoretical analysis based on cavity expansion theory has been developed to analyze the stress and displacement in the soil under the semi-infinite elastic half space and in a semi-confined cylindrical boundary. It indicates that a close simulation of the field boundary condition as prevailed in a semi-infinite soil mass subjected to cone penetration in a calibration chamber of limit size is possible if the induced radial stress and strain can be stipulated on the chamber wall. This may be accomplished by incorporating a compressible layer on the inner face of the rigid wall in a conventional chamber.

A laboratory investigation of cone penetration test (CPT) in a developed calibration chamber that is capable of reducing and minimizing the boundary effect of conventional calibration chamber was then performed in NTU Geotechnics Workshop. A series of CPT tests in Changi sand by using a standard cone were carried in the developed calibration chamber. The test results were interpreted and verified to evaluate the performance of the new calibration chamber.

The key findings are summarized as follows:

(1) The boundary effect of the calibration chamber with rigid wall for CPT tests is obvious and significant for medium dense and dense sand samples. For very loose sand, the boundary effect can still be detected but is small enough to be negligible. This is consistent with previous researchers' findings, such as Parkin (1988) etc.

(2) Existing correlations between $q_c$ and Dr proposed by Jamiolkowski et al. (1985) and Baldi et al. (1986) are applicable for Changi sand. The $q_c$ measured in the chamber tests on Changi sand are within the range of the values predicted by their proposed equations.

(3) It can be seen from the literature that there were some contradictions in which boundary condition will result in the highest $q_c$ value. Is the highest $q_c$ under rigid boundary condition or field condition? The CPT test in a calibration chamber is a complex problem that is controlled by many factors. Interpretations of CPT by various authors contain significant difference in relating $q_c$ to soil parameters. The conflicting conclusion as to which are the main factor which affect $q_c$ could be due to difference in laboratory setups as well as analytical procedure (Huang and Hsu, 2004). The experimental setup of this project also has some drawbacks and should be improved in the future study by others.

(4) When $q_c$ is converged, the value of $q_c/q_{c,R}$ for medium dense sample and dense sample in this study are equal to 0.86 and 0.80, respectively. It can be concluded that the boundary effect of the calibration chamber is reduced by the chamber buffer wall. The difference between $q_c/q_{c,R}$ of this study and $1/K_q$ derived from Equation (2.2) is probably because of the smaller diameter chamber (0.65m) used in this investigation. A larger boundary effect than the chamber of 1.2m diameter used by Jamiolkowski et al. (1985) is therefore expected.

(5) The experiments have shown that it is possible to develop a chamber with a lining of buffer material to simulate the far field in a chamber. The development of such a chamber would greatly help to establish a $q_c$-Dr relationship for a particular sand. As shown by various researches there is

no universally applicable correlation for all sand. The correlations are evidently site specific and hence the need to develop a simple, yet reliable calibration chamber to establish the applicable correlation for each type of sand. It has however also been demonstrated that this is not an easy task and much research work has still to be done. Hopefully some lessons can be learnt from the work done in the project and the following section discusses some of the possible future directions for research.

## 9.2 Recommendations for future research

(1) It was difficult to obtain ideal buffer material from the market that can perfectly match the elastic properties that were derived from theoretical analysis for the buffer layer. In this study, the sponge rubber sheets bought from Singapore's market were adopted as the buffer layers. The Young's modulus of the sponge rubber was feasible for the chamber wall design in this study but was slightly low. It is suggested that other materials with higher Young's modulus should be investigated in the future.

(2) The compression tests of the rubber sheets were conducted in the compression machine. Therefore, the strains of the rubber sheets in the compression tests as shown in Figures 6.3 to 6.8 were higher than the typical strains at the boundary wall during cone penetration test in the chamber. It is important to study the stress-strain behaviour in small strain range to check whether there is a linear stress-strain relationship of buffer layer. This point is recommended for future work if a more precise compression machine that is capable of conducting the small strain compression test of buffer layer is available.

(3) Due to a lack of time and the labour intensive nature of the experiments, the CPT tests in the chamber were carried in normally consolidated Changi

sand with an initial confining pressure of 100 kPa. It is suggested that the effect of different initial confining pressures on sand sample and the effect of stress history of sand in terms of OCR should be investigated in future studies.

(4) This research work should ideally be undertaken by a team of researchers. In the case of a single researcher, provision should be made for adequate assistance during the labour intensive part of the experimental work.

(5) When this type of calibration chamber is well-developed in the future which can perfectly simulate the far field soil mass, it is recommended to establish practical correlations between CPT measurements and intrinsic soil properties and soil-state variables for general use in practice.

# REFERENCES

Baldi, G., Bellotti, R., Ghionna, V., Jamiolkowski, M. and Pasqualini, E. (1982) "Design parameters for sands from CPT". Proceedings of the 2nd European Symposium on Penetration Testing, ESOPT II, Amsterdam, Vol.2, pp.425-432.

Baldi, G., Bellotti, R., Crippa, V., Fretti, C., Ghionna, V., Jamiolkowski, M., Pasqualini, E., Pedroni, S. and Ostricati, D. (1985) "Laboratory Validation of In-situ Tests". AGI Jubilee Volume-IX ICSMFE, San Francisco.

Baldi, G., Bellotti, R., Ghionna, V., Jamiolkowski, M. and Pasqualini, E. (1986) "International of CPTs and CPTUs; 2nd part: drained penetration of sands". Proceedings of the 4th International Geotechnical Seminar, Singapore, pp.143-156.

Baligh, M. M. (1985) "Strain path method". Journal of Geotechnical Engineering, ASCE, Vol. 111, No.9, pp 1108-1136.

Been, K., Lingnau, B. E., Crooks, J. H. A., and Leach, B. (1987) "Cone penetration test calibration for Erksak sand". Canadian Geotechnical Journal, Vol.24(4), pp.601-610.

Been, K., Crooks, J. H. A. and Rothenburg, L. (1988) "A critical appraisal of CPT calibration chamber tests". Proceedings of the International Symposium on Penetration Testing, ISOPT-1, Orlando, Vol.1, pp.651-661, Balkema Pub., Rotterdam.

Begemann, H.K.S. P. (1965) "The friction jacket cone as aid in determining the soil profile", Proceedings of the 6th International Conference on Soil Mechanics and Foundation Engineering, Montreal, Vol.1, pp17-120.

Bellotti, R. Bizzi, G., and Ghionna, V. (1982) "Design, construction and use of a calibration chamber". Proceedings of the 2nd European Symposium on Penetration Testing, ESOPT-II, Amsterdam, Vol.2, pp.439-446.

Bellotti, R., Crippa, V., Pedroni, S. and Ghionna, V.N. (1988) "Saturation of sand specimen for calibration chamber tests". Proceedings of the International Symposium on Penetration Testing, ISOPT-1, Orlando, Vol2, pp.661-672.

Bishop, R. F., Hill, R. and Mott, N. F. (1945) "Theory of indentation and hardness tests". Proceedings of the Physical Society, London, 57, pp. 147-159.

Bolton, M. D. (1986) "The strength and dilatancy of sands". Geotechnique, Vol. 36(1), pp. 65-78.

Bolton, M. D., Sun, H. W., & Britto, A. M. (1993) "Finite element analyses of bridge abutments of firm clay". Comput. Geotech, Vol. 15, pp 221-245.

Bolton, M. D. and Whittle, R. W. (1999) "A non-linear elastic/perfectly plastic analysis for plane strain undrained expansion tests". Geotechnique, Vol. 49 (1), pp. 133-141.

Bonita, J. A. (2000) "The Effects of Vibration on the Penetration Resistance and Pore Water Pressure in Sands". Ph.D Thesis, Department of Civil Engineering, Virginia Polytechnic Institute and State University.

Cao, L. F. (1997) "Interpretation of in-situ tests in clay with particular reference to reclaimed sites". Ph.D Thesis, Nanyang Technological University, Singapore.

Cao, L. F., Teh, C. I., and Chang, M. F. (2001) "Undrained cavity expansion in modified Cam clay I: theoretical analysis". Geotechnique, Vol. 51, No. 4, pp 323-334.

Cao, L. F., Teh, C. I., and Chang, M. F. (2002) "Analysis of undrained cavity expansion in elasto-plastic soils with non-linear elasticity". International Journal for Numerical and Analytical Methods in Geomechanics, Vol.26, pp.25-52.

Carter, J. P., Booker, J. R., and Yeung, S. K. (1986) "Cavity expansion in cohesive frictional soils". Geotechnique, Vol. 36 (3), pp. 349-359.

Chadwick, P. (1959). "The quasi-static expansion of spherical cavity in metals and ideal soils". Q. J. Mech. Appl. Math, 12, pp. 52-71.

Chang, M. F., Teh, C. I. and Cao, L. F. (2001) "Undrained cavity expansion in modified Cam clay II: application to the interpretation of the piezocone test". Geotechnique, Vol. 51, No. 4, pp 335-350.

Chang M. F. and Cao L.F. (2001) "Conceptual design of a calibration chamber for cone penetration test in sand". Internal Progress Report for RCC 1/99, School of Civil and Environmental Engineering, Nanyang Technological University, Singapore.

Chapman, G. A. (1974) "A calibration chamber for field test equipment". Proceedings of European Symposium on Penetration Testing, Stockholm, Vol.2.2, pp.59-65.

Chu, J., Lo, S-C.R. and Lee, I. K. (1993), "Instability of granular soils under strain path testing", Journal of Geotechnical Engineering, ASCE, Vol.9, No.5, pp.874-892.

Collins, I. F., Pender, M. J. and Wang Y (1992) "Cavity expansion in sands under drained loading conditions". International Journal for Numerical and Analytical Methods in Geomechanics, Vol. 16. pp 3-23.

Collins, I. F. and Yu H. S. (1996) "Undrained cavity expansions in critical state soils". International Journal for Numerical and Analytical Methods in Geomechanics, Vol. 20, pp 489-516.

Davis, E. H. (1969) "Theories of plasticity and the failure of soil mass". Soil Mechanics (ed. I. K. Lee), London: Butterworths.

Douglas, B. J. and Mitchell, J. K. (1975) "Static penetration resistance of soils". Proceedings Conference on In-situ Measurement of Soil Properties, American Society of Engineers (ASCE). Raleigh, North Carolina, June 1975, Vol.1, pp.151-188.

Douglas, B.J. and Olsen, R.S. (1981) "Soil classification using electric cone penetrometer. Cone Penetration Testing and Experience". Proceedings of the ASCE National Convention, St. Louis, pp.209-227, American Society of Engineers (ASCE).

ENEL (Milan), ISMES (Bergamo) and University of Turin (1985) "Laboratory validation of in-situ tests (in Geotechnical Engineering in Italy, an overview 1985)". Jubilee Volume for 11th International Conference of Soil Mechanics and Foundation Engineering, San Francisco, pp.251-271.

Gan, C. L. (2002), "Instability of granular soil under general stress conditions", MEng Thesis, Nanyang Technological University, Singapore

Ghionna, V.N, and Jamiokowski, M. (1992) "A Critical appraisal of calibration chamber testing of sands". Proceedings of The International Symposium on Calibration Chamber Testing, pp.13-40.

Gibson, R. E. and Anderson, W. F. (1961). "In situ measurement of soil properties with the pressuremeter". Civil Engng Public Works Rev, 56, No. 658, pp 615-618.

Gunn, M. J. (1992). "The prediction of surface settlement profiles due to tunneling". Predictive soil mechanics, Proceedings of the Wroth Memorial Symposium, Oxford, pp. 304-316.

Houlsby, G. T. and Withers, N. J. (1988) "Analysis of the cone pressuremeter test in clay". Geotechnique, Vol. 38 (4), pp. 575-587.

Houlsby, G. T. (1991) "How the dilatancy of soils affects their behaviour". Tenth European Conference on Soil Mechanics and Foundation Engineering, Florence, Italy.

Holden, J. C. (1971) "Laboratory research on static cone penetrometers". Internal Report CE-SM-71-1, University of Florida, Gainesville, Department of Civil Engineering.

Holden, J. C. (1977) "The calibration chamber of electrical penetrometers in sand". Internal Report 52108-2, Norwegian Geotechnical Institute.

Holden, J. C. (1992) "History of the first six CRB calibration chambers", Proceedings of The International Symposium on Calibration Chamber Testing, Potsdam, New York, 1991, pp.1-12.

Hsu, H. H. and Huang, A. B. (1998) "Development of an axisymmertic field simulator for cone penetration tests in sand". Geotechnical Testing Journal, GTJODJ, Vol.21(4), pp.348-355.

Huang, A. B. and Ma, M. Y. (1994) "An analytical study of cone penetration tests in granular material". Canadian Geotechnical Journal, Vol.31(1), pp.91-103.

Huang, A. B., and Hsu, H. H., (2004) "Advanced calibration chambers for cone penetration testing in cohesionless soils," Keynote Lecture, Proceedings. ISC-2 on Geotechnical and Geophysical Site Characterization, Porto, Portugal, Vol 1, pp. 147-167.

Huang, A. B., and Hsu, H. H., (2005) "Cone Penetration Tests under simulated field conditions,", Geotechnique, Vol IV, No.5, pp. 345-354.

Jacobsen, M. (1976) "On pluvial compaction of sand". Report No.9, Laboratory for Fundamentering, Inst.of Civil Eng., Univ. of Aalborg, Denmark.

Jamiolkowski, M., Ghionna, V. N. and Lancellotta, R. (1988) "New correlations of penetration tests for design practice", Proceedings of the International Symposium on Penetration Testing, ISOPT-1, Orlando, Vol.1, pp.263-96, Balkema Pub., Rotterdam.

Jamiolkowski, M., Ladd, C. C., Germaine, J. T. and Lancellotta, R. (1985) "New developments in field and laboratory testing of soils". State-of-the art report. Proceedings of the 11th International Conference on Soil Mechanics and Foundation Engineering, San Francisco, Vol.1, pp.57-153, Balkema Pub., Rotterdam.

Jefferies, M., and Been, K. (1995) "Cone factors in sand". The International Symposium on Cone Penetration Testing, Linkoping, Sweden, Vol. 2, pp. 57-153.

Kulhawy, F. H. and Mayne, P. H. (1990) "Manual on estimating soil properties for foundation design", Electric Power Research Institute, EPRI.

Kolbuszewski, J. and Jones, R. H. (1961) "Preparation of sand samples for laboratory testing". Proceedings, Midland Soc. for Soil Mech. And Found. Eng., Vol.4, 107.

Konrad, J. M. and Law, K. T. (1987) "Undrained shear strength from piezocone tests." Canadian Geotechnical Journal, Vol. 24, No.3, pp. 3392-3405.

Ladanyi, B. and Johnston, G. H. (1974) "Behavior of circular footings and plate anchors embedded in permafrost". Canadian Geotechnical Journal, Vol.11, pp. 531-553.

Laier, J. E., Schmertmann, J. H., and Schaub, J. H. (1975) "Effect of finite pressuremeter length in dry sand". Proceedings, ASCE Spec. Conf. on In-situ Measurement of Soil Props., Rayleigh, N.C., Vol. 1, pp.241-259.

Lunne, T. (1992) "Practical use of CPT correlations in sand based on calibration chamber tests". Proceedings of the International Symposium on Calibration Chamber Testing, Potsdam, New York, pp.225-36.

Lunne, T. and Christoffersen, H. P. (1983) "Interpretation of cone penetrometer data for offshore sands". Report 52108-15, Norwegian Geotechnical Institute, Oslo.

Lunne, T. and Kleven, A. (1981) "Role of CPT in North Sea foundation engineering (in Cone penetration testing and experience, Edited by G. M. Norris and R. D. Holtz). Proc. Session sponsored by Geotechnical Engineering Division at Am. Soc. Civ. Engrs. National Convention, St. Louis (Missouri), pp.76-107.

Lunne, T., Robertson, P. K., and Powell, J. (1997) "Cone Penetration Testing inGeotechnical Practice". Blackie Academic and Professional.

Mayne, P. W. (1991) "Determination of OCR in clays by piezocone tests using cavity expansion and critical state concepts". Soil and Foundations, Vol. 31 (2), pp. 65-76.

Muhs, H. and Weiss, K. (1971) "Investigation of ultimate bearing capacity and settlement behaviour of individual shallow footing in non-uniform cohesionless soil". Journal of the German Soil Mechanics Society, University of Berlin, pp. 1-37.

Na, Y. M. (2002) "In-situ Characterization of Reclaimed Sandfill with Particular Reference to Dynamic Compaction". Ph.D Thesis, Nanyang Technological University, Singapore.

Parkin, A.K. (1988) "The calibration of cone penetrometers". Proceedings of the International Symposium on Penetration Testing, ISOPT-1, Orlando, Vol.1, pp.221-43, Balkema Pub., Rotterdam.

Parkin, A.K. & Lunne, T. (1982) "Boundary effects in the laboratory calibration of a cone penetrometer for sand". Proceedings of the 2nd European Symposium on Penetration Testing, ESOPT-II, Amsterdam, Vol.2, pp.761-768.

Rad, N. S. and Tumay, M. T. (1987) "Factors affecting sand specimen preparation by raining". Geotechnical Testing Journal, GTJODJ, Vol. 10, No. 1, pp. 31-37.

Randolph, M. F., Carter, J. P., and Worth, C. P. (1979) "Driven piles in clay – the effects of installation and subsequent consolidation". Geotechnique, Vol. 29 (4), pp. 361-393.

Rix, G. J. and Stokoe, K. H. (1992) "Correlation of initial tangent modulus and cone resistance". Proceeding of the International Symposium on Calibration Chamber Testing, Postsddam, New York, pp.351-62.

Robertson, P. K and Campanella, R. G. (1983) "Interpretation of cone penetrometer tests: Part I: sand". Canadian Geotechnical Journal, Vol.20(4), pp.718-733.

Robertson, P. K., Campanella, R. G., Gillespie, D. and Greig, J. (1986) "Use of piezometer cone data". Proceedings of the ASCE Specialty Conference on: Use of In Situ Tests in Geotechnical Engineering, Blacksburg, pp.1263-1280, American Society of Engineers (ASCE).

Robertson, P. K., Sasitharan, S., Cunning, J. C. and Segs, D. C. (1995) "Shear wave velocity to evaluate flow liquefaction". Journal of Geotechnical Engineering, ASCE, Vol.121(3), pp.262-73.

Rowe, P. W. (1962) "The stress-dilatancy relation for static equilibrium of an assembly of particles in contact". Proc. Royal Society of London, Vol. 269, Series A, pp. 500-527.

Salgado, R., Mitchell, J. K. & Jamiolkowski, M. (1997) "Cavity expansion and penetration and penetration resistance in sands". Journal of Geotechnical and Geoenvironmental Engineering, ASCE, Vol.123(4), pp.344-445.

Salgado, R., Mitchell, J. K. & Jamiolkowski, M. (1998) "Calibration chamber size effects on penetration resistance in sand". Journal of Geotechnical and Geoenvironmental Engineering, ASCE Vol.124(9), pp.878-888.

Schmertmann, J. H. (1970) "Static cone to compute static settlement over sand". Journal of the Soil Mechanics and Foundations Division, ASCE, Vol.96(SM3), pp.1011-43.

Schmertman, J. H. (1975) "Measurement of in situ shear strength". Proceeding of the ASCE Specialty Conference on In Situ Measurement of Soil Properties, Raleigh, North Carolina, Vol.2, pp.57-138, American Society of Engineers (ASCE).

Schmertman, J. H. (1978) "Guidelines for cone penetration test: performance and design". Report FHWA-TS-78-209, US Dept. of Transp., Fed. Hignways Admin., Office of Research and Development, Washington (DC).

Shuttle, D., and Jefferies, M. (1998) "Dimensionless and unbiased CPT interpretation in sand". International Journal for Numerical and Analytical Methods in Geomechanics, 22, pp. 351-391.

Skempton, A. W. (1986) "Standard penetration test procedures and the effects in sands of overburden pressure, relative density, particle size, aging, and overconsolidation". Geotechnique, Vol.36(3), pp.425-47.

Sweeney, B. P. and Clough,G. W. (1990) "Design of a large calibration chamber". Geotechnical Testing Journal, ASTM, Vol. 13(1), pp.36-44.

Taylor, D. W. (1948) Fundamental of Soil Mechanics, John Wiley & Sons, New York.

Teh, C. I., Houlsby, G. T. (1991) "A analytical study of the cone penetration test in clay". Geotechnique, Vol. 41, No.1, pp 17-34.

Teh, C. I., Cao, L. F. and Chang, M. F (2001) "Stiffness parameters from in-situ tests in sand". Proceedings Insitu 2001, Bali, pp 17-35

Veismanis, A. (1974) "Laboratory investigation of electrical friction cone penetrometers in sands". Proceedings of the European Symposium on Penetration on Penetration Testing, Stockholm, June, 1974, Vol 2.2, pp.407-419.

Vesic, A. S. (1970) "Tests on uninstrumented piles, Ogeechee River site". Journal of the Soil Mechanics and Foundations Division, ASCE, Vol.96(SM2), pp.561-584.

Vesic, A. S. (1972) "Expansion of cavities in infinite soil mass". Journal of the Soil Mechanics and Foundations Division, ASCE, Vol.98 (SM3), pp.265-290.

Villet, W.C.B and Mitchell, J.K. (1981) "Cone resistance, relative density and friction angle". Cone penetration testing and experience: Session at the ASCE National Convention, St. Louis, 178-207, American Society of Engineers (ASCE).

Wesley L. D. (2002) "Interpretation of calibration chamber tests involving cone penetrometers in sands". Geotechnique Vol.52(4), pp.289-293.

Yu, H. S. (1990) "Cavity expansion theory and its application to the analysis of pressure meters". Ph.D Thesis, University of Oxford, Oxford, London.

Yu, H. S & Houlsby, G. (1991) "Finite cavity expansion in dilatant soils: loading analysis". Geotechnique, Vol.41(2), pp.173-183.

Yu, H. S., Herrmann, L. R. and Boulanger, R. W. (2000) "Analysis of steady cone penetration in clay." Journal of Geotechnical and Geoenvironmental Engineering, ASCE, Vol. 126. No.7, pp.594-605.